A Feasibility Study on Using CT Image Analysis for Hardwood Log Inspection

By

Dongping Zhu

Dissertation submitted to the Faculty of the
Virginia Polytechnic Institute and State University
in partial fulfillment of the requirements for the degree of

DOCTOR OF PHILOSOPHY
in
Electrical Engineering

APPROVED: Richard W Conners

Richard W. Conners, Chairman

A. L. Abbott

A. Lynn Abbott

D. Earl Kli

D. Earl Kline

Yilu Liu

Yilu Liu

Paul E. Torgersen

April 22, 1993

Blacksburg, Virginia

A Feasibility Study on Using CT Image Analysis for Hardwood Log Inspection

by

Dongping Zhu

Chairman: Richard W. Conners

Electrical Engineering

Abstract

To fully optimize the value of material produced from a log requires information about the log's internal defects prior to log breakdown. Studies have shown that a 7 to 21 percent improvement in log value recovery can be achieved if the location and identity of internal defects are known. Recent developments in advanced nondestructive testing methods such as CT and MRI offer, for the first time, the possibility of finding internal defects in logs prior to breakdown. Our ability to detect and recognize defects using this data depends critically on our understanding of wood structure and our ability to devise reliable method for automated image interpretation. While a lot of work has gone into demonstrating that certain types of defects manifest themselves in such sensor imagery, there has not been a systematic approach toward making the automatic inspection of logs a practical reality. This dissertation describes work aimed at creating a viable automated technology for locating and identifying log defects. The imaging modality used in this dissertation is CT. An important first step is to establish a data base of imagery and the ground truth information to determine how the various defects manifest themselves in this imagery. The second step is to study defect characterization and determine exactly which defects are detectable. The final step is to develop a basic method of approach to automated image analysis. A data base has been created from two hardwood species. It is representative of hardwood logs in the sense that it contains almost all the major defects. Visual inspection and analysis of these CT images have shown that most defects manifest themselves in CT imagery. These defects can be detected by features such as intensity, 3-d shape, and texture. As a means of automated image analysis, a knowledge-based vision system has been developed. It consists of three components: a data acquisition unit, an image segmentation module, and scene analysis module. A 3-d adaptive LS filter has been developed in the segmentation module that is efficient in removing annual rings while preserving other needed high frequency detail. Images are segmented using a multiple threshold scheme and regions are grouped using a 3-d connected volume growing algorithm. To represent the 3-d nature of wood defects, a set of *basic features* have been defined and used to design a set of hypothesis tests. These features seem to be adequate for defect recognition. To cope with imprecision and ambiguity the Dempster-Shaffer model for knowledge representation is used in the vision system. As a viable alternative to Bayesian-based theory, the Dempster's method of evidential reasoning is employed that uses previously unavailable information such as the amount of ignorance and ambiguity a hypothesis exhibits. As such, the proposed vision system seems to be able to recognize a number of hardwood defects. This dissertation also explores wood texture as an additional feature in defect recognition, and contributes the first application of robust Spatial Auto-Regressive modeling to wood texture analysis. Based on a correlation measure, two simple but efficient texture discrimination schemes are proposed. Incorporating a texture test in the scene analysis should improve the vision system's recognition power. As a pilot research, this dissertation has explored a number of important issues in creating a vision system for automated log inspection. Clearly, more work is needed to make the system more robust with additional species. Nevertheless, preliminary results seem to indicate that a machine vision system for automated hardwood log inspection can be developed.

ACKNOWLEDGMENTS

I would like to express my gratitude to Dr. Richard W. Conners, my principal advisor, who introduced me to machine vision and suggested the dissertation topic. His guidance, support, wisdom, and enthusiasm were essential throughout the course of my dissertation studies. For the successful education and pleasant memories I have from my years at Virginia Tech, a special thanks belongs to Dr. Paul E. Torgersen, former long-time Dean of Engineering College, whose vision, encouragement and assistance could always be counted on. I wish to thank Drs. A. Lynn Abbott, Yilu Liu, and D. Earl Kline for serving on my dissertation committee. I also wish to thank Dr. A. A. (Louis) Beex for teaching signal analysis courses and for the many insightful discussions on stochastic modeling.

I am very grateful to Mr. Philip Araman for his help and support in this project. I wish to thank Dr. Daniel Schmoldt for his friendship and for the stimulating conversations on log scanning. I also want to thank C. Ng, T. Cho, R. Avent, T. Drayer, S. E. Cline and R. Lineberry at the SDA Laboratory for their friendship and support. Also warm thanks to friends who made my stay at Blacksburg an enjoyable experience. I express my special gratitude to Dr. Kristian Peschmann and InVision Technologies, Inc. for providing the invaluable support, and to Dr. Kaarlo Heiskanen for giving his nuclear physics expertise.

Special thanks to my parents for my early education in discipline and integrity, and for their trust, encouragement and support in my life. Finally, I wish to thank my wife Jing for her love, and for the many days and nights she spent with me by the computers during the long winters in Virginia and the long summers in California. Without her love, devotion, support, and patience, this work would not have been completed.

TABLE OF CONTENTS

Chapter 1
Introduction

1.1 Motivation

The steadily increasing cost of raw material and labor in the manufacturing of lumber and veneer demands improved methods for the processing of wood. Since at the present time in the United States, logs constitute about 80 percent of the cost of the product in a sawmill, optimization of wood conversion into useful products is an economic necessity. There are approximately 5,000 sawmills in North America. The daily average volume of lumber processed by these mills is approximately 50,000 and 7,000 board feet (BF) for hardwood and softwood, respectively.

Hardwood timber, in particular, represents a substantial economic staple in the Eastern United States where there are many hardwood lumber processing facilities that produce more than 10 billion board feet of hardwood lumber annually. Improving processing would not only raise mill profits, but also enhance the utilization of the hardwood resource. However, hardwood sawmills are faced with two major difficulties [ARA90]. First, less than *optimal* processing has caused inconsistent product quality and reduced both volume and value recovery from logs. Second, log costs have been increasing faster than lumber prices; with cost of logs being increased from 20 to 80 percent of total production costs in the last 30 years [HOD90]. These circumstances dictate that sawmill operations be more efficient and improve yield (grade) from the available log raw material.

Automated log inspection systems hold much promise for the hardwood processing industry [HOD90] [CHA89]. These systems could increase productivity, and increase the grade of the material, either veneer or lumber, derived from logs. As such these systems hold the promise of addressing the problems facing primary hardwood processors.

The value of hardwood lumber or veneer cut from a log depends on the grade of the product. The grade of lumber or veneer depends on the size and number of clear areas on a board's surface or veneer flitch. It seems reasonable to suppose that if one could locate and identify the internal defects of a log prior to initial breakdown, one should be able to formulate a method for cutting the log into lumber or veneer that has the highest possible grade. Numerous studies suggest that at least 10 to 21 percent improvement in lumber value would result if an *optimal* breakdown strategy could be formulated [MAL56] [CHA89] [STE89] [OCC89] [HOD90] [KLI90]. While no formal studies have been conducted to determine the possible value improvement in veneer, it is believed that optimal processing would raise veneer value by as least the same percentage as that of lumber. It is for this reason that the primary wood processor's dream has always been to be able to "see" into a log's interior.

Currently log inspection is performed by human experts; experts that use bark distortions as surface indicators to infer the corresponding internal features of a log. Their performance is, however, quite limited due to a number of factors. First and foremost is the fact that while bark anomalies are indicative of some defects, it is unclear as to exactly how accurate "bark reading" actually is. Next, experts in any field are all subject to the *human equation*; their performance is affected by boredom, fatigue, and etc. Finally, to optimize wood recovery the expert must not only determine the locations and identities of all defects, and the 3-d log shape, he must also utilize this information to create an "optimum strategy" for processing the log. Formulating such optimum strategies for each log processed is a difficult task that calls for the application of more quantitative methods.

To this end, a number of log scanning methods have been studied over the last few decades. Optical scanners [LEE91], ultrasonic scanners [BIR91], microwave scanners [MAR87], and laser scanners [KIN79] have all been tried. Unfortunately, the crucial limitation of these scanning systems and the human expert is that neither can tell what the log looks like internally before it is cut. Without the necessary information about the internal structure of a log, it is impossible to design an *optimal* processing strategy that turns out products with the highest value.

Technology has developed to the point that wood defects can indeed be "seen" in the interior of logs using non-destructive *imaging* techniques. Most recently, log scanning using methods such as magnetic resonance imaging (MRI) and computed tomography (CT) imaging has been studied in laboratory experiments, and their ability to differentiate some internal defects in logs has been, in part, demonstrated [CHA91] [WAG89]. For some time, these highly advanced imaging devices have been considered too expensive for log inspection. However, according to a recent market analysis conducted with a number of the largest sawmills in North America, it is anticipated that earnings in sawmills over the next 5 years will increase by 15.5 to 17 percent. This clearly indicates that mills are profiting on the increased value of logs, due to high demand but decreased availability. In 1992, one major sawmilling company reported that it had raised its lumber price by 23%, while the lumber prices in the South increased on average by 50 percent during the first half of 1993. Given the increasing profits of sawmilling industry, it is expected that they will invest in innovative technologies, such as CT log scanning systems, that could help them produce higher value lumber products.

Unfortunately, the studies to date employing these advanced sensing systems all have a number of shortcomings. First, none of the studies has attempted to establish a data base of log images that illustrates the ways defects manifest themselves within logs of one wood species, or within logs across wood species. The data collected to date have all been from either a single log or a very small number of logs. Part of the reason for this is the high cost of collecting the imagery. Second, the studies have not attempted to provide much *ground truth* information. To verify the location and extend of a defect in an image slice requires at least a color photograph of the log cross-section at the position the sensor image slice was taken. These studies have also not addressed the issue of how the various internal defects depicted with a sensor's imagery can be automatically located and identified. For optimal processing to be commercially viable requires automatic methods for locating and identifying internal defects, and automatic methods for computing an optimal breakdown strategy based on internal defect location and identities.

While the recent work in [FUN85] [GRU91] represents an important step toward this goal, none, if any, has investigated the potentiality of creating a general machine vision system using such an imaging device for automated analysis of log images. There is no general method available for analyzing log CT image data.

1.2 Limitations and Scope

Because of the relatively high cost in creating a high quality image date base, this study has a number of limitations.

(1) The costs associated with obtaining CT and MRI image slices precluded obtaining data from both scanners. Only data from CT scanner are considered in this study.

(2) Due to the high cost of collecting CT image date, the number of hardwood species considered had to be limited. The species considered were red oak (ring porous) and yellow poplar (diffuse porous). These two species represent the extremes in the spectrum of the hardwood species.

(3) Because the desire is to determine how internal defects manifest themselves through a volume of space, the number of defects that could be imaged was limited. In collecting data on a defect in a log, scanning was started in the clear wood area just prior to the defect. Slices were collected starting at this clear wood section all the way through the volume affected by the defect into a part of the log that was again all clear wood. Using this procedure means collecting data on any one defect requires a number of CT slices to be collected.

(4) Given that little research work has gone into developing optimal processing strategies for veneer recovery based on internal defect location and identity, or into determining the impact of an optimal processing strategy would have on veneer value recovery from logs, this study concentrates on optimizing board values obtainable from log breakdown. Hence the internal defects of interest are those that affect hardwood lumber grades. Note that methodologies for optimizing value in veneer recovery could be of even greater importance than optimizing value in board recovery [DEA91].

1.3 Assumptions

The underlying assumptions behind this study are as follows.

(1) The performance and cost of all the required technologies will be such that these technologies can be profitably applied to the internal defect detection and/or optimum log breakdown problem by hardwood sawmillers.

(2) The same lumber grading defects, e.g., knots, splits, holes, decay, mineral streak, bark pockets, etc., manifest themselves in CT imagery as well as in MRI imagery. The available literature seemingly supports this assumption [SHA88] [WAG89] [GRU91] [CHA91].

(3) General imagery analysis methodologies based on adaptive and robust vision algorithms can be implemented regardless the imaging modality used. In particular, it is assumed that methodologies developed for CT imaging could be modified to handle imagery from other imaging modalities, such as MRI or ultrasound.

(4) Computerized methods for optimizing log breakdown based on the location and identification of internal log defects can be effectively implemented.

1.4 Objectives

The general goal of this dissertation is to establish the feasibility of using CT scanner imagery to power an optimal log breakdown system for optimizing the value of lumber obtainable from hardwood logs. This general goal can be subdivided into three objectives. These are as follows:

(1) *Objective 1*: Establish a log image data base. The purpose of this data base is two fold. First, it allows one to determine how and which hardwood defects manifest themselves in CT imagery. Second it allows one to correlate visual defects in a log with areas in CT imagery. It consists of a set of CT images scanned from various hardwood logs, and a set of color pictures of the corresponding cross-sections of these logs.

(2) *Objective 2*: Determine which hardwood lumber grading defects can be detected in CT imagery. The determination is very important in assessing the technical feasibility of using the CT imaging to optimize lumber value recovery from logs.

(3) *Objective 3*: Illustrate the feasibility of automatically locating and identifying a subset of hardwood lumber grading defects in CT imagery. A machine vision system using a knowledge-based expert system has been developed for automatically analyzing log CT images. The purpose of this machine vision system is to *find quantities that are automatically derived from the CT imagery with reasonable ease and which are useful for locating and identifying internal defects accurately.* This vision system can be conceptually decomposed into 3 components (Fig. 1.1):

1) a data acquisition unit,
2) an image segmentation module, and
3) a scene analysis module.

Fig. 1.1 The machine vision system diagram.

The segmentation module can be further divided into three components (Fig. 1.2):

1) filtering,

2) thresholding, and

3) 3-d labeling.

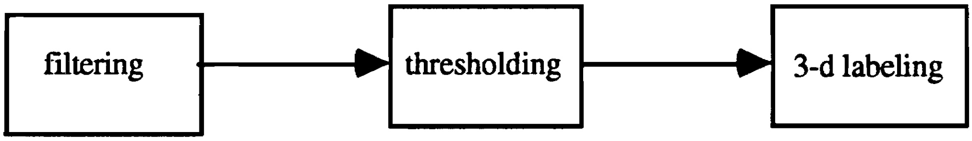

Fig. 1.2 The segmentation module

The scene analysis module consists of the following four steps (Fig. 1.3):

1) feature computation,

2) belief mapping,

3) evidence combination, and

4) decision making.

The input to the vision system is the 3-d image of a log acquired by a CT scanner, and the output provides information about the location, size, orientation, and identity of each defect in the log. To be effective, the vision system must be able to operate in a species-independent manner so that the same procedures can be applied across different hardwood species without any loss in efficacy.

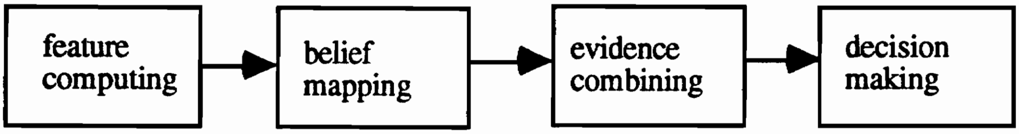

Fig. 1.3 The scene analysis module

1.5 Contributions

This dissertation makes a number of contributions to the machine vision research as applied to hardwood log inspection problem. These include:

(1) Creating a representative hardwood image data base. This data base represents the extremes in the spectrum of the hardwood log species: ring porous and diffuse porous species.

(2) Establishing the relationship between wood physiology and wood CT image characteristics, in particular, those relationships between various defects and their CT image manifestations, including intensity, shape, and orientation.

(3) Developing an adaptive 3-d image smoothing method that seems to be able to eliminate annual rings from log CT images while preserving other needed image detail. As such,

it facilitates the tasks of image segmentation and scene analysis in the machine vision system for log inspection.

(4) Defining a set of basic features that seem especially suited to the representation of 3-d objects that have complex and arbitrary shapes for which exact geometric models are difficult, if not impossible, to obtain.

(5) Developing an efficient defect recognition procedure that is based on the Dempster-Shafer theory of evidential reasoning. This procedure is able to propagate evidence at different stages or from different knowledge sources, and achieve consensus among conflicting pieces of evidence.

(6) Applying a Spatial Auto-Regressive (SAR) model to the analysis of wood texture of hardwood CT images, as well as developing two simple but efficient texture discrimination schemes in order to improve the scene analysis module's performance.

1.6 Outline

The rest of this dissertation is organized into 7 chapters. Chapter 2 provides background on the log grading and sawing problem. It reviews previous work on automated wood inspection. Finally it addresses the applicability of CT imaging to log inspection. Chapter 3 discusses wood anatomy, grading defects, and the characteristics of CT images. Chapter 4 is concerned with data collection and analysis. Chapter 5 describes the image segmentation module. Chapter 6 presents the scene analysis module. Chapter 7 addresses the image texture modeling and analysis problems. Finally, Chapter 8 concludes this dissertation with directions for future research.

Chapter 2
Problem Background

This chapter provides background on the hardwood log inspection problem. This includes a description of current log grading and log sawing methods, together with some comments on the limitations of current methods. The chapter reviews previous work on improving lumber value yield. It also addresses issues associated with applying various non-destructive testing (NDT) techniques to the hardwood sawmilling industry. Finally, it briefly discusses knowledge-based machine vision systems for industrial inspection.

2.1 Lumber Grading

2.1.1 Defects in Wood

From the point of view of economics, a defect in wood is any feature that lowers its market value. It may be an abnormality that decreases the strength of the wood or a characteristic that limits the board's use in a particular application. However, what is judged to be definitely unsuitable for one application may prove to be ideal for a different application, and some defects may be useful for special applications, such as the wood decorating surfaces.

Many grading defects are not natural abnormalities in a strict sense but are simply the product of natural tree growth. Variations from the normal shape of a tree trunk, knots and reaction wood are all natural defects whose formation man has only limited control over while the tree is growing. Other common sources of defect are insects and fungi that can attack living trees, logs, lumber or processed wood products. Chapter 3 contains a detailed description of the physiological and geometric characteristics of some most commonly occurring defects in logs.

Wood defects, such as knots, worm holes, stains, mineral streaks, splits, decay, and etc., all affect the grade of lumber. The fewer defects a board has, the higher its grade. There are two categories of wood grading defects: general defects and species-dependent defects. The former includes knots, wane, worm holes decay, pith and etc. in most wood species. The latter includes gum pockets in maple and some other defects that appear only in particular types of wood species. Below is a brief description of some of the grading defects (see Section 3.1.2 for detailed descriptions).

Knots: a branch included in the wood by growing around tree base.
Holes: round or oval shaped, caused by insects, rot or mechanical wound.
Stain: dark, solid wood caused by staining fungi inhabiting in the wood.
Decay (white or brown *Rot)*: decomposed wood caused by decaying fungi.
Mineral Streak: caused by bird pecks and mineral concentration.
Wane (*bark* or lack of wood): the outmost layer of wood covering the tree.
Splits or *Cracks*: lengthwise separation of wood due to wood tearing.

2.1.2 Lumber Grading Rules

All native hardwood lumber is graded according to the rules set forth by the National Hardwood Lumber Association (NHLA). The rules are complete and detailed so that they permit accurate lumber grading with a minimum of personal judgment. A complete description of the lumber grading procedure is beyond the scope of this dissertation, but can be found in other publications, such as the NHLA publication [NHLA86]. Basically, lumber is evaluated using several criteria such as overall lumber size, type and size of defects, the relative area of clear-face cutting pieces, and the total lumber surface area or surface measure. Higher grades require larger lumber dimensions, and require a higher percentage of clear-face cutting areas in very few cuttings. According to NHLA rules, the standard grades of hardwood lumber are

Firsts,
Seconds,
Selects,
No. 1 Common,
No. 2 Common,
Sound Wormy,
No. 3A Common, and
No. 3B Common.

In the above grades, Firsts and Seconds are usually combined as one grade, called FAS. Since Selects have FAS grade on one side and Common grade on the other, they are usually combined with No. 1 Common as one grade, named No. 1 Common. Sound Wormy is a grade used for species where insect damage is prevalent, and is not used very often. Thus it can be deleted from the above list. No. 3A and No. 3B Common may be combined as one grade, named No. 3 Common. Therefore, the 4 simplified lumber grades, FAS, NO. 1 Common, No. 2 Common, and No. 3 Common, are generally used in lumber grading with FAS being the highest grade.

The NHLA rules have specific criteria for each grade of lumber. For example, a board having the grade FAS must be: 6 or more inches wide, 8 to 16 feet long, and a 91% (Firsts) or a 83% (Seconds) clear-cutting face. This grade also has some other specific requirements for different defects, i.e., the average diameter of a knot or a hole should not exceed one-third of the surface measure, splits shall not exceed twice the surface measure, and wane shall not exceed one-twelfth of the surface measure, and etc. Table 2.1 lists the basic specifications for standard hardwood lumber grading [NHL86].

In general, higher grade lumber has a higher price in dollars per board foot (BF). Roughly speaking, when a piece of lumber is upgraded by one grade, its value can be almost doubled. For example, the prices (per thousand BF) in 1993 of green 4/4 Appalachian red oak are listed in table 2.2.

Table 2.2 1993 Lumber Prices by Grade (Appalachian Red Oak)

Lumber Grade	Price (per thousand BF)
FAS	$1,100
No. 1 Common	$650
No. 2 Common	$395
No. 3 Common	$205

Table 2.1 Hardwood Lumber Grading Rules[a]

Lumber Grade	Length[b] (ft)	Width (in)	Yield[g] (%)	Size of cuttings (in x feet)	Number of cuttings[c]
First and Second	8	6	$83\frac{1}{3}$	4 x 5 or 3 x 7	1 to 4
Selects[d]	6	4	$91\frac{2}{3}$	4 x 5 or 3 x 7	1 to 4
1 Common[e]	4	3	$66\frac{2}{3}$	4 x2 or 3 x 3	1 to 5
2 Common	4	3	50	3 x 3 or 3 x 2	1 to 7
3A Common	4	3	$33\frac{1}{3}$	3 x 2	no limit
3B Common	4	3	25[f]	$1\frac{1}{2}$ x variable length	to give 36 in^2

Note:

a. National Hardwood Lumber Association, 1974. These are minimum requirements.

b. Percentage of short lengths limited by grade; e.g., in FAS only 15% can be 8 to 9 ft; in 2C, 10% can be 4 to 5 ft.

c. Number varies with surface measure (SM) of piece; e.g., 1C with SM of 5 to 7 ft, 2 cuttings allowed; in 1C with SM of 11 to 14 ft, 4 cuttings allowed.

d. One cutting allowed. For pieces 2 and 3 ft (SM), reverse sound or not below 1C. Pieces 4 ft plus (SM) shall Greg on one face as required in seconds with reverse side of board not below 1C for reverse of cutting sound.

e. Including sound and wormy 1C. Full log yield of 1C and Better, with worm holes, knots, etc. (not over 3/4 inch), and stain, admitted.

f. sound cuttings.

g. Yield of rough lumber in clear-face cuttings (percent).

Given this fact about the price difference for hardwood lumber based on grade, it is very important for sawmillers to obtain the highest possible grade of lumber from the logs they saw up. As such it can be concluded that developing ways of improving the grade of lumber obtained from a log is very important to the primary hardwood forest products industry.

2.2 Log Grading and Sawing Methods

2.2.1 Log Grading

Trees can generally be classified as either hardwoods or softwoods. Hardwoods, such as oak or poplar, may be distinguished by their deciduous foliage. Softwoods, on the other hand, may have an evergreen foliage. Hardwoods are primarily used in furniture-making (lumber) and fine-finish woodworking (veneer), because of their rich, dark, colorful heartwood. Softwoods, on the other hand, are used mainly by the construction industry as a building material where the appearance of the material surface is not so important.

Owing to the end use of hardwoods, grading defects in hardwood are surface features that largely affect the visual appearance of lumber or veneer. Section 3.1.2 of this dissertation contains a list of major hardwood grading defects along with detailed descriptions of these defects. Knots, splits, decay, stain, worm or bird holes, etc. are considered grading defects. According to the hardwood log grading rules set forth by the U.S. Forest Service, the major factors that affect the grade of sawlogs are: 1) the position of logs in tree (butt or upper); 2) the size of log, especially diameter; 3) log straightness; 4) the amount and distribution of scalable defects that reduce the lumber volume; and 5) the defects in the usable wood outside the heart center [RAS73]. All defect indicators judged to indicate log grade defects are counted equally except for a few special cases. Hardwood logs are classified into grade 1, grade 2, and grade 3, with grade 1 being the highest value grade. There is a special grade, called veneer grade, that is applied to very high-quality hardwood veneer logs. The log grading rules place a high value on defect-free logs. Normally log prices are published as quarterly reports, such as the Pennsylvania Timer Market Report. For example, in September 1992 the published prices per thousand feet board at sawmills (mill prices) for veneer grade, grade 1, 2, and 3 of northern red oak sawlogs were $807, $551, $369, and $134, respectively .

Two steps are involved in log grading, face grading and end grading. In face grading, after taking into account the size and soundness of the log, the grader visually squares the log full length into 4 faces so oriented as to give the largest number of good faces. Each of these faces is evaluated the same way lumber would be evaluated. After eliminating the poorest face, the grade of the log is determined by the poorest of the remaining 3 faces. This face is called the grading face.

The major problem in grading saw logs is the manner in which one locates clear cuttings on the grading face. If clear cuttings can be determined, necessary measurements on the grading face can be made by the grader to decide the grade of a log. However, locating clear cuttings requires that one properly evaluates log surface indicators for internal defects. Except for such things as branch stubs and knot overgrowths, most other surface indicators are not only difficult to detect but very hard to interpret. For example there no surface indicators for internal stain or splits yet these features are very important in assigning accurate grades to log faces.

Once the faces have been graded, end grading is performed. End grading involves examining a log for grade defect indicators that may not show on the log surface. To evaluate the end defects, a log end is divided into two major zones, the heart center and the quality zone [RAS73]. The heart center is the core of the log with a "radius" equal to 20 percent of log diameter. The quality zone, the portion of the log outside the heart center, has a "radius" equal to 30 percent of log diameter. The quality zone, which produces quality material from the log, can be further divided into two sub-zones, the inner quality zone and the outer quality zone, with each taking up half of the quality zone. Consequently, special instructions are provided for evaluating log ends by measuring various defects in these two different zones. For example, a surface abnormality, if determined to extend into a depth more than 15 percent of the diameter at the point of occurrence, is considered a log grade defect. Otherwise, it should be disregarded.

As in the face grading, end grading depends largely upon information about the internal defect configuration of the log which, unfortunately, can not be directly seen by the grader. He must rely on finding surface indicators that may be indicative of some internal defects.

To illustrate the grades of saw logs, let us consider a straight, sound tree. The logs cut from this tree will have grade 1, grade 2, or grade 3 respectively, if 5/6, 2/3, or 1/2 of its grading-face length is clear. Clearly the sizes and locations of defect on a board dictate the quality and value of boards and logs from which boards are cut. The value yield of a board, VYB (in dollars), is calculated by the following equation [LEE91]

$$VYB = P_g \left[\frac{L \times Ac}{12(\text{inch}) \times 1000}\right] \text{ dollars,} \qquad (2\text{-}1)$$

where P_g is the price of 1,000 board feet lumber, L is the length of board in feet, A_c is the cross-sectional area in inch squared. The number of board feet in any board is defined by multiplying the thickness in inches by the width in inches by the length in feet and dividing the result by 12. Hardwood lumber is divided into four grades, which will discussed in section 2.2.2 of this chapter. For example, in April 1993 the P_g value of 1 x 4 inch red oak boards in the state of Virginia is $1,100, $650, $395, and $205 respectively for the 4 different grades. The values of the same size southern pine boards are $550, $380, $230, and $195 respectively.

Given the value of each board, the value of a log can be determined by the total value of the boards sawn from it. Suppose a log is cut into n boards. Let VYB(i) be the value yield of the *i*th board. The log value yield (VYL) with respect to this particular cut is the sum of the n VYBs, expressed as

$$VYL = \sum_{i=1}^{n} VYB(i) \tag{2-2}$$

2.2.2 Log Sawing

To produce lumber or veneer from a log, a sawing strategy needs to be designed. There are two possible strategies in log sawing, 1) volume recovery, and 2) value recovery. In volume recovery, logs are sawn to obtain boards that have the most board feet possible. This sawing strategy is typically adopted by the softwood industry. In value recovery, logs are sawn in order to obtain boards that have the highest grade possible - this must be the desire of every hardwood sawmiller. Note that maximizing board volume does not necessarily give near the profit of maximizing board value. Since human beings cannot "see" into the interior of a log to determine where all the defects are, the strategies they formulate cannot be optimal. In this study on hardwood log inspection, an optimal strategy is one that maximize the grade of lumber produced during log breakdown, as suggested by Eq. (2-2). The way to achieve the best value yield from a log is to adopt the cutting pattern that produces the highest possible grade of lumber.

To maximize volume yield of a log, the cutting pattern needs to be optimized by using the information about a log's internal defects. The cutting pattern of a log is determined by the set point diameter d_{sp}, as shown in Fig. 2.1 (a). The set point diameter of a log depends on the length l, the top diameter d_t, and the bottom diameter d_b of the log, as expressed by the following relation [LEE91],

$$d_{sp} = d_b - \frac{96(d_b - d_t)}{l}. \qquad (2\text{-}3)$$

The optimal cutting pattern of a log with a d_{sp} equal to 9 inch, for example, is shown in Fig. 2.1 (b).

There are two different log sawing methods, 1) live-sawing, and 2) grade- or around-sawing. Around-sawing is used only in hardwoods. Live-sawing is used mostly in softwoods though studies conducted by academicians suggest that this is the best say to saw up hardwood logs. Live-sawing is a relatively simple one-pass method that produces a parallel cutting pattern. In around-sawing, the log is sawn consecutively on 4 orthogonal faces, in effect boxing-in the log core or pith around which defects are usually found. The purpose of around-sawing is to contain the defects and to extract the most defect-free lumber possible. These two sawing patterns are illustrated in Fig. 2.2.

The most significant limitation in the traditional log sawing is the lack of the ability by the human sawyer to see the location and orientation of grading defects inside the log prior to sawing. Without information about the internal defects, the sawyer has to rely on what is visible on the surface. The only way the sawyer can tell where the internal defects lie is to saw a first cut, also known as the *opening face*. This method for determining internal defect information is piecemeal, and the information is only partial at best. Moreover, by the time the internal defects are revealed by these opening sawcuts, the remainder of the log is already constrained to a particular sawing pattern.

2.3 Value Recovery Improvement

As pointed out in the last section, there are two different strategies in log sawing, volume recovery and value recovery. The first strategy emphasizes on boards that have the most board feet possible, while the second strategy aims to obtain boards having the highest grade possible. Since the 1950s, numerous methods for increasing the volume of lumber produced from log have been studied [CHA89] [HAR91] [HOD90] [KLI88] [STE89]. The research involved evaluating alternative systems that incorporate a knowledge of external indications of log defects and log geometry. The studies revealed that volume yield depends on both the method of sawing and the characteristics of the log. One investigation found that factoring taper and external defects into sawing decision increased red oak lumber yield by as much as 9.4 percent for all logs and by 20.8 percent for grade 2 logs [MAL56].

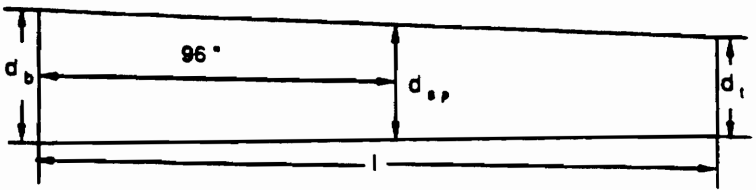

(a) Side view

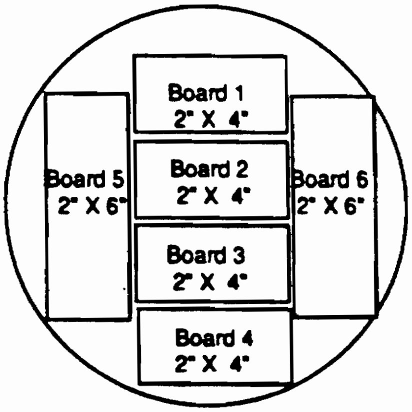

(b) Top view

Fig. 2.1 A 9"-set-diameter log and its cutting pattern

LIVE-SAWING

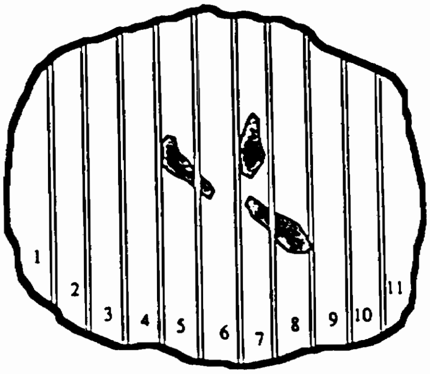

AROUND-SAWING

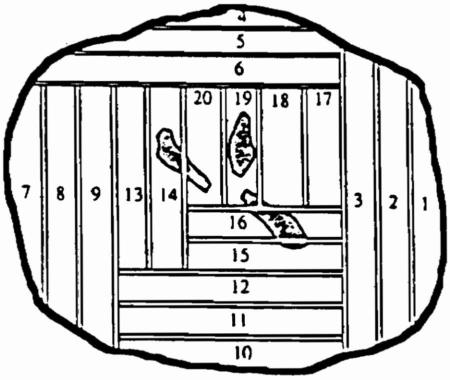

Fig. 2.2 Common log sawing patterns: live sawing (top), and around sawing (bottom)

In studying log value yield, Wagner [WAG89] demonstrated that the average value of lumber sawn from both hardwood and softwood logs may be increased by as much as 7 to 21 percent, by selecting the optimum log orientation and sawing pattern. Furthermore, eliminating operator turning error in a automated sawmill might increase yield by an additional 7 percent [MCM84].

In recent years, much research on hardwood timber processing has been focused on two closely related topics, optimal breakdown strategy and log scanning, while little has been done on analyzing the scanned data to optimize cut-up decisions.

2.3.1 Work on Optimal Breakdown

The maximum log value yield can be achieved by adopting an optimal sawing pattern that produces the highest possible grade of lumber. Instead of blindly sawing a log regardless its shape, its size, its location and orientation of its internal defects, a few efforts are being made to determine the optimal breakdown strategy [OCC89] [STE89]. Most of these efforts to date have involved simulations aimed at determining the economic importance of optimizing breakdown to increase value recovery.

In [STE89], the influence of defect location in hardwood logs on the value of lumber sawn from the logs is studied by simulating log sawing at different orientations. In this study, a value increase of 10.5 and 10.9 percent was achieved respectively with live sawing and around-sawing. There are 5 steps to collect the data required for this computer simulation. These steps are:

1) Log Cross-Cutting. Logs are cross cut into thin disks, and the outlines of the visible defects and the log are digitized by a sonic recorder. The digitized points represent the shape of the defects and log [STE89].

2) Log Reconstruction. These disks are then reassembled to create a "log" complete with all its internal defects. This reconstructed log is stored as a 3-d array in the computer.

3) Computer Sawing. Software is used to "saw" the reconstructed "log" into lumber using the above described live-sawing and around-sawing strategies. Each log is rotated through 360 degrees and sawn at 15-degree intervals, to test a total of 24 (6 for around-sawing) rotational positions per log.

4) Lumber Grading. The boards "sawn" from the log are then graded by a grading program to assign a value yield to each board. The value of a log is calculated as the sum of values of the individual board sawn from it.

5) Assessment. To assess the influence of defect positions on log value, the best and the average log value are computed from a set of all possible log values generated at the 24 (6 for around-sawing) sawing positions. Then the value increase, expressed as the percentage increase of the best value over the average value, is calculated for both sawing patterns.

Another study used a CAD-based graphic simulation of log sawing to create a pattern directed sawing method for hardwood log breakdown [OCC89]. Based on a 3-d input data base of a log obtained by a non-destructive imaging technique, this pattern directed inference approach can determine an optimal breakdown plan specific to each log, thereby eliminating the use of the traditional sawing pattern. The system can be conceptually described by the following 5 modules.

1) Defect Mass Computation Module. A 3-d input data base is used to map the 3-d data to 2-d images. Then boundaries are extracted for the defects and concatenated to form a hull. This hull permits the accumulation of defects to appear in the form of major axes, which are later used in determining a breakdown plan.

2) Configuration Search Module. The hull that is formed by the mass of defects will exhibit a configuration, called defect configuration. This configuration extracts a representation of the amount of information on internal defects (that can be detected by a sawyer from the graphic images of the 3-d data), and has distinctive patterns that will be characterized by the next module.

3) Configuration Characterization Module. This module describes a defect hull in terms of major features, regarding the aggregate location and orientation of internal defects -- the axial dominance of the hull. Major features of a defect hull include the number of axes, the direction and dominance score of each axis, and the minimum bounding rectangles for the defect hull and for the log profile.

4) Plan Prescription Module. The configuration characterization will enable a breakdown planning model to determine an appropriate breakdown plan specific to the defect patterns present in the log. In a study performed on a graphic sawing simulator for hardwood logs, it was shown that higher grades of lumber were consistently obtained by this pattern directed sawing approach [OCC88].

2.3.2 Work on Log Scanning

While attempts described above are being made to improve sawing patterns, during the last 10 years some computer controlled sawing systems have been introduced into sawmills. Generally, these systems analyze data and attempt to determine external log shape based on information from a set of light beams and photo-sensors or from a close-circuit video camera. Because these systems measure the log shape more accurately than a human operator, to some extent they are able to improve the volume yield of the log. These systems, however, do not address optimizing the value yield of the log.

Other log inspection methods have been tested in order to measure log shape. These include using microwave [MAR87], laser [KIN79], ultrasound [BIR91], and optical scanners [LEE91]. For example, an optical scanner is used in [LEE91] to obtain a set of log profile data, and a parametric paraboloid model is fitted for knots. Based on this mathematical model, a recognition method is developed to predict information on the location, shape, size, and orientation of the internal knots. This information is then used to in the knot-related grading rules so that an optimal log cutting pattern can be designed. In the experiment performed using 10 test logs, this system improved the value recovery by 7.5 percent.

Despite the experimental success of the above scanning methods, however, a common drawback with them is that they can only scan the log to obtain a set of 1-dimensional (1-d) data, which needs to be interpreted in an effort to infer information on internal defects. In fact, this inference process is an ill-posed problem, i.e., recovering the complete 2-dimensional (2-d) information from partially observed 1-d data. These scanning methods have some crucial limitations, i.e., they can not obtain a complete picture of the log by "seeing" into it.

Recent efforts to improve value recovery from sawlogs have used new technologies to obtain 3-dimensional (3-d) information about internal log defects. Of the various methods for doing internal log scanning, the two methods that seemingly have the greatest promise are computed tomography (CT) and nuclear magnetic resonance (NMR) which is commonly called magnetic resonance imaging (MRI).

A study using a CT imaging system was conducted in 1984 [TAY84]. In this study, it was noted that water present in green logs and the small disparity in density between knots and the surrounding wood tissue make it difficult to detect knots. Moreover, the expensive medical CT units used in the study did not meet the requirements for lumber production speeds at sawmills. Although cost has been a problem in terms of the economic viability of CT scanners in sawmills, perhaps the most serious technical difficulty is speed. Since a processing rate of 0.5 log per minute is not uncommon in many sawmills, little time is available in which to acquire and analyze an extremely large amount of CT image data. The amount of data generated presents a major problem for the computer and the human operator alike.

Recently, more rapid scanning has been made possible by a scanning electron beam CT scanner developed by Imatron, Inc. [WAG89]. In its ultra fast mode, the Imatron CT scanner acquires a pair of contiguous slices at the rate of 34 images per second. Compared with the rate of about 1 slice per second of the third and fourth generation CT units, this speed improvement is very significant. It demonstrates the technical possibility of developing a commercial CT scanning system for hardwood log inspection.

At about the same time CT imaging systems became commercially available, scientists were developing the MRI technology. Shortly before MRI became commercially available in 1984, early studies using MRI for wood scanning began. MRI medical scanners have been used to scan both white oak and black cherry for internal defects. Good quality images were obtained and these images seemingly permit identification of sapwood, heartwood, the growth rings, knots, wet wood, reaction wood, rays, pith, and gum spots [WAN89]. However, this study did not address such important issues as fast scanning, capability for automatic image analysis, and economic viability.

2.3.3 Work on Data Analysis

An initial study of CT's feasibility for sawmill use evaluated this technology's knot detection capabilities [TAY84]. Comparing CT images with knots visible on the cross-sawn log sections indicated that CT provides an effective means for locating knots, this study did not develop any image analysis method for image data interpretation.

A more complete evaluation of CT's usefulness for identifying defects was reported in [FUN85] which involved development of automated image analysis methods. CT-scans were taken with a Siemens Somatron DR2 medical scanner. To identify different regions on each individual CT slice, three features are derived from these images and used in the recognition process. These three features are: 1) pixel density, 2) object shape, and 3) growth ring texture patterns. In its decision-making stage, the vision system discerns knots by pixel density and 2-d shape, clear wood by the circular patterns of the growth rings, rot by density and growth ring patterns, and background (air) by density. This system can successfully identify knots, rot, holes, and clear wood in CT-scans of sawlogs.

The work in [FUN85] represents the first attempt to automatically infer wood internal structure by analyzing the scanned log data. Not surprisingly this study has several limitations. First, it was not tested on defects other than those reported, e.g., decay, bark, and compression wood. Second, the methods were tested only on images of log samples from 3 softwood species. Hence the species-independence of the system has on hardwoods has not been established. Third, no attempt was made to deal with the possible "noise" problem inherent in imaging. For example, the unwanted annual rings in log images, if not eliminated at an early stage, will misguide the identification task. Furthermore, since annual rings are present in most part of a log image, processing them will significantly slow down the speed of the overall system. Fourth, its identification was not based on sufficient information. Image features presented in the 3-d image, such as topological relation between defects and 3-d geometric and volumetric properties, were not utilized.

Up till now, there exists no general method for automatically analyzing and interpreting log CT images. However, a number of researchers have reported progress toward developing machine vision systems for surfaced lumber and rough lumber inspection [CON83] [KOI89] [CHO90]. A common feature of these vision systems is that they combine sufficient information and a reasoning process in decision making, using either texture pattern related measures [CON83], decision tree [KOI89], or knowledge-based system [CHO91]. The successful applications of machine vision systems to lumber quality inspection indicates that they might also be adopted to the log inspection problem if appropriate imaging method is used.

2.4 Available Scanning Technologies: A Critical View

To optimize sawing decisions to maximize value recovery, there is a need for an automated, real-time evaluation of log dimensions and quality. Recent progress in computer technology and electro-mechanical design has increased the use of automation in the mechanical conversion of wood. While substantial progress has been made in automated measurement of wood dimensions, little has been done to address the accurate automated inspection for determining log quality.

Technology has developed to the point that wood defects can indeed be "seen" in the interior of logs using non-destructive imaging techniques. Most recently, log scanning using more sophisticated methods such as magnetic resonance image (MRI), and x-ray computerized tomography (CT) *imaging* have been studied in laboratory experiments, and they ability to differentiate some internal defects on logs has been in part demonstrated [CHA91] [WAG89] [KLI90]. This dissertation only discusses the technologies available for *log* inspection. [SZY81] provides an excellent, comprehensive review on the potential applications and limitations of several *lumber* inspection technologies, including optical method [KIN79] [LEE91], ultrasonic method [BIR91], microwave method [MAR87], x-ray method [MUL84], and neutron method [SZY81]. A scanning method that used the color information of wood defects for rough lumber inspection was reported in [CHO91].

As pointed out in sections 2.1 and 2.2, current log grading and sawing methods are limited by the invisibility of log internal defects. All the recent developments in overcoming this crucial limitation of invisibility are only made possible by the advances in the use of non-destructive imaging technologies, such as the X-ray computed tomography (CT), ultrasonic computed tomography, and magnetic resonance imaging (MRI) [KAK88]

[FUN85] [WAG89] [CHA91] [ZHU92a]. Of these three imaging modalities, ultrasound is basically used to differentiate fluid from solid tissue, CT and MRI have greater potential for industrial application because of their high penetrating power. Since CT and MRI are the two major imaging modalities that have been the most tested for possible application to log inspection, the following discussion will be confined to comparing CT and MRI for log inspection.

CT units became commercially available in the early 1970's while MRI units which were not available until 1984. MRI has a number of disadvantages that make it inferior to CT when applied to log inspection. First, MRI imaging is based on the distribution of hydrogen in the water within an object. Hence the significant moisture variation between heartwood and sapwood generates inconsistent MRI images. It has been shown that bark, and sapwood in some cases, can not be captured by MRI due to the small amount of moisture they contain [WAN89]. This situation is alleviated to a large extend with CT, because CT imaging is based on the concept of line integration which is not so directly related to the moisture distribution within an object.

Second, CT appears to be the preferred method because it seemingly can handle the log flow rate in high-volume commercial sawmills. Recent studies of hardwood logs using ultra-fast x-ray CT scanning [WAG89] have stimulated a major Australian hardwood company to evaluate the economic impact of CT technology on processing large volumes of hardwood logs [DAV92]. With the fifth generation (most advanced) CT scanner [WAG89], a scanning speed of 34 images per second is reported. That is a significant improvement in speed over more conventional CT scanners which can image only 1 slice per second. At the same time CT image reconstruction methods have also been progressing because of the rapid development that has taken place in microelectronics technology. At present, CT images can be reconstructed at the rate of at least 2 images per second. However, the data acquisition speed of a MRI scanner has, so far, not reached 1 image per second [CHA89].

Third, MRI units are far more expensive than CT units because they require the expensive superconducting magnet. The price of a medical MRI unit ranges from $750,000 to $2,000,000 [CHA91], while medical CT units range from $96,000 to $120,000 apiece [HER78]. As a matured technology, CT has the greatest potential for further price reduction, since many of the niceties found in today's medical CT units have no relevance to industrial inspection applications. These unneeded features can be eliminated in industrial applications, thus reducing the cost of CT units. For example, a special industrial CT unit for wood inspection can be built at a cost of about $4,000 [SHA88], although the speed of this unit is very slow. This great disparity in cost between CT and MRI should attract potential sawmillers to use CT as the major imaging device for automated sawmilling.

Fourth, MRI units are seemingly less "safe" than CT units when operated in a sawmill or a veneer plant. The X-ray tube of a CT scanner generates X-ray radiation that is hazardous to the human operator. However, this hazard can be easily prevented by lead shielding the scanning gantry of a CT scanner as has long been done in the many hospitals. The magnetic field required by MRI units can pull any magnetic material (such as nails) out of saw logs and veneer logs as they are being imaged. If this happens serious damage to the superconducting magnet would most certainly result. Furthermore, the magnetic field induced around the outside of the magnet is also very intense. Care must be taken not to get any iron or steel tools close to a MRI unit, or they would be drawn toward the superconducting magnet causing damages to the imaging unit and possibly to the human operator. Whereas CT does not pose such safety problems.

Given the above arguments about CT and MRI, it can be concluded that CT could be technically and economically more applicable than MRI to the log inspection application. It was for these reasons that the CT imaging technique was chosen for the data acquisition component of the proposed vision system that is to be discussed in this dissertation.

2.5 Principles of CT Imaging

The mathematical basis of computed tomography is usually attributed to Radon (1917) [HRE78], who established that a complete set of projection data of some relevant physical variables of an object could be used to reconstruct a cross-sectional **image** of that object. One type of projection is produced by the differential attenuation of radiation passing through the object. Projections are described mathematically through the Radon transform, and the process of image reconstruction from these projections is known as the inverse Radon transform. The inverse Radon transform was first used to reconstruct image from projections by Bracewell in 1956 [HER78] [KAK88].

However, it was not until the work of the joint Nobel Price winners in medicine, Geoffrey Hounsfield and Alan Cormack, that computed tomography, as we know it today, was implemented. In 1972, Hounsfield, an engineer at EMI, built the first CT scanner as a medical diagnosis tool for examining human heads. More recently, this technique has been used in other non-medical environments such as testing of concrete, steel, wood, paper rolls, and the mapping of underground resources via cross-borehole imaging.

To illustrate the basics of CT, consider a homogeneous object and a narrow incident beam of x-rays. Let the incident x-ray intensity be I_o, and the transmitted intensity in the same direction as the incident beam is I, then the attenuation of the beam is described by

$$I = I_o \exp(-\mu t) \tag{2-4}$$

where t is the object thickness traversed by the beam, and μ is the linear attenuation coefficient, which is dependent on the x-ray energy, the electron density, and the material composing the object. Note that a mono-energy x-ray source is assumed throughout this discussion, unless otherwise stated.

Since most objects will be nonhomogeneous, the above equation needs to be changed into the following form

$$I = I_o \exp\left(- \int_0^t \mu(x)\, dx \right) \tag{2-5}$$

which is a line integration of the attenuation coefficient u(x) of the object along the line's direction. This equation can be linearized by taking the natural logarithms of both sides giving

$$\ln(I_o/I) = \int_0^t \mu(x)\, dx \tag{2-6}$$

The line integral (ray sum) is the Radon transform of $\mu(x)$ discussed above. If enough projections are obtained in different directions, an approximate 2-d image or "slice" can be obtained using a reconstruction method. There are three fundamental reconstruction methods, summation, Fourier transform, and convolution.

1) Summation: The summation method is the simplest one. It distributes every ray sum over the image cells along the ray. Where there are N cells, increment each such cell by a number equal to the ray sum divided by the total number of directions used. This step is called back projection. Repeating this process for every ray results in an approximate version of the original image [KUH63].

2) Fourier Transform: Another way of reconstructing the original image is to use the Fourier transform (or some other orthogonal transforms) of the projections to define points in the Fourier or transform space. The undefined points of the transform are interpolated from known points. Finally the inverse transform is taken to obtain the reconstructed image.

3) Convolution: The convolution method is the natural extension of the summation method. Since the summation technique is equivalent to blurring (degrading) the image by convolving it with a certain point-spread function, one can remove the degradation by a deconvolution. The straightforward way to accomplish this is take the Fourier transform of the degraded image, multiply this result with an estimate of the transform function in frequency domain, and then take the inverse Fourier transform to obtain the reconstructed result. However, since all the operations are linear, a faster approach is to deconvolve the projections before performing the back projection. Owing to its speed and the fact that deconvolutions can be performed while the data are

being acquired, this fast convolution approach is the method employed in most CT imaging systems.

CT scanning generates a sequence of CT images, also referred to as CT tomographs, CT-scans, or CT slices. Each pixel (picture element) in the CT image has a gray level called CT number ranging from -1024 to 1024 (11-bit data) where water has a CT number of 0, or from 0 to 2047 by a gray level transform where water has a CT number of 1024. Since X-ray attenuation depends on the density of the material, the CT number is a density measurement. A detailed description of the mathematical and physical concepts of CT can be found in [HER78] [KAK88].

2.6 Machine Vision for Industrial Automation

Vision is a biological perceptual task that bas been the subject of much study and interest. Early vision research in this century was carried out mostly by investigators in the field of psychology. Some of the main results of these studies are the Gestalt principles of organization (1912-1935), the theory of space perception (1950) , and ecological approach (1979). With the increasing use of digital computers during the last two decades, vision has also become a subject of study in Computer Science and Engineering. *Machine vision* is the study of applying human vision principles to solve such problems as automated inspection and robot vision with the aid of some imaging mechanism. More recently, *machine vision* has been widely applied to such fields as web inspection, PCB inspection, log inspection, and etc. It is hoped that this combined effort will bring additional insight into the vision problem and its associated industrial applications.

Machine vision systems typically start with a digital *image*. A digital image is an array of picture elements (henceforth denoted as *pixels)*, whose values represent visual sensory information obtained from a video camera or other such imaging device, and digitized to a certain number of quantization levels. The task of the vision systems is to identify and describe the nature of the real world objects that give rise to the digital image. The extent and exact nature of that description depends, of course, on the goals and expectations of the observer. This task has proved to be , in general, an extremely complex one.

There are normally two levels of information processing in machine vision: low-level vision and high-level vision, or image *segmentation,* and image *interpretation* or *understanding*. The task of image segmentation is to separate the part(s) of interest (*objects*) from the rest of the image, while image interpretation is to identify or label the objects in the image. To deal with the various uncertainty factors that actually arise during interpretation, new methods such as *fuzzy logic* and *uncertainty reasoning* have been applied to vision research and have proven to be very useful.

2.6.1 Image Segmentation

In many respects, the low-level portion of a vision system is designed to mimic the early stages of visual image processing in humans. In these early stages, it is believed that scenes are partitioned to some extent into *regions* that are homogeneous with respect to some set of perceivable features (i.e., feature vector) in the scene [BAL82]. Objects of interest in an image can be segmented from the rest of the image by several methods. The most commonly used method in industrial vision applications is the so called *thresholding* method. In this method, object features such as gray level or texture are thresholded against a preset value. Pixels or groups of pixels that have a feature value within the preset range will be assigned a *label*, those that have a feature value outside this range will be assigned other different labels. Thus, the original image is divided into regions, each with a distinct label. Next, properties of each region of the segmented image are computed and stored to be passed on to the high-level vision module. These properties are called knowledge sources in *expert systems*. However, the identity of each such region at this stage of processing is still unknown. In general, low-level vision tasks are regarded as a transformation from a lower to a higher level of representation for image information.

2.6.2 Advanced Image Interpretation

When the segmented image together with its extracted properties are forwarded to the high-level image interpretation module, domain-specific knowledge and reasoning are used to correctly infer the identity of as many objects as possible in the image.

It is clear that no segmentation is perfect. There will be regions that overlap semantically distinct visual entities. Or there might be regions that are oversegmented, i.e., multiple regions that partition a single semantic entity. These anomalies are due, in part, to several unavoidable realities of the visual domain. Imaging machinery such as CT scanners will simultaneously lose meaningful information and introduce bogus information, e.g., noise or distortion. Thus, the data from which a segmentation must be produced are an imperfect abstraction of the scene a system is expected to understand. Also, semantic information about objects in a scene cannot be contained entirely in the image data. As a consequence, some regions will partition a single visual entity. Still other regions may enclose multiple semantically distinct visual entities.

During the last decade, expert systems have found great use in the field of machine vision [NAG80] [BAR88] [CHO91]. In expert systems, knowledge sources extract image feature information from a subset of regions in a segmented image, feature information that can include spectral, texture, shape, and spatial attributes of regions. Based on their perceptions, knowledge sources form opinions about the presence or absence of features they are capable of observing. It logically follows that beliefs based on these opinions will be imperfect. At best, such opinions can be viewed as only *evidence* to suggest the presence or absence of semantically meaningful entities in a particular scene of interest.

To represent the inexactness in expert systems, *fuzzy logic* and *inexact reasoning* methods have been studied [ZAD65]. It has been found that a pure probabilistic-based approach to reasoning in complex domains is overly restrictive. As a consequence, pure probabilistic approaches are typically compromised by making *ad hoc* modifications to Bayes' rule [GOR85]. The Dempster-Shafer theory [DEM67] [SHA76], on the other hand, has recently been applied to uncertainty reasoning in knowledge-based machine vision systems [CHO91] [HEN88] with impressive results. In principle, it is a formal and uniform representation of ignorance, and it can distinguish disbelief from belief. The benefit of employing such techniques is that the vision system is able to correctly label a significantly greater number of regions in an image, by using previously unavailable information such as the amount of ignorance or ambiguity that a label (classification) hypothesis exhibits. In the context of industrial machine vision systems applications, this means that using this advanced reasoning method will bring about much more accurate inspection or detection.

2.7 Summary

Sawmillers have long looked into the problem of detecting the invisible defects in logs prior to primary breakdown. Previous scientific studies have demonstrated a 7 to 21 percent improvement in log value recovery when defect knowledge is incorporated into cutup decisions. As a preferred and matured technology, CT can be used for log scanning at relatively affordable cost. It is concluded that log scanning has come to the point where a general image analysis methodology, such as the machine vision approach, needs to be developed. Combining this methodology with existing grading and sawing methods will help realize the potential of increasing value yield from logs.

Chapter 3
Wood Characterization by CT

The digital CT imagery of a log encodes much information about the log's internal characteristics. This information is manifested primarily through spatial intensity (CT-number) variations which correspond to variation in some physiological, physical or chemical characteristics of defects, such as the high density of knots and the directional textures of annual rings, and etc. Our ability to decode these intensity variations and to produce a correct interpretation of the CT imagery depends critically upon our understanding of wood anatomy and our ability to devise intelligent methods for image processing and analysis.

This chapter introduces the basic anatomy of hardwoods. It describes the important internal defects of hardwood logs and describes these defects' physiological and physical characteristics in terms of density, textural structure, and relational positions. A number of experiments on wood characterization using CT imaging are described. They establish the fact that most wood defects manifest themselves in the CT imagery and thus lend themselves to be easily detected using a CT-powered machine vision system.

3.1 Basic Wood Anatomy

3.1.1 Tree Structure

Chemically, wood cell walls consist of three components, all three of which affect wood's characteristics as a structural material [WIL91]. Two of these components, ***cellulose*** and ***hemicellulose***, are carbohydrates, formed by linking sugar molecules end to end. Cellulose is the most important because it supplies most of wood's strength. The other carbohydrate component is hemicellulose (sugar molecules). The main function of hemicellulose is as a matrix substance, supporting the skeletal framework of cellulose microfibrils. The third major cell wall component is *lignin* which is a very large, amorphous molecule whose chemical structure we do not completely know. Lignin is generated after the cell wall is fully formed and acts to encrust the cellulose microfibril framework. The function of lignin is to surround and stiffen the microfibrils, holding them together and making them rigid. Lignin is what makes wood "woody", i.e., hard and brittle as opposed to soft and mushy. According to [BRO63], wood is composed of 30 - 50 % cellulose, 15 - 35 % hemicellulose, and 15 -`30 % lignin. The impact of these wood constituents on wood density is analyzed in section 2 of this chapter.

Wood also contains small quantities (0.2 - 1.0 % of dry weight) of extraneous materials, called *extractives*. These are chemicals not directly involved in determining the strength of wood that are formed primarily at the transition from sapwood to heartwood. Although they play little role in strength, they are totally responsible for many of wood's other properties, such as color, odor, taste, decay resistance, shrinking, swelling, and permeability, and density.

Wood in the tree trunk (1) supports the branch and leaf structure, (2) conducts water solutions (sap) to the crown, and (3) stores the carbohydrates, that are synthesized in leaves and flow as dissolved sugars down in the inner bark to migrate from the bark into the wood. These three functions determine wood's essential functions. For the purpose of designing an automated vision system for log inspection, our discussion on wood structure will be limited to the following major wood features that are directly related to grading defect recognition. A complete treatment of wood anatomy and chemistry can be found in [KOL68] [WEG84] [WIL91].

Heartwood and sapwood: Cross-sections of tree trunks typically show *bark*, a pale zone of *sapwood* surrounding *heartwood*, and the *pith* dot in the center (Fig. 3.1). A trunk's main parts are sapwood and heartwood. In young trees all wood is sapwood. As the years pass on, some sapwood becomes heartwood, the transition starting near the pith and progressively seizing rings farther out. New sapwood continues to grow in the cambia zone so that the sapwood zone continues to retain its same approximate width. Wood in the transition line, in most species, ceases to conduct sap and gives up its food reserves for good. Heartwood is defined as wood that no longer participates in the life processes of the tree.

The transition involves death of the last surviving parenchyma cells; the detectable criterion of heartwood is absence of living cells. This detectable criterion of heartwood can be transformed into other equivalent criteria depending on the detection methods used. For instance, in x-ray CT imaging of logs, the pixel values of the heartwood portion of a tree are generally greater than those of the sapwood, since some heartwood deposits remaining in cell cavities are higher-density oils that repel water and some are minerals that are hard enough to dull cutting tools. These oils, also called fat acids or extractives, are chemically described as Terpinene ($C_{10}H_{16}$), an organic compound that has a density (0.845 g/cc [LID90]). This density value is higher than that of sapwood (see sub-section 3.2.3).

Other deposits infiltrate cell walls in the hardwood and may influence strength and moisture content slightly. These deposits reach substantial proportions, on the order of 10 to 20%, only in a few species, such as redwood and black locust. In these species, heartwood is slightly stronger and less hygroscopic than sapwood, and shrinking and swelling may be substantially reduced [WIL91]. Other species, however, accumulate tannins, oils, and other heartwood deposits, which are either formed along the transition line or pass in from young sapwood and may originate in the leaves. Generally heartwood is dark-colored, since many deposits are of particular color, e.g., red-tinged brown in red oak, red in rosewood, and nearly black in ebony. The linear attenuation coefficient is very sensitive to deposits in heartwood since these deposits can markedly affect material density. As will be seen this makes CT imaging a very effective tool for separating heartwood from sapwood.

Knots: knots are the basis of limbs embedded in the tree trunk that are revealed when cutting the stem during manufacture. As the trunk increases in diameter, trunk wood gradually encompasses the wood base of a branch and makes it a knot. In general, knots devalue wood. They are not tolerated in furniture. They render sawing, planing, gluing, and finishing difficult. They also can cause drying checks and warp. They deprive lumber of strength, and restrict the use of many pieces. As such knots are grading defects and are by far the most prevalent grading defect in timber, lumber, plywood, and other wood products. The fact that each knot is a portion of a branch explains the essential knot characteristics. In particular, knots have a number of unique features that make them easy to detect in CT imagery and other imagery as well.

In a tree almost all branches originate at the stem's very tip, which later becomes the trunk pith. Hence practically all knots extend to the pith (Fig. 3.2). Closely related is the

Fig. 3.1 Sample image RK05.41 with defects

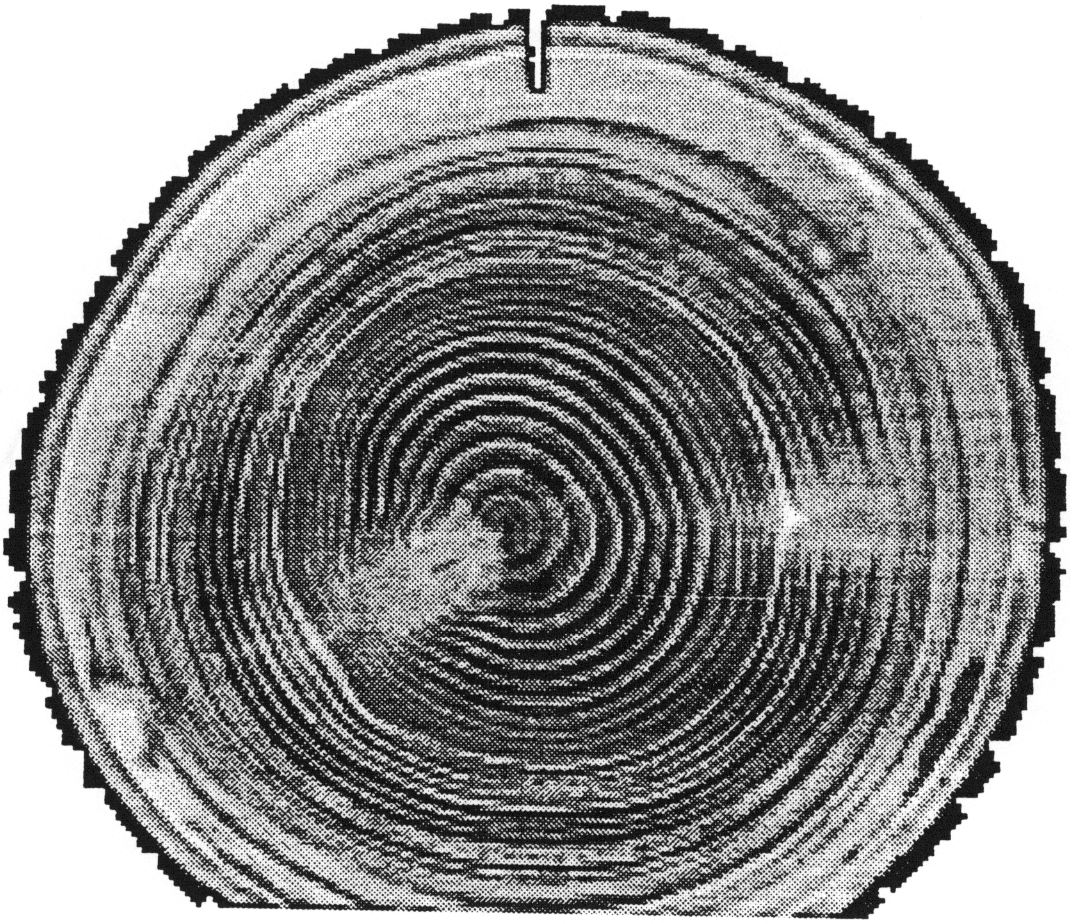

Fig. 3.2 Sample image YP06.25 with knots pointing to the pith

fact that branches grow radially or in the radial-longitudinal plane out of the stem. Therefore, the radial section of edge-grained lumber exposes branches as elongated *spike* knots, whereas the tangential surface of flat-grained lumber lies perpendicular to horizontal branches and has *round* knots. Knots from steep branches at tangential surfaces, and all knots at intermediate surfaces are between the round and the spike type - i.e., they are *oval.*

In addition, branches grow in thickness except in the trunk; therefore, knots diameters increase with the distance from the pith. Knots resemble cones whose tips point to the pith (Fig. 3.2). In chapter 6 of this dissertation, these features of knots are encoded into an efficient knot recognition procedure that is based on the uncertainty reasoning theory [DEM67] [SHA76]. Growth increments of the trunk and of live limbs interlace with each other without forming a line of demarcation; knots of live branches are *intergrown.* At dead limbs the wood formed in the tree trunk makes no further connection with the limb but grows around it, causing an *encased*, loose knot that tends to fall our of lumber.

In branches the fibers run parallel to the axis of the branch as needed for branch strength; hence the direction of knot fibers is entirely different from that of the fibers in the trunk. Furthermore, branches need more strength than the trunk. This is not only because of winds, but also because branches must support their own weight, together with the weight of any rain, snow, and ice that clings to them. The knots are correspondingly *dense* and *hard*, a fact that further contributes to their causing drying defects such as dry checks and warp. These facts have been incorporated into the wood defect recognition procedure of the automated log inspection system discussed later in this dissertation [ZHU91d] [ZHU93].

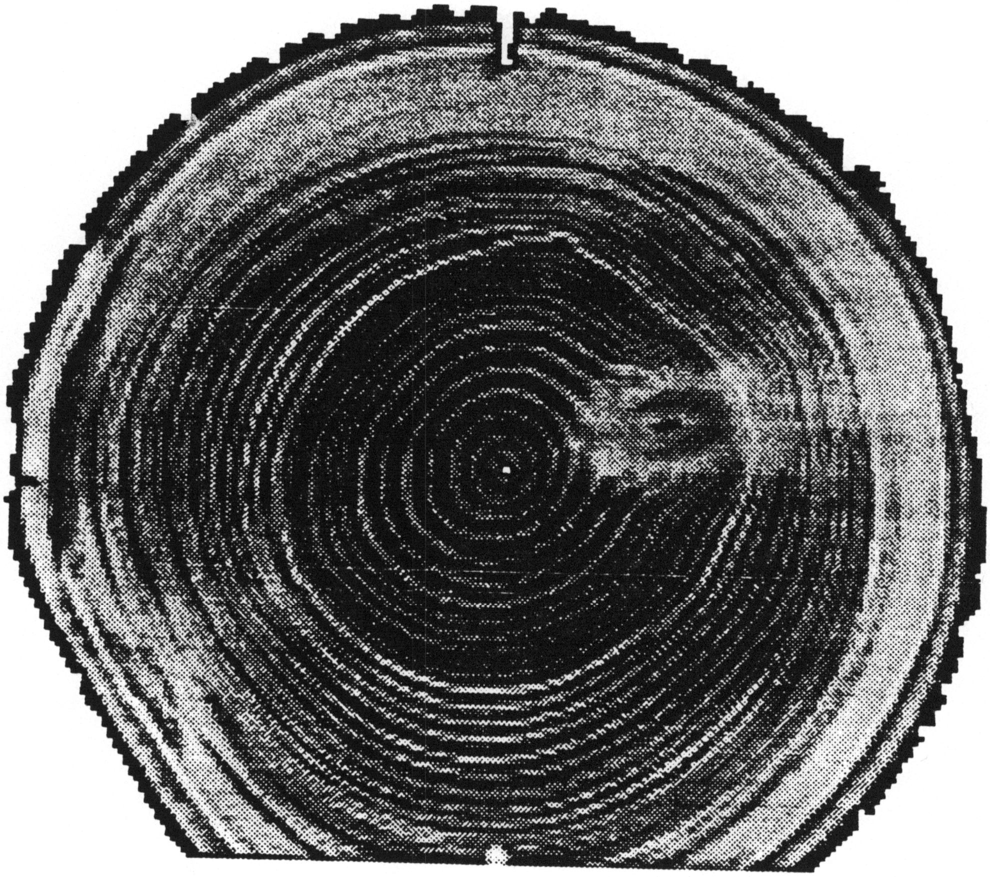

Fig. 3.3 Sample image YP04.09 with pith and reaction wood

Wood Splitting: Wood is distinctly anisotropic, meaning that its properties vary depending on direction. The anisotropy shows spectacularly in *splitting*, when fibers separate along their directional orientation. Splitting requires less energy than any other method of wood disintegration. Wood splits when it is nailed and screwed, during planing and in veneer cutting. It splits most easily in the plane of ray bands of thin-walled parenchyma cells. Low-density woods tend to split less because their air space and thin cell walls accommodate nails and similar objects without forcing the tissue apart.

Tree Growth and Annual Rings: Tree grows lengthwise and in thickness. Growth in length is restricted to the tips of stems, branches, and roots. The tissue formed at the tips appears as *pith,* the small soft core occurring near the center of a tree trunk, branch, or root. In many species the pith is too small to be visible with the unaided eye; in others it can be seen at the central lateral surface as a fine dark line or narrow band, and at the transverse surface as a dot (Fig. 3.3). Pith downgrades lumber and, hence, is a grading defect.

Wood cells consist of cell walls and empty cell cavities. In many tree species the *wall-to-cavity ratio* changes during the growing season. First-formed earlywood or springwood has relatively thin walls and large cavities and is more porous than *latewood* or *summerwood.* In cross sections of logs, earlywood and latewood appear as circular growth layers known as *annual rings.*

Annual rings together with wood rays and knots give surfaces a particular *figure*, a figure that is useful for wood defect detection [ZHU93]. In ring-porous hardwoods - such as most oaks, elm, ash, and hickory - earlywood vessels are many times wider than latewood vessels and form distinct rings or narrow bands. By contrast, in the diffuse-porous species - maple, yellow poplar, and others - the vessels are of uniform size throughout the annual ring, the ring being marked only by narrow line of thick-walled fibers and/or parenchyma cells at the very edge.

Density Variation within Trees: Organic tissue generally changes with the age of the growing organism. It is of interest to know whether similar differences also exist in trees, particularly whether wood properties depend on the age at which the wood grew. The question has significance, since the curvature and width of annual rings show the approximate age of each species. Actually, properties of clear wood do differ within the tree. Some of the variations follow regular patterns.

In many trees, especially softwoods, the wood of the first 5 to 25 annual rings around the pith is *juvenile*, that is, relatively light, having short thin-walled fibers, with the cellulose microrfibrils lying at a large angle from the fiber axis, and containing less cellulose than the mature wood of later annual rings. The properties of juvenile wood change progressively with increasing distance from the pith until they reach the fairly uniform level of mature wood. Many tree species have juvenile wood, no matter how fast they grow. In some species the juvenile wood may lack one or more of its four basic characteristics - low density, short fibers, flat microfibril angle, and little cellulose - but each of the four characteristics has the same effect: they cause juvenile wood to be structurally weak. In addition, because of the flat microfibril angle, coniferous juvenile wood tends to shrink excessively in the fiber direction and contributes to the warp during lumber drying.

Mature wood also varies with distance from the pith, but much less than does juvenile wood. The changes do not follow a simple pattern, but two major groups of species show some regularity. Since annual growth tends to diminish as trees grow old, wood formed late in the life of ring-porous hardwood is relatively light. Conversely, in most sunlight-demanding conifers, density may peak in the growth increments of mature trees.

The width of each annual ring sheath also depends on the height of the tree. The rings are narrow near the base of the trunk and become wider toward the crown, reaching a maximum in the vicinity of the crown base, narrowing again toward the top. This growth pattern causes the stem to be cone-shaped (tapered) in the crown area and nearly cylindrical in the trunk below the crown. Because of the influence of height, new wood in ring-porous hardwoods is relatively dense at the base of the crown, whereas in sunlight-demanding softwood it is frequently relative light.

Reaction Wood: Many of the undesired variations within trees result from changes in the environment. Drastic changes lead to formation of *reaction wood* tissue, which is a major cause of warp in lumber. Trees always grow upward no matter how one bends them. Reaction wood is wood that *re-orients* the tree into more favorable positions. As an abnormal tissue, reaction wood occurs in stem wit bents. It also appears in straight stems that in a repeatedly changing environment bend for one period to one side, then for another period to the other side, remaining fairly straight all the time.

Reaction wood appears as *compression wood* in coniferous and as *tension wood* in broad-leaved trees. Forming on the upper side of leaning trees, tension wood develops as a reaction to lean or wind forces in the radial direction. The stress in tension wood is due to fibers attempting to contract longitudinally during maturization, while older wood restrains this contraction. Correspondingly, it can be assumed that compression wood attempts to expend in the fiber direction when lignin forces cell-wall components apart; compression wood indeed contains much more lignin than normal wood.

The most prominent features of reaction wood are their color and density. In the photograph of a log cross-section, the lignin-rich compression wood appears darker than normal wood; in reality it looks reddish. Compression wood features relatively large proportions of latewood and frequently lacks the demarcation between earlywood and latewood. Tension wood appears less conspicuous; being rich in cellulose, the constituent that provides tensile strength, it is generally relatively light in color and has a sort of sheen. Reaction wood exceeds normal wood in density and in strength, as might be expected from its function in the tree, but curiously enough it is not as strong as normal wood of the same density, despite being more dense (compacted). In the CT image of a log, reaction wood appears brighter than normal wood due to its higher density (Fig. 3.3).

In summary, trees exhibit a variety of properties and wood defects exhibit their own particular features, such as color, odor, taste, shape, size, density, and relational geometry. CT imaging of logs, however, can only utilize a sub-set of these features in automatically detecting and identifying the internal defects in them, due to its intrinsic limitations. The question now is how to devise such an automated system based on the limited sub-set of wood features, so that it can meet the forest industrial requirements on defect inspection.

3.1.2 Descriptions of Hardwood Lumber Grading Defects

From the point of view of economics, a defect in wood is any feature that lowers its value on the market. It may be an abnormality that decreases the strength of the wood or a characteristic that limits its use for a particular purpose. However, what is judged to be definitely unsuitable for one application may prove to be ideal for a different use.

Many so called defects are not abnormalities in a strict sense, but are simply the product of natural growth. Variations from the normal form of a tree trunk, knots, and reaction wood are natural defects whose formation man can control only within certain limits. Closely allied to these, but directly attributable to environmental factors of wind, heavy snow, severe cold, heat or lightning, are other natural defects which are called environment- or site-related defects. Examples of site-related defects include insects and fungi which can attack living trees, logs, lumber or processed wood products. The following is a brief description of the characteristics of some most commonly occurring defects in hardwood logs [KOL68]:

Knots: Knots are the principal grading defect. A knot has a higher density than the wood around it. Although a knot may have many different shapes from different angles, it appears mostly round or elliptical in a 2-d plane, and ellipsoidal in the 3-d space.

Tension Wood: Tension wood is a hardwood reaction wood which is named for woody tissues produced in certain parts of leaning trees. Its presence can be indicated by eccentric growth and wider rings.

Holes: Holes are caused by a variety of factors, such as wood-boring insects, rotted-wood, or an external mechanical wound. Normally holes appear as round or oval shape in 2-d plane, and as cylinder in the 3-d space. Their density is much lower than that of wood, and in some cases is very close that of air since the holes typically contain at least some air.

Splits (*Cracks*): A split or crack is a lengthwise separation of the wood, due to the tearing apart of wood cells. Splits or cracks are formed across the growth rings of the wood as frost injuries (in cold areas), or as frost rings following the general pattern of the growth rings, or as damages caused by excessive drying. Their presence can be characterized by darker, straight, long, and narrow areas which are close to the heart of log and point in the radial direction. They are one of the less important natural defects which arise while trees are growing.

Bark: Bark is not categorized as grading defect. Covering the tree, it is the outmost layer of wood material in the tree. Its density varies greatly with different wood species and with individual samples of the same species. Densities higher and lower than that of wood have been observed with red oak logs used in this study.

Bark Pockets: Bark pockets are patches of bark that are included in the wood, grown over after some damage to the tree has occurred. They appear most commonly near knots or holes. They are of unknown origin in some cases, but traceable to insects or birds in others. Their density is normally lower than that of the clear wood and comparable to that of bark in some cases. A bark pocket is a grading defect.

Mineral Streak : Mineral streak frequently appears across the growth rings in trees damaged by bird peck and other openings into the tree. Because of its prominent color mineral streak markedly degrades the appearance of hardwood lumber and thus is a grading defect. This environment- or site-related defect is reportedly due to something boring into the tree and causing a chemical action, or a concentration of minerals. This concentration of minerals may increase the density of mineral steak due to their high-density chemical compound (see section 3.2) and causes the marked discoloration in lumber sawn from the tree. Mineral streak has various shapes, and can appear at different locations in the tree.

Stain: Stain is a biological deterioration of wood and is caused by the staining fungi that might inhabit a tree. Due to the chemical nature of the fungi, they cause mild discoloration or staining of the wood. As the initial evidence of decay, it is formed when the fungi in the tree "eat up" the chemicals stored inside the cell walls of the tree (deriving their nourishment from the wood holocellulose) without destroying the walls themselves. Hence, stain is still solid wood with different color than normal wood. Depending on the stage of growth, stain may appear in various shapes at various locations in the tree. Despite darker color, its density is close to that of the clear wood. Stain is a grading defect.

Decay: Decay, also called *rot*, is caused by the decaying fungi in the tree that "eat up" the cell walls and decompose the wood substance. It tends to disrupt the wood growth ring pattern, and has a density lower than wood and yet not quite as low as that of a check. Two common rots are white-rotted wood and brown-rotted wood. The former has a white and bleached appearance, while the latter is reddish-brown. Like stain, decay has varying shape in the tree. Decay (rot) is a scalable defect because it lower the volume of lumber.

3.2 X-ray Attenuation Coefficient in CT-Scanning

3.2.1. Definition of CT-Number H

Most CT images are displayed as 2-d plots of the linear attenuation coefficient μ (also called absorption coefficient) on a square grid. The square grid elements, pixels, are given a magnitude (gray level) that indicate the calculated, average attenuation coefficient for the corresponding volume in the object cross-section. The pixel dimensions are usually chosen to be directly related to the ray sum sampling distance, or effective detector separation [SHA88]. Thus, a scanner that has a sampling distance of 0.5 mm and gathers projections, each of 512 equally spaced ray sum samples, will most likely result in an image on a grid spanning 256 mm x 256 mm. The pixels represent volume elements due to the finite thickness of x-ray beam - the slice thickness.

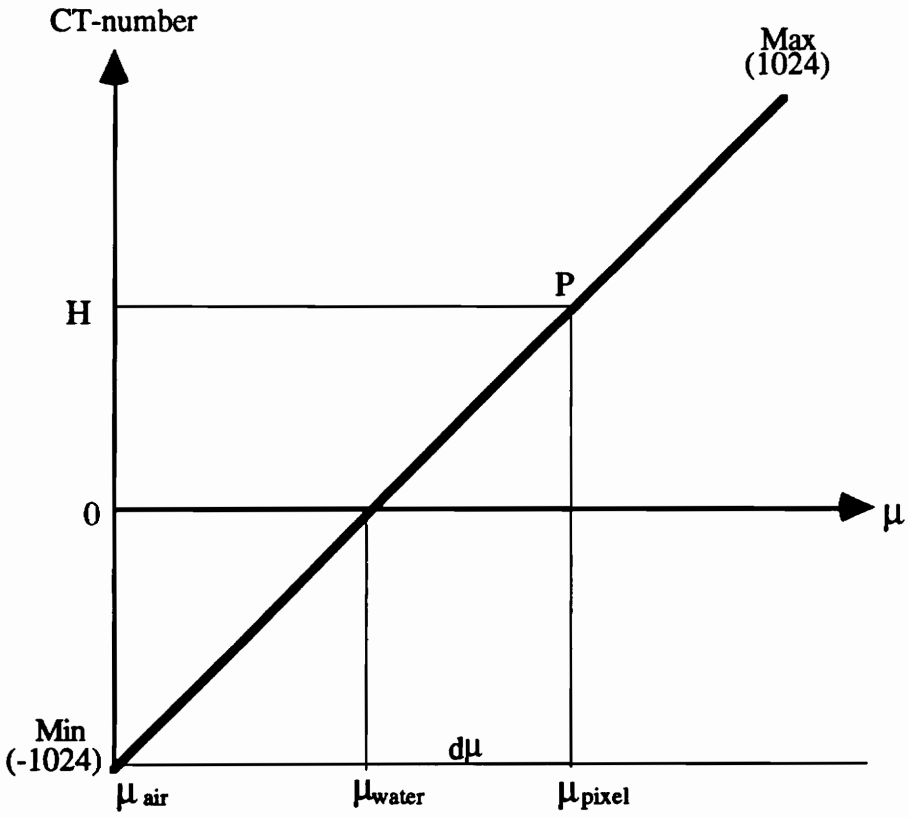

Fig. 3.4 Calibration of the CT-number.

In most instances, and always with hospital CT scanners, the pixel gray values are not presented in value of μ_{pixel} (in units of inverse length, say mm^{-1}), but in normalized units called Hounsfield numbers, H, or CT numbers. A Hounsfield number can be defined in several different ways. One possible definition is illustrated in Fig. 3.4. In this figure, the bold, slanted line is a straight line that is obtained by assuming a linear relationship between the μ values and the CT-numbers. The value Min (-1,024) and Max (1,024) are the minimum and maximum CT-numbers obtained from image reconstruction. To calibrate a CT scanner, the CT-number of water is usually assigned to 0 and its attenuation coefficient is denoted as μ_{water}. Since there is no X-ray attenuation in air, the value of μ_{air} is 0. Then for any given point P on the bold straight line with attenuation coefficient μ_{pixel}, its CT-number, H, must satisfy the following relationship

$$\frac{H}{d\mu} = \frac{|Min|}{\mu_{water} - \mu_{air}}$$

where $d\mu = \mu_{pixel} - \mu_{water}$, and $\mu_{air} = 0$. Manipulation of the above equation gives

$$H = |Min| \frac{d\mu}{\mu_{water}}$$

$$= |Min| \frac{\mu_{pixel} - \mu_{water}}{\mu_{water}}$$

i.e.,

$$H = 1{,}024 \; \frac{\mu_{pixel} - \mu_{water}}{\mu_{water}} \qquad (3\text{-}1)$$

When the X-ray energy is 0.15 MeV, μ_{water} is about 0.26 [ENG66]. The normal μ value of wood is about 0.24 [LIN91]. In addition, since wood's density is smaller than that of water, the H values for wood will always be negative, according to the above definition. For purposes of this dissertation, Eq. (3-1) has been modified by adding a constant of 1,024 to H. In this case, the CT-number becomes 1,024 for water, 0 for air, and positive value for wood. This normalization procedure allows meaningful comparisons between images of the same object, or different objects, from different scanners operating under varying conditions and at different x-ray energies.

3.2.2 Wood Density and Specific Gravity

When traversing through a material, x-rays attenuate due to the interaction of photons with the atoms of the material. We denote the distance traveled by x-rays as d, the incidental and transmitted x-ray intensity as I and Io respectively, and the linear attenuation coefficient of the material as μ. By definition, the level of attenuation of x-ray intensity, ΔI, is proportional to the incidental intensity and the distance traversed by the photons (material thickness), Δd, i.e., $\Delta I = -\mu I_o \Delta d$, where μ is the proportional constant with unit photon numbers/gram [HER78]. After integration of the equation, the following equation is obtained:

$$I = I_0 e^{-\mu d} \tag{3–2}$$

Taking logarithm on both sides of Eq. (3-2) leads to

$$\ln\left(\frac{I}{I_0}\right) = \mu d = \left(\frac{\mu}{\rho}\right)\rho d = (\mu_m \rho) d \tag{3–3}$$

where ρ is density of the material traversed by the x-rays, and μ_m is called *mass attenuation coefficient* which is defined by

$$\mu_m = \left(\frac{\mu}{\rho}\right) \tag{3-4}$$

For a compound that consists of several different elements, each with a mass attenuation coefficient $\mu_m(i)$, the total mass attenuation coefficient of the material can be calculated as

$$\mu_m = \Sigma w_i \mu_m(i) \tag{3-5}$$

where w_1, w_2, ..., are the fractions by weight of the elements which make up the absorbing material.

The physical significance of μ_m is defined as the probability of the interaction between the x-ray photons and the atoms of the element. Each chemical element exhibits a distinct μ_m distribution, as a function of the electron energy (in the unit of eV). One eV unit is the energy that is needed to carry 1 electron across the voltage difference of 1 volt between the anode and cathode of a x-ray tube. As a generic rule, all materials have a broad minimum μ_m at around the electron energy of 1 MeV [ENG66].

Note that mass attenuation coefficient μ_m is independent of the material density ρ, while linear attenuation coefficient μ is a density-related coefficient. Normally, μ_m is tabulated for each of the chemical elements [ENG66], while μ has to be measured using one method or another. At fixed electron energy, same materials will have the same mass attenuation coefficient μ_m.

From Eq. (3-1), it can be seen that CT-number of a material is directly proportional to the material's linear attenuation coefficient μ, and from Eq. (3-3) we can readily derive the following relationship:

$$\mu = \mu_m \rho \tag{3–6}$$

As can be seen from Eqs. (3-1) and (3-6), for a material with mass coefficient value of μ_m, the material's CT-number, H, for a given x-ray energy, is directly proportional to the material density ρ, i.e.,

$$\rho = \alpha H \tag{3-7}$$

In the above equation, constant α is a proportion factor. This relationship between the CT-number H and the density ρ of a material is the basis for nondestructive evaluation using CT imaging technology. In log CT scanning, the pixel value at each point of the image, i.e., the normalized CT-number, represents the density value of the wood material at the cross-section scanned. Since gravitation acceleration varies with latitude and elevation above sea level, weight also varies in a similar manner. To eliminate discrepancies, specific gravity is frequently used to express the relative weight per unit volume of various substances.

Specific gravity serves as a measure of other properties, representing the simplest and best indicator of wood quality in general. Most wood properties are directly, and more or less linearly, related to specific gravity - a wood with twice the specific gravity as another will be about twice as strong, have twice the shrinkage, and so on. Specific gravity is a strong predictor of wood properties and wood performance.

Wood specific gravity is defined as the ratio of the oven-dry weight of a wood sample to the weight of a volume of water equal to the volume of the sample, at the specified moisture content level (commonly at 12% moisture content). Accordingly, the specific gravity of a sample, D, is defined as

$$D = \frac{\rho}{\rho_w} = \frac{m/v}{m_w/v_w} \qquad (3\text{–}8)$$

where ρ is used for density, m for mass, v for volume, and the subscript w indicates the corresponding value for water. Setting the volume of the substance, v, to the volume of water, v_w, Eq. (3-8) simplifies to

$$D = \frac{m}{m_w} \qquad (3\text{–}9)$$

Therefore, the specific gravity of a material is defined as the mass (or weight) of the material divided by the mass (or weight) of an equal volume of water. This property is independent of all gravitational forces and therefore is a constant for a given material [ROW84].

The definition of specific gravity in Eq. (3-8) treats the volume of the material as well as that of the water as constant. However, below fiber saturation the volume of wood substance is subject to change, so it is necessary to specify the volume at which specific gravity is measured. Three different volumes are used: oven-dry, air-dry, and green. Consequently, three different specific gravity values can be calculated, D_o (oven-dry), D_a (air-dry), and D_g (green), one for each particular volume.

For example, Sitka spruce has an air-dry specific gravity $D_a = 0.38$, and a green specific gravity $D_g = 0.355$. The volume of wood in the *green* condition (above the fiber saturation point) is relatively *constant* and can be readily reproduced. Therefore, D_g, specific gravity based on green volume, is now more widely used than the other specific gravity measuring method.

From Eq. (3-8), we can write D in the following form

$$D = \frac{\rho}{\rho_w} \qquad (3\text{–}10)$$

However, water has a ρ_w value of about 1.00 g/cm^3, as such $D = \rho$. Therefore, it can be concluded that density D (in units of grams per cubic centimeter) is numerically identical with specific gravity ρ, the ratio of a particular density to the density of water.

In most instances, to account for the effect of different moisture conditions in the wood, the *average specific gravity* , D_{ave}, is used instead of specific gravity D. The average specific gravity of wood species is defined as the average value of D_a, D_o, and D_g of the material. For instance, the average specific gravity D_{ave} of water in the cell wall of wood is 1.017.

Standard texture books on wood science contain tables of D_g or D_{ave} values for various wood species in Northern America [PAN70] [KOM80]. Further discussion of the issue is beyond the scope of this dissertation. Details about the relationship between moisture content and specific gravity can be found in [ROW84] and other literature on wood science.

Table 3.1 and Table 3.2 list the average specific gravity of some hardwood and softwood species [KOM80].

Since the D values for most wood species are given in standard textbooks or operator's manual, the wood density ρ can be easily calculated from D using Eq. (3-10). Then the CT-number, H, of the species can be estimated from ρ by Eq. (3-7). However, this estimate of H from ρ is not very accurate and is not used very much in practice.

In [DAV92], a method of estimating H from ρ is proposed that is especially suited to CT wood measurement. It points out that a complete calibration should be undertaken to express μ in terms of more suitable variables. From Eq. (3-7), it can be seen that density ρ is an obvious choice in practice, particularly for wood, where a rough rule-of-thumb calibration indicates that

$$\rho\ (\mathrm{kg/m^3}) = H + 1{,}000 \qquad (3\text{–}11)$$

may be used for an accuracy of about 10 percent. For feasibility studies, this expression is often adequate [DAV92].

3.2.3 X-ray Attenuation Coefficient μ

In previous studies on wood characterization, methods have been developed for measuring density of wood by calculating the linear attenuation coefficient μ of the material. These methods are different from the specific gravity-based method, discussed in the previous sub-section, in that they study the relationship between the chemical composites in wood and the x-ray photons at certain energies.

Table 3.1 Average Specific Gravity of Hardwood

Species	Average Specific Gravity D_{ave} [1]
Red Alder	0.37
White Ash	0.55
Black Cherry	0.47
American Chestnut	0.40
Sugar Maple (hard)	0.56
California Black Oak	0.51
Red Oak	0.54
Water Oak	0.56
Black Walnut	0.51
Yellow Poplar	0.40

Table 3.2 Average Specific Gravity of Softwood

Species	Average Specific Gravity D_{ave} [1]
Western Red Cedar	0.31
Douglas-fir (coast type)	0.45
Pacific Silver Fir, White Fir	0.35
Subalpine Fir	0.31
Hemlock (eastern, western)	0.38
Ponderosa Pine	0.38
Red Pine	0.40
Redwood (old-growth)	0.38
Red Spruce	0.38
Sitka Spruce	0.37

1. Based on weight when ovendry and volume when green.

Mull found an accuracy of 10 kg/m^3 in density measurement for 7 different wood species using an Ohio Nuclear 2010 scanner [MUL84]. Hattori et al. measured wood density and moisture content using a Toshiba TCT-20A scanner [HAT85]. The measurements were made within a circle that contained 60 percent of the actual specimen area. An empirical relationship was determined for the density with an accuracy of 5 kg/m^3. Lindgren found a relationship between wood density and CT-number for a GE 9800 Quick-scanner that showed an accuracy of 4 kg/m^3 in whole test pieces [LIN88]. Similar relationships for a Siemens DR 1 scanner were also found. As expected, the relationships were not identical for the two scanners according to Levi et al. [LEV82].

Tsai et al. [TSA76] developed a model for calculating x-ray attenuation coefficients for different materials. Denote the coefficient caused by the photo-electric effect and the Compton scattering of photons by μ_p and μ_c respectively. Then, regardless of other interactions between photons and the material, the total x-ray attenuation coefficient for each particular type of atom of the material, μ, can be approximately expressed as

$$\mu = \mu_p + \mu_c \qquad (3\text{–}12)$$

where

$$\mu_p = (K_1 \rho\, n_o Z^{1/m}) / E^{3.10} \qquad (3\text{–}13)$$

$$\mu_c = K_2 \rho\, n_o f(E) \qquad (3\text{–}14)$$

where K_1, K_2 are constants, ρ is density of the material, n_o is the electron density, Z is the effective atomic number of the molecule, E is the photon energy (e.g. 73 keV at 120 kV power supply), m is a material related constant (e.g, m=4.4 when Z < 16 and $\rho < 2.0$ g/cm^3), f(E) is a complicated function of E.

Eq. (3-12) to Eq. (3-14) make it possible to calculate the absorption coefficient of any material once its density and chemical composition is known. According to [WIL80], the absorption coefficient in a material consisting of different materials can be calculated by the following equation for a compound in which all the atoms are uniformly distributed

$$\mu = \Sigma w_i \mu_i \tag{3–15}$$

where μ_i is the absorption coefficient of the *i*th material, and w_i is equal to percentage by weight of the *i*th material.

Now that the total absorption coefficient of the compound is calculated, the CT-number of the compound can readily be computed from Eq. (3-1). In summary, the absorption coefficient and the CT-number of a material can be calculated as soon as the chemical composition and the density of a material is known. These values can also be calculated for a compound consisting of different materials, each with known density, chemical composition, and percentage by volume.

In [LIN91], CT scanning and its relationship to *softwood* density were studied with a GE 9800 Quick medical scanner. It describes how x-ray attenuation coefficient μ and CT-number can be calculated for dry and wet wood. It shows that wood density ρ could be measured with high accuracy, that wood with same green density but different amount of water have different μ values and different CT-numbers, and that CT-numbers differ between manufacturers and even between scanners from the same manufacturer.

Chemical composition of softwood: As pointed out in section 3.1, wood contains 30-50% of cellulose, 15-35% of hemicellulose, and 15-30% of lignin. Cellulose and lignin can be chemically regarded as $C_6H_{10}O_5$ and $C_{10}H_{13}O_2$ respectively, and hemi-cellulose, averaged over the different softwoods, can be regarded as $C_{5.9}H_{11.8}O_{5.8}$. It is assumed that the densities of these constituents are equal and calculated as 1.5 g/cm^3 [LIN91].

Calculation of μ and CT-number for dry wood: When Eqs. (3-12) through Eq. (3-14) are used to calculate the attenuation value μ, results are obtained for the three constituents of wood and listed in Table 3.3.

Table 3.3 Calculated μ for 3 wood constituents (at 70mA, 8 sec. scan time)

Constituents		μ
cellulose	$C_6H_{10}O_5$	0.2684
hemicellulose	$C_{10}H_{13}O_2$	0.2655
lignin	$C_{5.9}H_{11.8}O_{5.8}$	0.2608

However, wood is a porous material that contains a large portion of air in addition to cellulose, hemicellulose and lignin. For dry wood, the total volume, V, consists of wood volume V_{wood} and air volume V_{air}, i.e. $V = V_{wood} + V_{air}$. If we denote the density of wood substance in kg/cm^3 by ρ_{wood}, the wood volume can be calculated as a portion of the total volume, according to the following relationship [LIN91]

$$V_{wood} = \frac{\rho_o}{\rho_{wood}} V \qquad (3\text{–}16)$$

where ρ_o is the dry density of wood (when without water and inorganic salts), ρ_{wood} is the density of wood substance in kg/m^3.

To determine how different volume distributions of cellulose, hemicellulose and lignin within the volume V_{wood} influence the total attenuation coefficient μ and the CT-number, H, different volume percentages are chosen for a softwood with dry density of 500 kg/m^3 (or 0.5 g/cm^3) [LIN91]. For each of the distributions, the total attenuation coefficient μ and CT-number are calculated and listed in Table 3.4.

Table 3.4 The Influence on CT-number by Wood Constituents

Cellulose vol. %	Hemicellulose vol. %	Lignin vol. %	μ	CT number
50	25	25	0.08775	-527
25	25	50	0.08753	-528
50	40	10	0.08799	-526
10	10	80	0.08715	-530

From table 3.4 it can be seen that changes in volume percentage between cellulose, hemicellulose and lignin result in only small changes in CT-number and μ value. This also implies that the CT-numbers for *heartwood* and *sapwood* of softwoods are the same, since the C, H, and O relationships (percentage by volume) do not change after heartwood transformation.

According to [WEG84], wood contains 0.1 - 1.0% by weight inorganic salts. Although they play little role in strength, they are totally responsible for many wood's properties, such as color, taste, and decay resistance. They may also affect shrinking and swelling, by taking space between microfibrils which would otherwise be occupied by water molecules [WIL91]. To study how the μ value and CT-number dependent on the changes in inorganic salt content in softwood, the same softwood as above is used to calculate the changes in μ and CT-number for different inorganic salt contents in wood [LIN91]. In the study, salt is chemically expressed as $CaCO_3$ with a density of 2.17 g/cm^3.

It has been shown in [LIN91] that small change (e.g., 0.5% by volume) in inorganic salt content in wood results in large change in the CT-number (e.g., 2 CT units). The calculated CT-number is -527, -525, and -523 for 0.0%, 0.5%, and 1.0% salt content by weight, respectively. The corresponding μ values are 0.0878, 0.0882, and 0.0886. Thereby, relationship between CT-number (and μ) and wood density ρ must be assumed to be sensitive to inorganic salt contents. However, this relationship may be different for softwood and hardwood, since the inorganic salt contents by weight may be different in them. In fact, differences can be expected even between different hardwood species, as their inorganic salt contents sometimes show large differences.

In the same study on wood attenuation, Lindgren assumed 0.5% by weight inorganic salts in softwood. This results in a linear attenuation coefficient for wood $\mu_{wood} = 0.2646$. Using this value, CT-numbers for eleven oven-dry densities of the wood are measured using CT scanner, and calculated using Eq. (3-12) to (3-14). After linear regression, the result can be expressed by the following linear relationship between the measured CT-number, H, and measured dry wood density ρ

$$\rho = 1.052\,H + 1053 \qquad (3\text{–}17)$$

Calculation of μ and H for wet wood: Suppose that water is added to wood so that the total volume V_{tot} has increased by α %, i.e.,

$$V_{tot} = (1+\alpha)\ V \tag{3-18}$$

The density at moisture level u (percentage by weight), ρ_u, is

$$\rho_u = \frac{V_{wood}}{(1+\alpha)V}\rho_{wood} + \frac{V_{water}}{(1+\alpha)V}\rho_{water} \tag{3-19}$$

where ρ_{wood}= 1.5 g/cm^3, ρ_{water} = 1.0 g/cm^3. In analog to the above equation, the attenuation coefficient at moisture level u, μ_u, can be expressed as

$$\mu_u = \frac{V_{wood}}{(1+\alpha)V}\mu_{wood} + \frac{V_{water}}{(1+\alpha)V}\mu_{water} \tag{3-20}$$

where μ_{wood} is the attenuation coefficient of wood (=0.2646), μ_{water} is the attenuation coefficient of water (=0.1856).

To illustrate how to calculate the CT-number, H, and attenuation coefficient, μ, for wet wood, consider the following example. Suppose the volume of wood plus air is 300 dm^3, and that the oven-dry density 0.5 g/cm^3. Then the mass of wood is 150 kg, and V_{wood} is dm^3 according to Eq. (3-16). If the moisture contend is 30% (u = 0.3), the mass of water is 45 kg. If all water swells the wood, the total volume including water increases to 345 dm^3. Therefore, (1+α) = 345/300 = 1.15.

According to Eq. (3-20), the total attenuation coefficient μ_u is,

$$\mu_u = \frac{100}{345}\,0.2646 + \frac{45}{345}\,0.1856$$
$$= 0.1009$$

From Eq. (3-1), the CT-number of the wet wood, H, is

$$H = 1{,}000 \times (0.1009 - 0.1856) / 0.1856$$
$$= -456.$$

In [LIN91], 50 CT-numbers for green wood containing water are calculated with moisture content ranging from 6% to 117%. The relationship between the CT-number, H, and the green density, ρ, is expressed by the following linear equation

$$\rho = 0.993\,H + 1015 \qquad (3\text{–}21)$$

As expected, the relationships between dry/wet wood density and CT-number are not the same, by comparing Eq. (3-17) with Eq. (3-21). Due to different dry densities, wooden test pieces containing different amounts of water may show the same green wood density. Furthermore, an increase in wood density by adding wood substance results in a larger increase in the attenuation coefficient than a corresponding increase in density by adding water.

3.3 Wood Characteristics in CT Imagery

Conventional methods for wood testing, such as composition analysis, static bending, or fracture tests, are destructive tests, performed using standard pieces of wood of specific size and from selected parts of a tree. These tests cannot be applied to hardwood logs which are not sawn up. On the other hand, CT imaging can circumvent these problems since it is nondestructive and can be used to scan any part of a tree. To determine how effective the CT imaging devices are in detecting wood defects, a number of studies have been conducted by different groups in recent years.

In [WAG89], a grade 2 water oak (*Quercus nigra*) log of a diameter of 15 inches and a length of 12 feet was scanned, using the ultra fast C-100 Scanner at Imatron, Inc. of South San Francisco. The purpose of this study was to compare the CT data with those acquired by sawing the log into thin sections (disks) and hand tracing the defect outlines. Fresh-cut sample of the log was cut into 2-feet long segments and shipped to Imatron sealed in plastic bags. Each segment was placed on the patient table and scanned in the low-resolution mode using a slice thickness of 8 mm. In all, 456 scans were obtained. In this scan mode, each pair of scans (covering 16 mm in thickness) was acquired in 50 micro-second. In addition to the low-resolution scans, one of the log segments was scanned at high resolution with a scan time of 100 micro-second per pair of slices, each of the same thickness of 8 mm.

Visual inspection of the CT images of the log showed that they are indistinguishable from photographs of a cut log. A careful examination reveals that the resolution of these CT images is approximately 7 lines/cm, which is not quite as high as that of a good photograph, and that, because a CT scan has a finite thickness, the image represents a density averaged over this thickness (8 mm in this case), rather than over a single plane like in a photograph. Nevertheless, wood grains, annual rings, and defects, including pith, knots, bark, splits, and holes can be seen clearly on the CT scans, as shown in Fig. 3.1. This indicates that CT can indeed be used to detect defects in hardwood logs.

In a log scan experiment with softwood logs using a Siemens Somatom DR2 scanner, Funt et al. reported a surprising similarity between the CT scan and the photograph of the logs [FUN85]. Three types of softwood logs were used, they were cedar, hemlock, and fir. In this test, many details of log's internal structure, such as its growth rings and knots, are visible in the scans. The scans reveal them because the scanner measures the x-ray absorption, which corresponds to a material's density. The density of knots and slow winter growth exceeds that of the fast summer growth, and this is depicted in the scan by the brighter pixels in these areas. In this test, knots are easily discerned by their whiteness and roughly elliptical shape. The air surrounding the log, as well holes and cracks, appears very dark, while good wood shows up in the circular pattern of growth rings. The hardest feature to distinguish tends to be rot which has dark shade and disrupts the growth ring pattern of good wood.

Besides density, other features of the wood material can also manifest themselves in the CT scans. The major axis of an elliptical knot region points toward the center of growth of the log, thus can be used to identify knots. The rational for considering the *orientation* of the knot region stems from the fact that knots are created by branches whose cross-section is roughly elliptical and points toward the center of the log (see section 1 of this chapter). In addition, most other high density regions in CT scans are caused by moisture occurring in the sapwood, so they tend to form circular bands concentric to the growth rings. The axes of these regions align with the growth rings rather than point toward the center, thereby distinguishing them from knots. Rot causes a breakdown in the growth ring structure so that presence of uniform growth ring *texture* indicates sound wood even if the wood has quite low density. Therefore, the low uniformity can be used as a measurement to detect rottenness in wood.

3.4 Summary

The digital CT imagery of a log encodes much information about its wood characteristics. This information is manifested primarily through spatial intensity variations which correspond to variation in some physiological, physical or chemical characteristics of the material in wood. Our ability to decode these intensity variations and to correctly recognize the internal defects in the log depend critically on our understanding of wood structure and our ability to devise reliable method for image analysis.

Trees exhibit a variety of properties and wood defects exhibit their own particular features, such density, shape, texture, and relational position. In CT imaging, major grading defects generally manifest themselves very well, rendering their detection by an advanced machine vision system. In particular, such defects as knots, splits, pith, holes, reaction wood, decay, and stains can be detected from CT imagery of hardwood logs, and their characteristic features are perceivable on the imagery. In addition, since CT-number is directly related to the density, chemical components, and moisture content of the material, CT imaging method can be used to measure the density, chemical constituent, and the moisture content of wood.

To increase wood value recovery by optimum sawing, all information required for determining log/lumber grade must be detected. This information includes log/board geometry and the location, size, and identification of all features considered as defects by NHLA [NHL86] grading rules. While significant advances have been made in defect detection research [LIN88] [WAG89] [LIN91], the type of detection system that can provide all of this information has not yet been developed. Systems that are considered technically feasible at present are able to detect only some of the features required for accurate lumber grade evaluation [SZY81] [LEE91]. In a practical study on how much log/lumber value recovery can be accomplished with limited input information for determining optimum sawing solutions [KLI92], the obtained result shows that it is possible to obtain lumber value higher than actual sawmill output from a computer-based optimization procedure, even if *not all* board defects are considered. From this and some other studies on wood value recovery [OCC88] [STE89] [REG91], it can be concluded that significant value recovery from logs will be achieved when CT imaging is used together with an intelligent machine vision system, since CT can reveal much of the needed information about various grading defects.

Chapter 4
Image Collection and Evaluation

This chapter argues the importance of creating a data base of CT imagery for establishing the feasibility of using CT for log inspection. It also discusses a number of performance measures for evaluating human and machine analysis of CT imagery. Finally it describes a procedure that was needed to create the required data base of log images. Visual inspection of images comprising this data base shows that almost all grading defects can be detected and identified based solely on CT imagery. This means that CT imaging modality can be used to easily detect the presence of almost all grading defects inside hardwood logs.

4.1 Purposes of An Image Data Base

In this dissertation study, an image data base was created 1) to determine which grading defects are detectable in CT imagery, 2) to establish "ground truth" as to exactly where these defects are located in the collected CT imagery, and 3) to train a machine vision system for log inspection. This data base consists of a set of scanned CT images and set of color photographs of the cross-sections of the scanned logs.

To determine the efficacy of using CT imaging for log inspection, a method for determining whether important defect information is contained in the imagery must be identified. This method must be able to determine which grading defects are detectable in

CT images. If the imaging device, whether CT or MRI scanners, can not capture the features defining internal log defects, then there is no hope of using CT data in the sawmilling application. A data base as collected in this study allows one to conduct a visual comparison so as to determine the detectable grading defects in logs.

Since this data base contains "ground truth" information about log internal defects, it can be used to locate the various grading defects. This location information along with the log geometry can be employed to help build a knowledge base for a machine vision system for log inspection. Then defect recognition procedures can be defined by using this knowledge as the contextual knowledge in the inference engine of the machine vision system.

A data base also provides a method by which the overall vision system performance can be evaluated. To develop any computer vision system requires a good deal of experimentation. The resulting vision system will be no better than the data base used in its development. If the data base of images is representative of the range of images the system will have to process in the real world environment, the system, once it is developed, will probably be effective in solving the problem it was intended to solve. If on the other hand the data base of images used to create the system is not representative of the real world image data, then the resulting system will probably not be able to perform its task effectively.

Machine vision system applications to industrial automation is still in its infancy, with much work, both in theory and in application, remaining to be done. As pointed out in Chapter 2, an industrial machine vision system consists of two major components, a segmentation component and a recognition component. The segmentation component separates areas of interest (AOI) from the rest of an image, and the recognition component is designed to identify the objects. First, most segmentation methods separate AOI from background using some type of thresholds, thresholds that can only be obtained from experiments with a large data base of object images. Second, the recognition component of a vision system identifies objects by their features. Most vision systems are based on concepts of artificial intelligence (AI) and expert systems, including such concepts as learning (training), recognition by reasoning, classification by example, and so on. All these concepts are closely related to a data base that is used to build the AI procedures and expert knowledge base. It is impossible to develop a machine vision system for a specific task e.g., hardwood log inspection, without an appropriate data base, a data base that can be used to establish algorithm robustness.

Furthermore, an image data base is needed to perform computer sawing simulation. In this type of simulation, information regarding the internal structure and geometry of the various wood defects are used as input to a computer sawing simulator [OCC88]. The input would include such specific parameters as the location, size, orientation, and type of each grading defect in log, as well as their topological relations. This input information can easily be obtained from a log image data base and combined to simulate the various configurations of internal defects in the log. Then lumber grades are computed from the lumber sawn according to the NHLA national standards. Different sawing patterns are searched in an effort to find an optimal cutting decision.

The image data base can also be directly used by the logging industry as part of a larger log image data base. Currently, there are only a few research centers in the world that are dedicated to the non-destructive testing of forest products. As technologies are advanced in fast pace, more and more wood processing factories will look to the scanned log images for optimum cutting solutions. For example, the CT scanning industry is planning to establish a CT Log Image Database on the west cost of the U.S. The idea is to use a mobile scanner to scan logs at different logging sites throughout the Northwest of the U.S., and store the scanned images as an industrial data base which is made accessible to any forest products business that is interested in these images. With this accessibility, workers at a lumber company would not need to go the logging site to pick up the desired logs. Instead, computer operators at the company can immediately view log images through the computer network, and efficiently obtain all the necessary information about logs at different sites to decide which logs to use. It is no longer a dream to "see into" the logs before cutting them for maximum value yield. As part of a more representative image data base, our collected data base of log images together with its analysis results could contribute to this new application of log scanning for the logging industry.

4.2 Evaluation of System Performance

The utility of using CT images on an application problem is directly related to the issue of how well the human visual system and, hence, any machine vision system, can locate and identify objects in these images. To evaluate any machine vision system requires the ground truth information about the objects to be inspected. One way to obtain the ground truth information is to have experts visually view the object's image scanned by a CT unit and record their responses. However, even for experts to accurately interpret CT images is a complex task that involves the human perception and a number of physical variables [NEW81]. Due to its limited scope, this dissertation does not address the human perception. To accurately assess the performance of a CT-powered vision system, it is, therefore, important to define and evaluate a number of scanner performance measurements for specific tasks. Since machine vision systems are typically designed to mimic human eye-brain system in many aspects, it is equally important to study the machine vision system performance through an image data base used to develop it.

The accuracy of interpretation of a CT scan depends on 1) the performance of the visual system of the observer (called observer performance), 2) certain physical variables (measurements) in the CT image, and 3) the decisions required to recognize and classify the wood abnormalities or defects (machine vision system performance). Each of these issues will be addressed in the following sub-sections. A good deal of research has been conducted on these topics by experts in medicine, radiology, psychology, and computer science [DOI69] [MET69] [GOO72] [STA75] [ROS73] [BAL82] . An especially informative and concise description of the topic is contained in [NEW81]. Much of the notation used in [NEW81] will be adopted in the following discussions.

4.2.1 Measurements of CT Imaging Performance

In automated industrial inspection the objects (defects) to be inspected, in general, have varying size, contrast, density range, and etc. For a CT-powered machine vision system to successfully inspect log defects, its imaging performance must meet the requirements of the log inspection task. For example, to accurately detect a grading defect 2.0 mm wide in a log using a CT scanner, the required resolution of this scanner must be 2.0 mm or higher. Otherwise, this scanner cannot be used to defect log defects that are smaller than 2.0 mm. Since CT is just recently being used for industrial inspection, there is a need to develop an industrial standard to measure the its imaging performance. There have been a number of performance measurements that are specifically defined to assess the imaging performance of CT in medicine [NEW81]. It is hoped that studying these medical CT performance measurements may help in defining similar performance measurements for industrial CT applications.

Typically, medical CT images contain 512 x 512 voxels (volume elements), with each voxel assigned one of 6,000 "gray levels." Because the human eye cannot discern such small differences in gray level, *the image which exists in computer memory contains far more information than the CT image viewed by an operator.* In order to produce images of this quality, the basic x-ray data must be acquired with extremely high precision and accuracy. Detector dynamic range is typically six orders of magnitude, and the analog signals are digitized to the equivalent of 22 bits. The number of views required to reconstruct an image is basically determined by the desired resolution. A 512 x 512 image can, in principle, be considered to be the solution of a set of 512 linear equations, each containing 512 elements - the minimum required for a unique solution. In practice, different means are used for reconstruction which require even more views, and are generally treated as the trade secret in the CT scanner business.

The issue of CT imaging performance can be described in analog to that of observer performance. There are several measurements of observer performance. The diagnostic process that determines observer performance consists of at least three basic steps: 1) "detection," in which a decision is made as to whether some (as yet unspecified) abnormality (defect) is present in the image; 2) "classification," in which decisions are made as to the attributes (defect size, shape, etc.) of any detected abnormalities; and 3) "recognition," in which decisions are made as to likely physiological conditions or geometric relations (the identity of defects) that correspond to the classified detected abnormalities.

Certain basic physical measurements obtained from CT imaging systems are related to the "detection" step of the diagnostic process. These physical factors influence perception of a diagnostic "signal" (physiological defect of wood), they include 1) contrast between the suspected abnormality and non-suspected areas (background of the image), 2) amplitude and character (standard deviation and spatial frequency content) of any image "noise" (e.g., the annual ring structure of wood) that may tend to diminish the perception of the abnormality, and 3) the rate of change of intensity at the boundary of the suspected abnormality. The latter factor, which is important because of the known human perceptual preference for sharp edges, is often referred to as sharpness, edge gradient, or acuteness. Edge gradient is the one of the most prominent features of the objects, which are used by the segmentation component of a vision system to separate defects from the rest of the image.

The evaluation of CT image, especially as it affects the detection performance of the human observer and machine vision system alike, is a complex task involving analysis of the following physical and psychological variables:

A. Image parameters
   1. signal (feature of defect) to be detected: size, shape, inherent contrast
   2. number of possible signals (a set of features)
   3. imaging system: spatial resolution, sensitivity, linearity, noise
   4. nonsignal structure: pixels, artifacts, and etc.

B. Psychological parameter
   1. display system: brightness, magnification, nonlinearity
   2. viewing condition: viewing distance, ambient room brightness

3. detection task
4. number of observations
5. a priori information
6. feedback
7. observer experience

A data base of CT images, as described in this study, provides the necessary data to conduct the evaluation of human visual system performance with regard to wood defect recognition. It can also be utilized to test the physical measurements from CT imaging systems. When comparing different imaging modalities, such as CT and MRI, the data base serves to assess a number of the imaging parameters associated with each imaging modality, such as resolution, contrast, amount of image data, and so on.

4.2.2 Evaluation of Machine Vision Systems

To develop a reliable machine vision system, its performance must be evaluated under the conditions for which it was designed. If a vision system does not perform reliably under the required condition, then it cannot be expected to perform under conditions other than the required one. A key part to any machine vision system is its algorithms, most of which are designed to be robust under varying conditions. The only way to verify this robustness is to test the algorithm on a data base of images. In addition, evaluating a vision system's performance against a data base can help one to predicate its potential performance in an unknown environment.

The experimental results of observer performance in medical radiology clearly indicate that concepts of signal detection theory (SDT), and in particular, receiver operating characteristic (ROC) curves [EGA75] (Fig. 4.1) may be applied to certain detection tasks in the industrial CT image analysis [COP93]. In particular, the perception and processing of the information content in CT images by a machine vision system may be evaluated quantitatively by studying its performance under different imaging conditions. A machine visions system can be tested under varying contrast, low and high sharpness, and different spatial resolutions.

Any inspection decision, made by a vision system under certain imaging condition, regarding the existence of a defect in the CT image of a log can be associated with two kinds of errors: (1) false positive (i.e., an incorrect decision that a defect is present) and (2) false negative (i.e., an incorrect decision that a defect is absent). According to [EGA75], we have to first specify what "signal" and "noise" are. In the CT log images that have been collected in the data base, for example, the signal can be given by the pixels representing areas of physical defects of the wood. In regard to noise, only a part of the background pixels (i.e., the annual ring structure in clear wood, and some other structures at the various locations of the log CT image) can deceive our observation and thus can be considered noise.

The true positive rate, or the "sensitivity" of a machine vision system, represents the probability that the system will respond correctly to the presence of a signal (defect). Likewise, the true negative rate is frequently called the "specificity" of the detection system. It represents the probability of the system responding correctly to the absence of the signal (defect) when the signal (defect) is not present. Another term often encountered in error analysis is "accuracy." The accuracy rate is related to sensitivity and specificity in that is may be defined as the number of correct decisions divided by the total number of decisions made [NEW81].

Generally speaking, the assessment of the performance of an automated machine vision system relies on reference descriptions that specify the objects (defects) to be described and their features such as shape, size, density, and so on. Unfortunately, in the field of log inspection, such a description is not available due to the difficulty associated with making direct measurements. Since the signal measurement in standard SDT is the number of times the signal (defect) occurs during the test, defect features, such as its area A_d (the total pixel number of the defect) can be used as the signal measure. Likewise, if we denote the true positives as TP and the false positives as FP, the following parameter can be evaluated:

$$C = FP / (FP + TP), \qquad S = TP / A_d$$

where TP and FP are expressed by the number of pixels, C is the complement of the *positive predictivity coefficient*, and S is the *sensitivity* of the observer [COP93]. Parameter C expresses how wrong the vision system is by saying "yes," i.e., the probability of false alarm, and parameter S expresses how many "yeses" the system says in comparison with the defect (pixel) occurrence number, i.e., the probability of the correct detection. For the sample CT image RK11.20 (Fig. 4.2), we have found Ad = 43691, TP = 37443, FP = 959, S = 85.7%, and C = 2.5%.

Like in medical imaging, the protocol of ROC analysis measures the ability of a vision system or an imaging modality (or an observer) to identify abnormalities. The ROC curves (Fig. 4.1) are plots of the true positive fraction as a function of the false positive fraction [EGA75]. In Fig. 4.1, P_d and P_f stand for the detection probability and the false alarm probability of a system. An ROC curve is obtained through data collected from the CT imaging specialists who report their findings using graded response. *Ground truth* is obtained from information not related to the images being compared. If two vision systems, or two imaging modalities, or two imaging devices of the same modality are studied, then the one producing the better statistically significant ROC curve (i.e., that with the largest area under the ROC curve) is judged to have produced better results with respect to the comparison task at hand [NEW81].

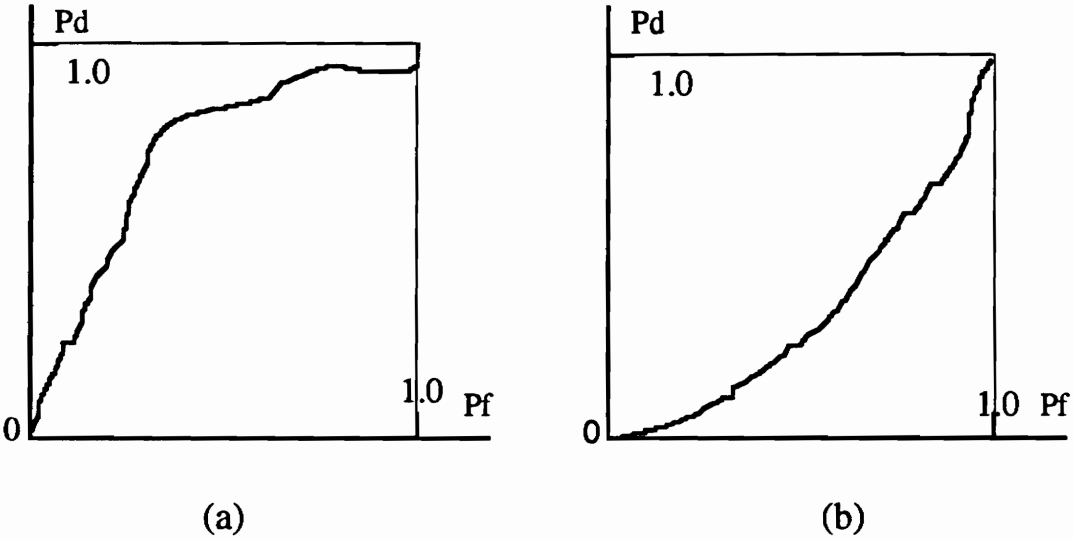

Fig. 4.1 ROC curves for 2 systems, system (a) has better performance than system (b) since the area under the curve in (a) is larger than in (b).

In ROC studies, the system performance is directly related to the concept of probability, the distribution of sample population. To achieve valid analysis results that bear statistical significance, a data base, that consists of a large number of image samples, has to be established. Machine vision system performance measures, as just discussed, present a potential significant improvement in the assessment of CT-based industrial vision systems in that the methodology implicitly includes measures of both sensitivity and specificity.

4.3 Significance of the New Data Base

Because of the above mentioned reasons, it is very important that at the beginning of any study to spend a good deal of time preparing an appropriate image data base. At the beginning of this research activity there was only one data base of CT images of hardwood logs available. This data base was the one created to perform the research work reported by [WAG89]. It was established by investigators at Mississippi State University (MSU) in cooperation with the Southern Forest Experiment Station of U.S. Forest Service, and with the Imatron Inc. of South San Francisco. The data base consisted of a series of 256 x 256 by 8 millimeter contiguous slices of a red oak log section 12 feet long.

This data base, while containing a number of slices, is not very satisfactory for the feasibility study for a number of important reasons. First and foremost was the way in which "ground truth" was established on this data base. Whenever attempting to create an automatic method for analyzing images, one must be able to compare results obtained from the automatic analysis with the way the image should actually be interpreted, i.e., the ground truth interpretation. An image interpretation is the creation of distinct regions within the image and the assignment of labels to these regions.

To establish ground truth for a CT image slice of a log requires cutting the log across the imaging plane used to create the slice and examine the log at the position of the cut to determine the location and extent of each defect. If a log has multiple contiguous image slices taken from it, establishing the ground truth for each of the slices becomes somewhat more complicated since the log must be accurately cut a number of times without any accumulative error build up. The problem is to make sure the surface of the log face visually inspected is accurately registered with the CT image associated with this surface.

The MSU data base was collected with the idea of being able to determine the ground truth for an entire log. The objective was to use this ground truth data to help determine the potential benefit of using internal defect locations to optimally position a log for cutup. As such an entire log had to be scanned and the log had to be handled just as it came from the forest. Because of this handling process, there was, only moderate, if not poor, registration between a log surface obtained from the cutup operation and the associated CT image slice obtained by the Imatron CT scanner.

Another problem with this data is that the ground truth information was in the form of *hand digitized outlines*. Hence, while one could compare the results of computer processing with the labeling assigned to these outlines, one could not control the error that might be caused by the hand digitizing method. The final problem with this data base is that it represents only one species, albeit a very important species, red oak.

Last but not the least, the log scanned for MSU seemed to be a dry log - the log sections must have been oven dried priori to scanning - there were too many drying splits in its CT images. According to chapter 3, dry wood differs from green wood in wood physiology and in defect properties. For example, since the moisture content of the dry wood is less than that of green wood, the CT numbers of the former are lower (due to more air in the wood) than those of the latter. Furthermore, the dry wood specific gravity and the linear attenuation coefficient variation pattern are different from those of green wood. All these differences could drastically affect the performance of the machine vision for hardwood log inspection.

To address these problems, a new CT image data base was created in Blacksburg, VA, in June 1991 for use in this research. The methodologies used to create this new data base differed markedly from those used in creating the Mississippi State data base. Collecting CT imagery of logs, or for that matter anything else, is very expensive, about $10 per slice. Hence, it is very important that each slice provide as much information as possible. Due to this side restriction, only two species of hardwood logs have been selected for scanning in this study, they are red oak, a ring porous species, and yellow poplar, a diffuse porous species. Nevertheless, these two species represent the two extremes of the hardwood spectrum, and inspection results obtained from them could be generalized to some extend to the whole population of hardwood species.

For the purposes of developing a computer vision system the "important information" contained in each slice of CT imagery is the way different defects manifest themselves in relation to one another and to clear wood. Since the vast majority of any log is clear wood, the really important part of any CT image slice is that portion of the slice that represents an internal log defect. Hence, low grade logs of red oak and yellow poplar species were individually selected and scanned, so that the image data base contains ground truth information of the common internal defects in hardwood logs for use in creating the data base.

4.4 A Systematic Image Collecting Procedure

To achieve the above objectives, a set of procedure for creating such a log CT image data base has been established. The log image data base consists of both the digital CT images and photographs of hardwood logs. This method can be categorized as the following five procedures: (1) log selecting, (2) section cutting, (3) slice scanning, (4) slice cutup, and (5) photographing.

1) *Log Selecting*: Hardwood logs were picked up from a local sawmill in Virginia; ones which may contain such defects as knots, holes, shake, stain, decay, end splits, and bark pockets. To provide information about the variations caused by inter-species differences in hardwood logs, log samples from two wood species were selected for consideration. They are red oak, a high value *ring-porous species*, and yellow poplar, a medium value *diffuse-porous* species. These have been selected because they represent the physiological extremes that exist between hardwood logs. The logs selected have diameters from 8 to 16 inches so that they are more likely to have internal defects that manifest themselves as bark anomalies, i.e., the so called bark distortions in wood science. Hence a visual inspection of those anomalies on log barks allows a human expert to more accurately determine that a possible internal defect is present at a particular location, and even allow one to determine the type of defect that is present.

2) *Section Cutting*: Log sections to be cut from each log need to be properly determined, numbered, and prepared for CT scanning. Each log used was first sawn so that it had one flat face. Log sections selected were then cut from the logs. Obviously, each section also had one flat face, a face it inherited from the log from which it had been cut. Marks were used to delineate the volumes of each section that were to be scanned. The flat face was used to rest a section on the bed infeed system of the CT scanner so that the log could be positioned on the scanner station during the CT imaging. The objective was to produce image slices perpendicular to the plane defined by the flat face.

Finally, a saw was used to make a straight groove down the side of the log section opposite of its flat surface. The groove was used to determine the beginning and end of CT imaging process and to align the section on the CT scanner so that slices would be imaged perpendicular to the line defined by the groove. Both the groove and the flat face were used so that good registration could be obtained between a cut made through a section and the associated CT image slice. Since there were some delay between the time the sections were cut and prepared for scanning and the time they were actually scanned and photographed, the log sections were stored in cold-storage to keep them from drying until they could be scanned. The objective of this step is to acquire the CT images of "green" material.

3) *Slice Scanning*: The volumes marked on the log sections were then scanned to produce CT images of these volumes. On average, the defect volumes of a section can be imaged using 20 CT image slices. The CT unit used is a Siemens Somaton CR system, operating at a voltage of 125 keV. This scanner has a resolution of 256 by 256 pixels, with an inter- and intra-slice spatial resolution of 2.5 mm and 8.00 mm, respectively. Each pixel is a CT number in the range of 0 to 2,047, representing the X-ray absorption of the material. CT number 1,024 represents the absorption of water. In our experiment, 9 sections of different red oak logs and 3 sections of different yellow poplar logs, each being 10 to 18 inches long, were shipped to a local hospital where they were scanned. A total of 490 digital images were generated, with one sequence of images coming from each log section.

Once scanned the images were stored on 10 inch floppy disks that are machine readable by Digital Equipment PDP-11 computers running the RT-11 operating system. The images on these double density disks were transferred to a VAX 11/785 computer for processing. All the CT images were then stored on magnetic 6250 bpi tapes. Several tape backup copies were made to insure that the CT image data base would not be lost. A single 16-bit CT image of size 256 x 256c pixels takes a memory of about 0.1 Mbyte when stored on the magnetic tapes.

4) *Slice Cutup*: After the sections were scanned they were returned to cold storage. Within a very few days each section was removed from cold storage and was cutup using a saw into very thin slice sections, so that each slice corresponds to a log volume appearing in one of the CT images. A local lumber company was hired to cut the sections into slices. To minimize kerf losses, a Woodmizer saw was used. As each slice was being cut from a section it was immediately labeled, washed, bagged with the other thin slices cut from the same section, and returned to cold storage. The goal was to perform all this additional processing without drying out the thin wood sections.

5) *Photographing*: The last step involved in creating the CT image data base was to take a 5 x 7 color photograph of each thin wood slice by a Pentax camera mounted on a Bogen copy stand. This copy stand used four tungsten halogen lamps for an acceptably uniform illumination. To capture high quality pictures with good color contrast and saturation, a color filter (by HOYA) was used to convert the spectral characteristics of tungsten halogen bulbs into the spectral characteristics of the afternoon sun. The film used was Kodak Gold ASA 100. Appearing in each photograph is information that allows one to determine the CT slice number for which this thin wood slice is supposed to correspond, the log section from which the thin slice was cut, the log from which this log section was cut, the species of this log, as well as a ruler measuring the slice diameter with clear scale marks. The film negative and the 5 x 7 color print of each thin wood slice have all been saved for archival purposes. These 5 x 7 pictures will be used to determine what exposures should be enlarged to obtain 8 x 10 color prints. Each color photograph roughly corresponds to a CT image, giving a full color view of what is created using X-rays. These 8 x 10 pictures were to be used to compare the inspection results from the vision system with the actual defects inside the log.

4.5. Results and Analysis

Through the above described 5-step procedure of image collection, a total of 490 CT image slices, color photographs, and film negatives have been collected, and they comprise this image data base, which resides at the Spatial Data Analysis Laboratory at Virginia Tech. These images require 48 Mbytes of memory. In these images, one can clearly see the annual rings, knots, decay, cracks, and other internal defects. The images are so detailed that if one was to take a black and white photograph of the actual slice of the log, it would be difficult to tell the difference from the CT image. A careful visual inspection of the above collected image data base reveals that almost all defect features can readily detected and clearly identified with the human eyes. This supports the argument that the CT imaging modality can be used for automated inspection of hardwood logs

4.5.1 Experiment Results

Fig. 4.2 shows the CT images of a cross-section of a red oak segment (sample RK11.20), which contains 2 knots, a split, a decay, bark, and clear wood. The knots have an elliptical shape, and it is located half way between the log center and bark since the location of this cross-section is half way between the two ends of the knot in the log. The CT-number of knots range from 1100 to 1300, while those of decay range from 560 to 800. The CT-number of bark ranges from 850 to 1050, and from 900 to 1150 for clear wood. The narrow split runs through the pith and has CT-number approximately from 350 to 550. Also visible on the image are the circular annual rings in the clear wood area.

Fig. 4.3 shows the CT image of a cross-section of another red oak segment (sample RK12.05), which has bark, a large dark area of decay at the center, several splits that run through the decay, and clear wood. The decay pixels have CT-numbers ranging from 450 to 730, the bark pixels are from 1050 to 1250, and the splits are from 290 to 450.

Fig. 4.4 shows the CT image of a cross-section of a yellow poplar segment (sample YP06.21), with bark, sapwood, heartwood, a knot, and the pith. The outmost layer of bark has CT values from 850 to 930, the knot is from 950 to 1050, and the pith's CT value is approximately 338. From this CT image, one can clearly separate sapwood from heartwood, since the former has CT-numbers from 990 to 1060 and the latter 550 to 620.

The CT image in Fig. 4.5 is from a second yellow poplar segment (sample YP01.15), which illustrates 2 elliptical knots growing in 2 different directions, part of the bark, the pith, and clear wood which shows no separation of sapwood and heartwood. The CT values of these two knots range from 600 to 850, the bark from 730 to 930, and the clear wood from 520 to 660. The pith is one dark dot on the slice and has a CT value of 250.

From visual inspection of these image scans, some features of the hardwood log defects are defined and examined over a large number of sample images from the two species. These features include CT-number, defect size (in pixels), geometric shape in 2-d (the 3-d shape will be discussed in detail in chapter 6), and their relational positions inside the log. The results are listed in table 4.1 and 4.2 respectively. The blank entries in these two tables indicate that the corresponding items are not available or cannot be determined.

In summary, for red oak the CT imaging system can detect most defects including knots, splits, holes, and decay. However some pixels of bark are mixed with those of stain. Furthermore bark cannot always be differentiated from clear wood. For yellow

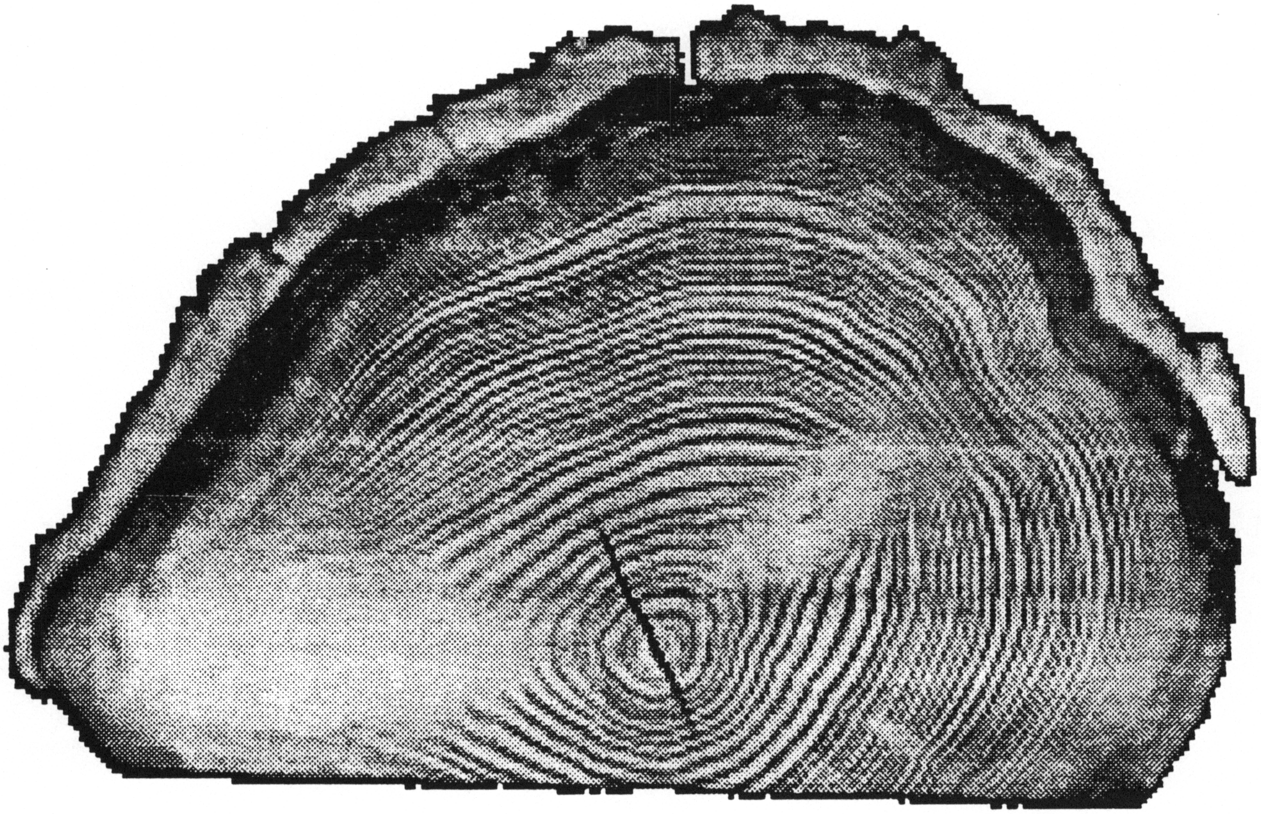

Fig. 4.2 Sample image Rk11.20 showing split, knots, bark, and decay

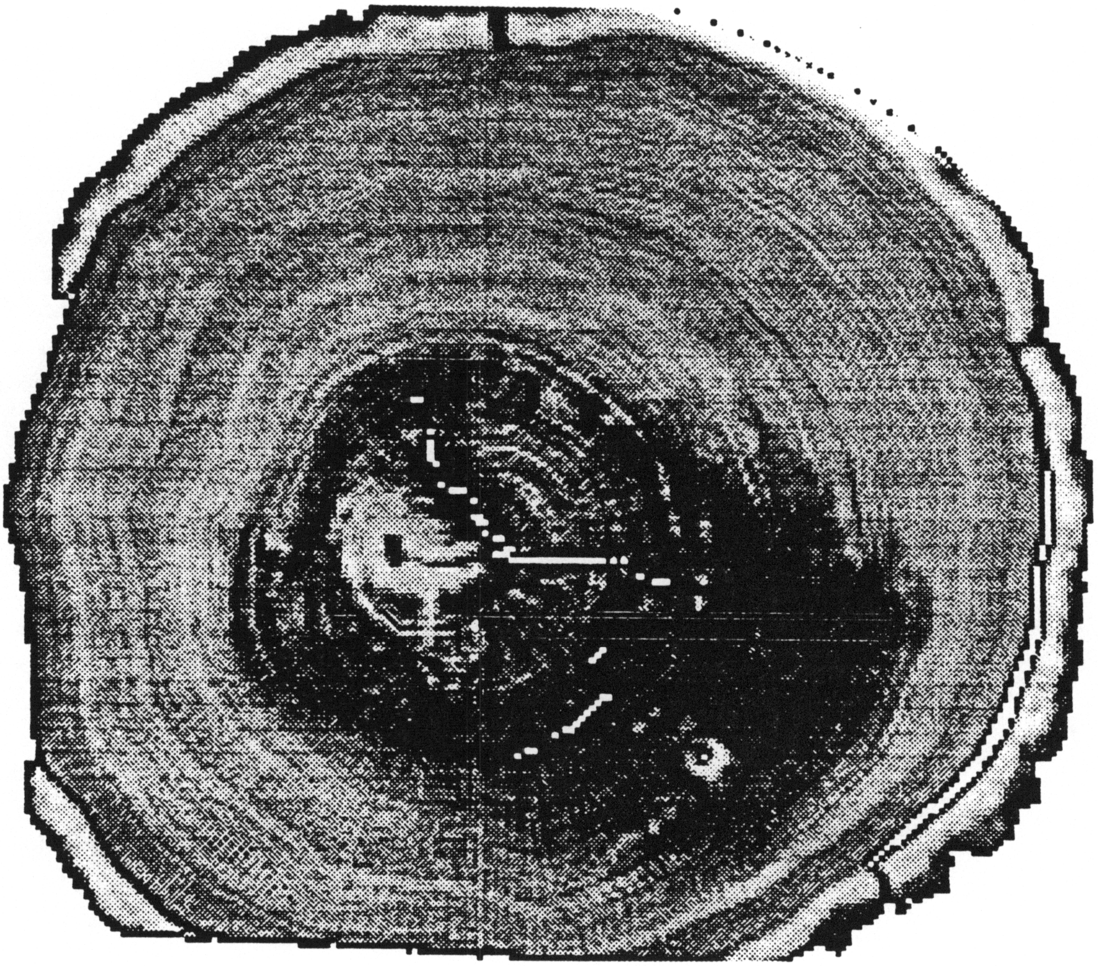

Fig. 4.3 Sample image RK12.05 showing decay, bark, and split

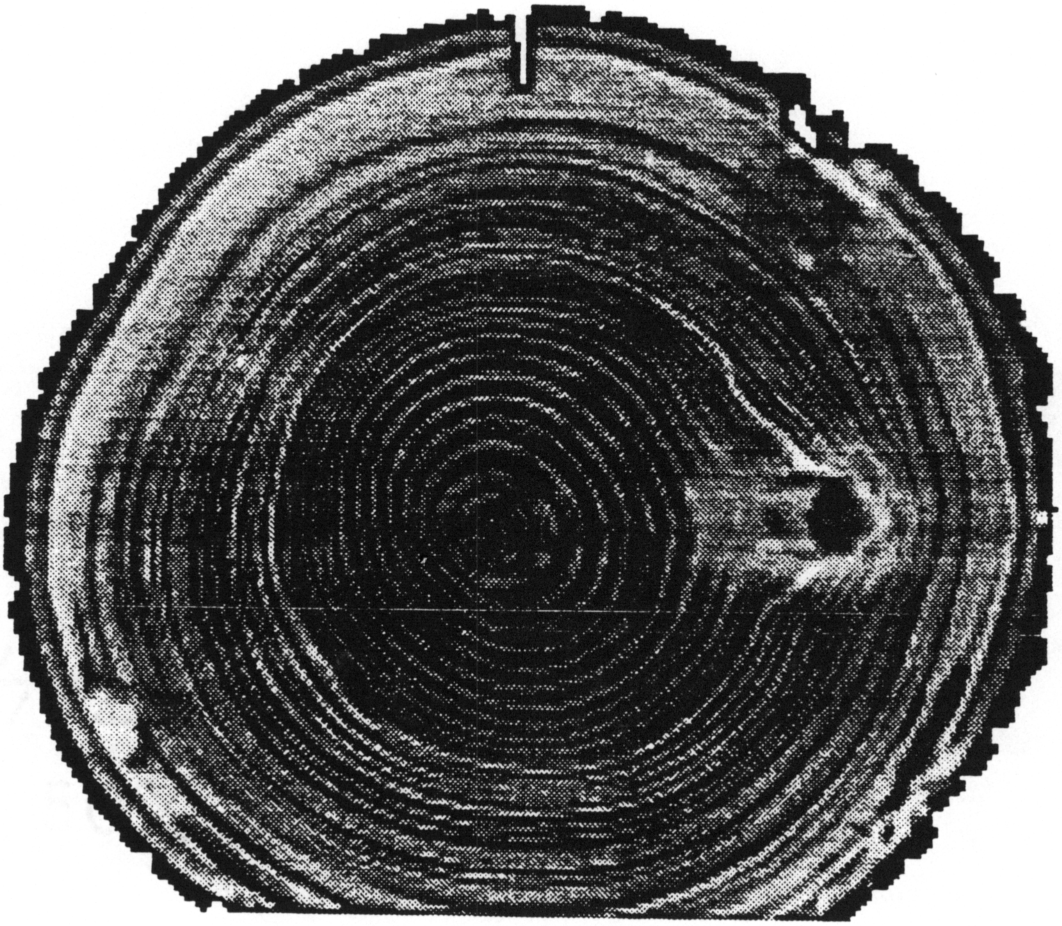

Fig. 4.4 Sample image YP06.21 showing sapwood and heartwood

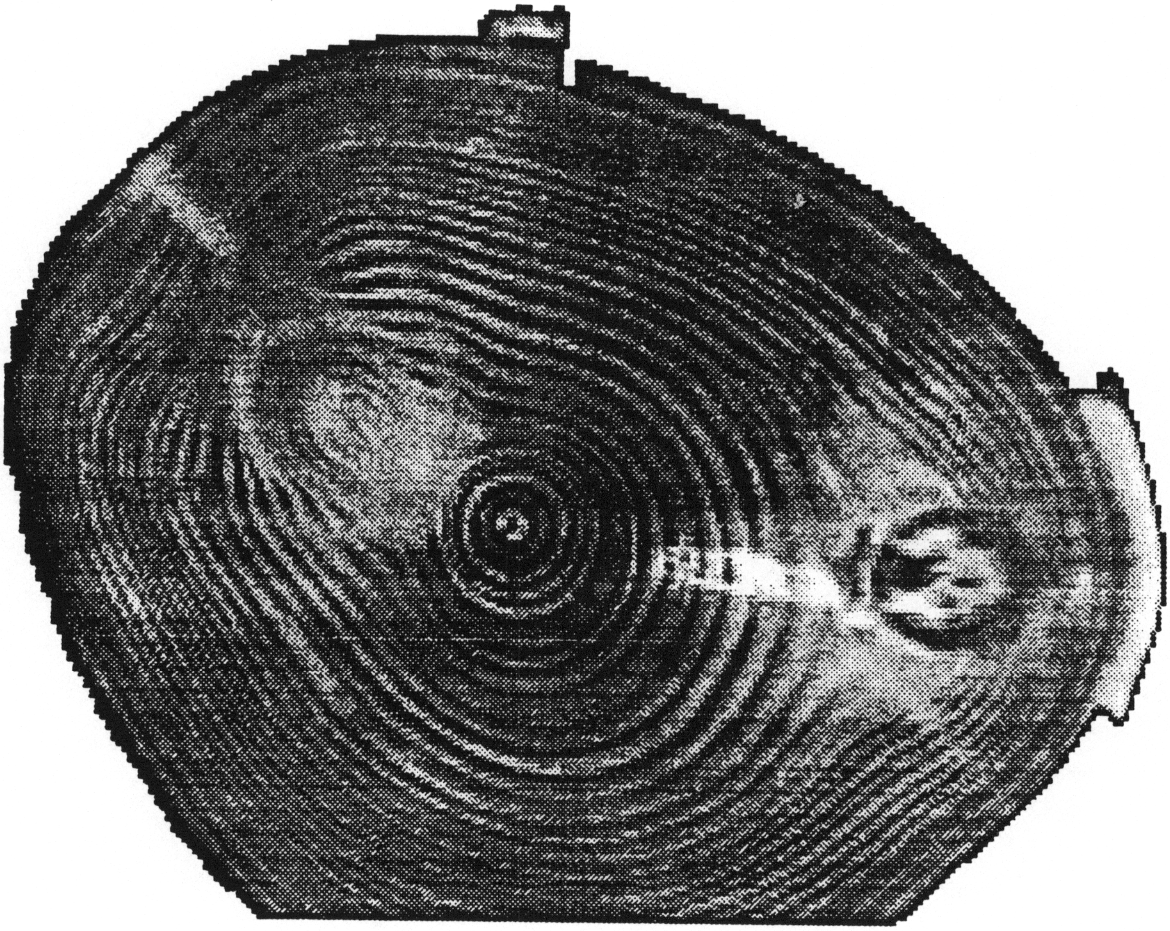

Fig. 4.5 Sample image YP01.15 showing two elliptical knots

Table 4.1 Experiment Results with Red Oak Images

Wood Material	CT-Number	Size (pixels)	2-D Shape	Position
knots	1140-1300		elliptical	from center outward
splits	390-550	30-150	narrow lines	run through pith
holes	200-500		circle	inside knots, in clear wood
stain/decay	500-800			inside clear wood
bark	850-1050		narrow band	outmost layer
pith	300-500	1-5	dot	trunk center, on splits
clear wood [a]	900-1100	largest area on a slice		

a. Sapwood can not be separated from heartwood.

Table 4.2 Experiment Results with Yellow Poplar Images

Wood Material	CT-Number	Size (pixels)	2-D Shape	Position
knots	800-1100		elliptical	from center outward
splits	NA[b]			
holes	250-450	10-100	circle	inside knots
decay/rot	600-800			inside clear wood
bark	800-1030		narrow band	outmost layer
pith	250-380	1-5	dot	trunk center
sapwood	880-1070		narrow band	next to bark
heartwood	420-860	largest area on a slice		trunk center

b. NA - Not available from the image samples.

poplar, CT numbers can differentiate knots, bark, and clear wood, as well as being able to differentiate sapwood and heartwood in green logs.

4.5.2 Discussions and Analysis

The image data base that has been collected is basically representative of most hardwood species, since they represent the two extremes of the hardwood species spectrum - ring porous and diffuse porous species. It is representative in the sense that it contains almost all the major hardwood grading defects with their representative features, features that can be used to recognize general hardwood defects by an automated vision system.

Although only CT images of two hardwood species, red oak (ring porous species) and yellow poplar (diffuse porous species), have been collected and examined in this study, the results that have been obtained from experiments with them can be extrapolated (generalized), to some extend, to the rest of the hardwood family.

For example, from table 4-1 and 4-2 it can be seen that all knots, whether in red oak or yellow poplar, have CT-numbers that are greater than those of clear wood and other defects, that they have the elliptical shape in 2-dimensions, and that they grow from log center outward. In addition, holes and splits in both red oak and yellow poplar have lower CT-numbers than do clear wood, and they have round and lengthy shape in 2-dimensions, respectively. In general, these defect features are expected in other hardwood species as well.

The major discrepancy between red oak and yellow poplar is that decay and stains exhibit slightly different patterns of x-ray intensity variations and different CT-numbers, which need to be carefully considered in designing the recognition algorithms of a machine vision system for log inspection. As previously pointed out in section 4.2, the image data as collected by a CT scanner contain far more information than the CT images viewed by the human operator. However, from the experiments and evaluation reported in the above, it can be argued that almost all hardwood defects can be manifested very well by the mapping of their x-ray attenuation coefficients on their CT images, and that a machine vision system approach can be adopted for the automated inspection of internal wood defects.

Due to the intrinsic limitations of CT imaging modality and the human visual system, some of the defects can not be differentiated easily in some cases. For example, pith is not readily recognized and in some cases is totally lost on some of the collected CT images (Fig. 4.1). This is so because the resolution of the CT scanner used is 2.5 x 2.5 mm (between pixels) which makes it impossible to detect a pith that is 1-2 mm in diameter. The wood decolorization, associated with decaying and staining fungi in heartwood, causes the wood to change to different colors, such as white decay and brown decay. The different colors of decay and stains may be manifested as similar CT-numbers, making them hard, if not impossible, to be discerned when the contrast of the display device is not appropriate.

Nevertheless, some visual improvements of CT images are possible so as to facilitate image analysis. The psychophysical considerations involved in the perception of CT images have been established. In particular, it has been shown that in examining an image, the human visual system and machine vision systems have response characteristics strongly dependent on 1) the luminance levels of an imaging device, including achievable levels of contrast and latitude, 2) the relative spatial and temporal frequency content of the image, and 3) the information density or noise levels present within the image (or the observer).

Due to the limited scope of this dissertation, however, the issues associated with these three aspects were not explored.

4.6 Summary

An image data base is needed to study the human and machine vision systems, and conduct computer sawing simulations. It also can be used to compare different imaging modalities. The data base collected in this study is representative of most hardwood species since it contains the two extremes of the hardwood spectrum. Visual inspection and analysis of these CT images show that most of the wood defects are manifested through attenuation coefficient variations, variations that may be recognized by a machine vision system.

The accuracy of interpretation of a CT image is closely related to observer performance, image properties, and the decisions made by a vision system. The performance of a vision system must be evaluated through a data base of images collected for its task. However, the evaluation of CT images is a complex task that involves the human perception and analysis of a number of physical and psychological variables. Instead, methods based on signal detection theory, such as receiver operating characteristics (ROC) curves, are often used in practice to evaluate the performance of machine vision systems. Due to the limited scope of this dissertation, we did not address the problem of how to use the methods described in this chapter to evaluate the vision system's performance in automated log inspection.

Chapter 5
Image Segmentation Module

This chapter proposes a 3-d image segmentation method for the low-level *segmentation module* of the machine vision system for hardwood log inspection. In particular, this method consists of four steps: (1) noise filtering, (2) image thresholding, (3) morphological operations, and (4) 3-d connected volume labeling. The results of the *segmentation module* are forwarded to the *scene analysis* module.

5.1 Problem Statement

5.1.1 Vision System Decomposition

As pointed out in Chapter 2, an important part of this research is to demonstrate the feasibility of developing a machine vision system for hardwood log inspection. A key element in establishing this feasibility is to create methods that can separate or detect various defects from clear wood and background (air). This will, on the one hand, generate a number of 3-d objects that are to be recognized by the recognition module of the vision system, and, on the other hand, speed up the overall vision system by eliminating the unnecessary processing time spent on non-defect data. After defect separation or segmentation, an object recognition stage is needed to identify the various defects detected in the segmentation stage.

Therefore, the proposed machine vision system can conceptually be divided into the following three basic components:

(1) a CT scanning unit for image data acquisition,
(2) a low-level module for image segmentation (object detection), and
(3) a high-level module for scene analysis (object recognition).

The function of the data acquisition unit is to acquire CT images by scanning the sample log according to prescribed requirements, which have been discussed in the previous chapters. The primary objective of the segmentation module is to separate grading defects from clear wood and background, while the objective of the scene analysis module is to classify the defects. This chapter concentrates on the image segmentation module, and the next chapter will treat the scene analysis module.

5.1.2 Objectives of Segmentation Module

The first objective of the segmentation module is to eliminate the unwanted noise (annual ring structure) from the log images. As demonstrated in chapter 4 on wood characterization by CT, the annual ring structures in hardwood log CT images tend to diminish the perception (by human observer) and detection (by machine vision system) of the grading defects in wood. If they are not removed before image segmentation, the regions that are detected by the segmentation module will not correspond to the actual defects in the image since most segmentation algorithms are very sensitive to high frequency noise (annual rings) [BAL82] [JAI89]. In this study, a 3-d spatial filtering algorithm has been developed as an image processing technique to smooth out these rings to insure efficient segmentation.

The second objective of the segmentation module is the 2-d image segmentation. To segment an image into meaningful parts needs to develop a feature extraction - decision rule algorithm that performs the object classification. In using CT to log inspection, the classes generally correspond to anatomic or physiological structure information. Examples of potential defect classes (objects) in log CT scanning include knots, decay, holes, splits, stains, bark, and clear wood. The successful application of image segmentation processes to the problem of structure recognition requires that some *a priori* information about the desired objects be used. This consideration is necessary because in a complex scene one must employ the knowledge about an object to extract the boundary of the object. To be successful in locating objects, the extraction method must be context sensitive.

The third objective of the image segmentation module is associated with the *labeling* process whereby groups of pixels are assigned individual labels, with each label identifying a distinct object in the image. Once an image has been segmented into parts (volumes in 3-d) that consist of grouped pixels, a label must be assigned to each of the parts. The label of a volume serves the purpose of identifying it as an distinct entity in the 3-d image. The criterion for region labeling can be any one of a number of well known methods [BAL82] [JAI89] [CHO91]. In this study, a 3-d volume growing method is developed based on a natural generalization of 2-d *connected component labeling* (CCL) [SHI87].

5.2 Image Processing Method

5.2.1 Image Processing Problem

Removing unwanted image detail can be an essential step in successful image interpretation (scene analysis). From the analysis of the CT image data base presented in

Chapter 4, the annual ring structure in a log manifests itself as a dense circular texture in the image (Fig. 4.2).

The major problem caused by these annual rings is that they produce artifacts or spurious regions during the image segmentation step. Fig. 5.1 illustrates a case where image segmentation produces false object regions due to the presence of these annual rings in the image. As such, the presence of annual rings can mislead any graylevel-based image segmentation method, e.g., the multi-thresholding method to be discussed next. Since the annual rings tend to adversely affect the quality of the image segmentation, they can also adversely affect the later scene analysis tasks of the machine vision system. Hence they must be removed by some image processing technique as the initial step in the machine vision system.

Therefore, an important problem in CT log image analysis is how to get rid of these unwanted annual rings while preserving other important image details, e.g., the small splits and holes. Since the actual effect of these annual rings on image analysis is like that of image noise, the rings can be regarded as high frequency noise for purposes of CT log image analysis. There are a number of noise removal techniques that have been studied in image processing. A commonly used method for noise removal is pre-processing operation based on an image model or image statistics.

5.2.2 Image Processing Techniques

Image processing can be defined as techniques, operations, or processes which modify an image or group of images to enhance the visibility (for either human visual system or machine vision systems) of useful information while suppressing "noise" or non-useful information.

Depending on the decision to be made about the information contained in an image, it is evident that the roles of information and noise in an image can be reversed. That is, in general, different aspects of an image are useful in making different decisions. There are thus no one optimal image-processing techniques; the nature of the image-processing algorithm depends on the desired information that needs to be extracted in specific applications.

It is important to note that image processing techniques do not create new information. The information content in the processed image is always less than or equal to that in the original image. Because no additional information is generated, image processing techniques alone cannot be expected to greatly enhance the object recognition (scene analysis) of a machine vision system.

There are many different image processing techniques [BAL82] [CON83] [KAS86] [SHI87] [JAI89], each designed specifically for particular types of problems. They include image smoothing, image optimal filtering (linear or nonlinear), image restoration or enhancement, image sharpening and unsharpening. As stated in the previous section, the objective of the image segmentation module of the vision system under study is to separate defects from clear wood and background (air) in the image. The discussion of this section will concentrate on the elimination of the unwanted annual ring structures from the clear wood area of the log CT image, by an image filtering method. Two most commonly used techniques of image processing are image smoothing and image filtering operations [BAL82] [JAI89].

Image smoothing: Smoothing techniques are those which selectively remove the higher frequencies in an image. They include gradient inverse smoothing, adaptive smoothing, and the nonlinear smoothing [WON81] [LEE80]. Smoothing is particularly appropriate for the enhancement of large, smooth objects with prominent high spatial frequency background noise, such as the clear wood area with annual ring structures, shown in Fig. 5.1. It should be noted that image smoothing causes a decrease in graininess in the image accompanied by a loss of fine detail (Fig. 5.1).

Image Filtering: Image filtering is used to filter an image so as to restore the signal while suppressing the noise, or to increase the signal-to-noise ratio (SNR). It is usually not possible to selectively remove the noise completely from the image by image smoothing, which is most of the time a linear operation. However, if certain characteristics of the noise are known, linear or non-linear filtering methods can be used to maximize SNR of the image. The most commonly used image filtering methods include Wiener filter, Kalman filter, median filter, and σ-filter [BAL82] [UNS90] [JAI89].

5.2.3 A 3-D Adaptive Filtering Scheme

For nonlinear smoothing of digital images, Lee's adaptive filter [LEE90] is particularly efficient. It computes a weighted sum of the noisy image and of the output of a moving averaging filter that provides an estimate of the local image average value. However, this approach assumes that the image noise is uncorrelated Gaussian, and that the image is locally ergodic and stationary so that local statistics can be used to estimate ensemble features. Unser's method [UNS90], on the other hand, adaptively computes a linear combination between a noisy image and a restored (filtered) version of this noisy image

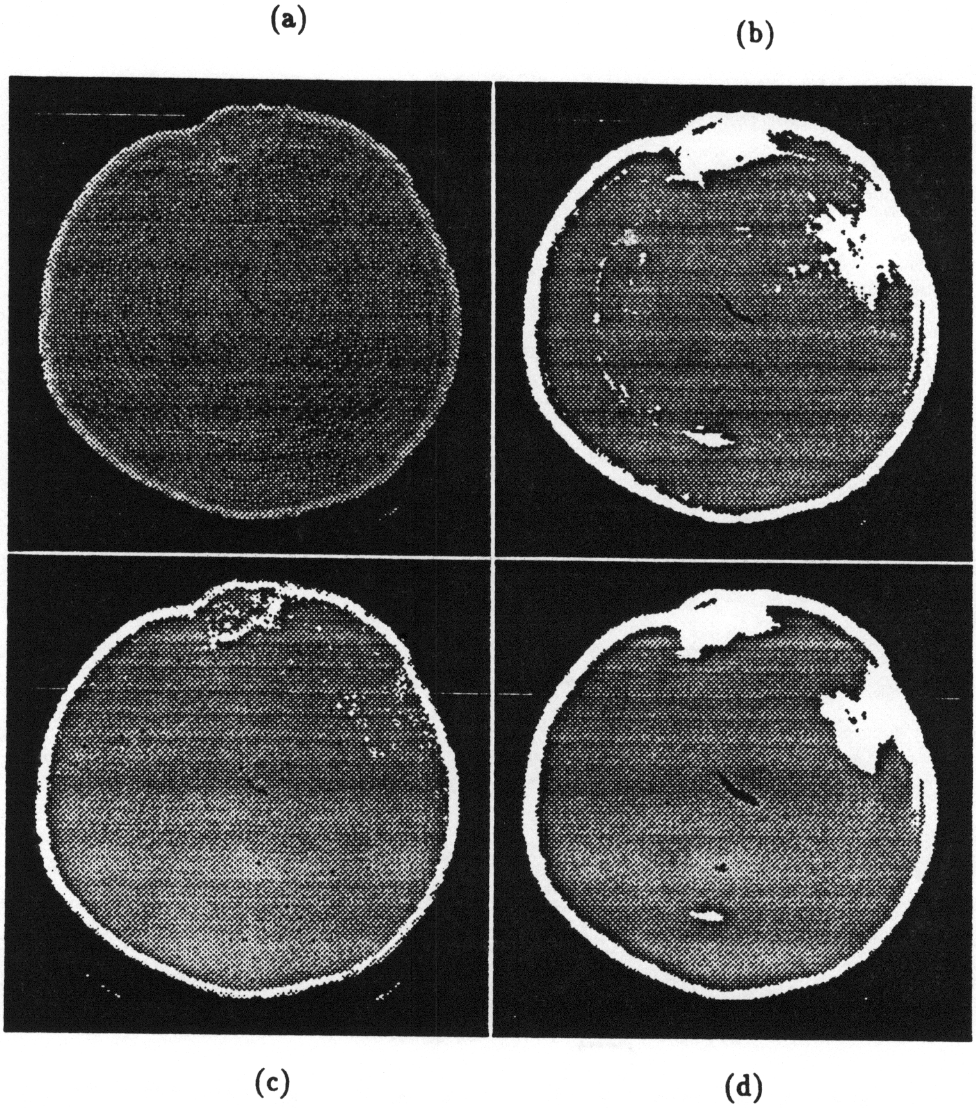

Fig. 5.1 Sample image Log4.65: original (a), segmentation using Unser's filter (b), Gaussian filter (c), and the 3-d adaptive filter (d)

obtained by an *initial filtering*. The purpose of this procedure is to improve image restoration performance by using a rather simple structure. In contrast with previous work, this approach is based on a filter of fixed structure rather than on simplifying assumptions about the signal model. Simulation and experiment examples indicate that it is capable of reducing noise efficiently while preserving image details. Apparently, image filtering or smoothing using this procedure depends heavily on the structure of the initial filter.

It is assumed that subscripts i, j, and k are used to represent the x, y, and z coordinates of an image in 3-d. As in most cases, the observed image signal $x_{i,j,k}$ at spatial location (i,j,k) consists of two uncorrelated components: the true signal $u_{i,j,k}$, and corrupting noise $n_{i,j,k}$ with known variance σ^2 (or the noise sample variance which can be estimated on a window of data taken from the background area). Thus a 3-d image $x_{i,j,k}$ can be expressed as

$$x_{i,j,k} = u_{i,j,k} + n_{i,j,k} \qquad (5\text{–}1)$$

Filtering or smoothing is adopted to improve the signal-to-noise ratio (SNR) at most points of the image. However, in regions of heavy edges or texture, filtering may degrade the image more than it actually reduces noise. In this case, a compromise would be not to do any filtering of the data (such as the pixels of a split in the log). On the other hand, for non-textured or non-edged areas (such as clear wood), we may want to filter them using some kind of filtering operation. Accordingly, to obtain an optimal estimate of the true image signal at point (i,j,k), $z_{i,j,k}$, a weighted sum of the noisy signal, $x_{i,j,k}$, and its filtered (or restored) version, $y_{i,j,k}$, is constructed by [UNS90]

$$z_{i,j,k} = a_{i,j,k}x_{i,j,k} + b_{i,j,k}y_{i,j,k} \qquad (5\text{–}2)$$

with $y_{i,j,k}$ as a convolution expressed by

$$y_{i,j,k} = x_{i,j,k} * h_{i,j,k} \tag{5–3}$$

In Eq. (5-3), $h_{i,j,k}$, called the initial filter, is a linear or nonlinear space invariant operator, $y_{i,j,k}$ an initially restored version of the noisy image by this operator. Note that $a_{i,j,k}$ and $b_{i,j,k}$ are the coefficients that are to be adjusted so that (1) for edged regions (such as splits), the noisy observation $x_{i,j,k}$ is retained by down weighting (through reducing $b_{i,j,k}$) the restored signal $y_{i,j,k}$; and (2) for non-edged regions (such as clear wood), the initial restored signal $y_{i,j,k}$ is retained by down weighting (through reducing $a_{i,j,k}$) the noisy observation $x_{i,j,k}$.

In general, the above defined 2-d filter structure works fine on 2-d images and outperforms some of the other image filtering or smoothing methods. In [UNS90] the 2-d initial filter $h_{i,j,k}$ is implemented as a simple 2-d moving averaging filter, and the 2-d output $y_{i,j}$ at point (i,j) from this initial filter is an average of the pixels in a window centered at that point. However, this spatial least squares (LS) method does not consider the important problem of how to choose the initial restoration filter $h_{i,j}$ for specific applications. Research indicates that it suffers from excessive edge smoothing and texture blurring when applied to CT log images. This 2-d method would smooth out some of the fine details such as splits and checks. For instance, Fig. 5.1 shows one such case where several segments of a fine split are lost after image filtering and segmentation.

It is noted that the pixel value $x_{i,j,k}$ at point (i,j,k) on the *k*th slice is closely correlated with those at its neighboring points on the (*k-1*)th and (*k+1*)th slices in a sequence. Hence one way of improving the filter performance would be finding the optimal solution for a

LS problem defined in a finite 3-d volume. By solving this 3-d problem, filter coefficients ai,j,k and bi,j,k in equation (5-2) can be computed from image data in consecutive slices of a sequence. This extended 3-d filter also uses consecutive cross-sectional images to perform the initial image restoration on the pixels in a volume V_y from these consecutive image slices. The output of this initial filter is expressed as

$$y_{i,j,k} = \sum_{l=-L}^{L} \sum_{m=-M}^{M} \sum_{n=-N}^{N} x_{i-l,j-m,k-n}\, h_{l,m,n} \tag{5–4}$$

where L, M, and N are the proper dimensions of the 3-d volume V_y on which the initial image restoration is performed, and their typical values are from 1 to 3, depending on input images. Operator hi,j,k can be chosen as the averaging filter as in [UNS90], the 3-d Gaussian smoothing filter, or other linear or nonlinear filters [UNS90] [ZHU91c].

To compute the optimum filter coefficients $a_{i,j,k}$ and $b_{i,j,k}$ for the final estimate of the image signal at each point (i,j,k) on the *k*th slice, a similar LS criterion is introduced to minimize the quadratic error over V

$$\varepsilon^2(a,b) = \frac{1}{N_r} \sum_{(i,j,k)\in V} (z_{i,j,k} - u_{i,j,k})^2 \tag{5–5}$$

where V is defined as a 3-d volume cubic with dimension D_v, and N_r is the number of pixels in the cubic. Typical value for D_v is from 3 to 7 [ZHU91c]. In order to find the optimum solution for the filter coefficients ai,j,k and $b_{i,j,k}$, let us assume, for the time being, that these two coefficients are constant over the volume V though they are later allowed to change at different spatial points. Note that $z_{i,j,k}$ is computed using Eq. (5-2), and that $y_{i,j,k}$ is defined by Eq. (5-4). For simplicity in the following discussion, the subscripts i, j, and k of all the variables will be omitted.

Following the procedure similar to that in [UNS90], the filter coefficients are computed by finding the optimal solution to Eq. (5-5). However, to insure that the average intensity (brightness of the image) at a given point (i,j,k) remains unchanged, i.e., $E[z] = u$ whenever $E[y] = u$, where $E[x]$ means taking the average of a variable x, the following additional constraint is necessary

$$a + b = 1, \qquad \text{or} \;\; g(a,b) = a + b - 1 = 0 \tag{5–6}$$

The minimization criterion then becomes

$$e(a,b,\lambda) = \varepsilon^2(a,b) + \lambda g(a,b) \tag{5–7}$$

where λ is a dummy Lagrange multiplier. Setting to zero the partial derivative of e with respect to a, b and λ leads to the following three equations:

$$\frac{\partial e}{\partial a} = 0, \frac{\partial e}{\partial b} = 0, \frac{\partial e}{\partial \lambda} = 0 \tag{5–8}$$

Simple mathematical manipulation of Eq. (5-8) gives the following system of equations

$$a\Sigma xx + b\Sigma xy + \lambda = \Sigma ux \tag{5–9}$$

$$a\Sigma xy + b\Sigma yy + \lambda = \Sigma uy \tag{5–10}$$

$$a + b = 1 \tag{5–11}$$

where integration Σ is taken over the volume V. This set of equations can also be expressed equivalently in the matrix form

$$\begin{bmatrix} \Sigma xx & \Sigma xy & 1 \\ \Sigma yx & \Sigma yy & 1 \\ 1 & 1 & 0 \end{bmatrix} \begin{bmatrix} a \\ b \\ \lambda \end{bmatrix} = \begin{bmatrix} \Sigma ux \\ \Sigma uy \\ 1 \end{bmatrix} \tag{5-12}$$

When replacing the unknown variables in this matrix by their expected values, we have

$$\begin{bmatrix} S_{xx} & S_{xy} & 1 \\ S_{yx} & S_{yy} & 1 \\ 1 & 1 & 0 \end{bmatrix} \begin{bmatrix} a \\ b \\ \lambda \end{bmatrix} = \begin{bmatrix} S_{ux} \\ S_{uy} \\ 1 \end{bmatrix} \tag{5-13}$$

where

$$S_{uv} = S_{uv}(i,j,k) = \frac{1}{Vr} \sum_{(i,j,k)\in V} u_{i,j,k} v_{i,j,k} \tag{5-14}$$

with $u_{i,j,k}$ and $v_{i,j,k}$ representing any two of the unknown variables under discussion.

Finally, by evaluating the matrix inverse, we find that the optimal solutions to the minimization criterion of Eq. (5-7) are given by

$$a_{i,j,k} = 1 - (1-\rho)\sigma^2/P(i,j,k),\ b_{i,j,k} = 1 - a_{i,j,k} \tag{5-15}$$

where constant ρ, called the residual noise correlation coefficient, is defined as

$$\rho = h(0,0,0) = [(2L+1)(2M+1)(2N+1)]^{-1} \tag{5-16}$$

if $h_{i,j,k}$ is defined as an averaging filter. P(i,j,k) is given by

$$P(i,j,k) = S_{(x-y)(x-y)}(i,j,k) > 0 \qquad (5-17)$$

which is a local estimate of the variance of the difference between the noisy and filtered signal which we will refer to as the residue. This is a particularly simple implementation of the adaptive constrained least squares filter.

Note that in Eq. (5-15), the term $(1-\rho)\sigma^2$ is the residue variance when filtering is not on the signal component, i.e., when the residue variance is due to noise alone. Hence whenever the residue energy is small, the adaptive scheme will allocate a prominent weight to the filtered signal. On the other hand, when the residue energy is greater than this level the weight is shifted to the unfiltered signal. The above argument is consistent with the fact that an unusually large value of P(i,j,k) is an indication that filtering tends to degrade the signal. Experiments using this 3-d adaptive filtering are presented later in this chapter.

5.3 Image Segmentation Method

As pointed out in the above, image segmentation is a process in which image elements representing the same material type are grouped together and referred to as a single entity. In general, there are two basically different methods for image segmentation: (1) methods based on edge detection, and (2) methods based on region detection.

5.3.1. Edge-based Segmentation

Edge Detection Methods: These schemes search for *edges* between regions [BAL82]. Most of these methods use a gradient operator, followed by a threshold operation on the gradient, in order to decide whether an edge has been found. Some methods use the constraints of neural networks or optimization. The results of edge detection is a binary image indicating where the edge points are or a list of the edge pixels, possibly with attached description such as direction and contrast. To form closed boundaries surrounding regions, a further step of linking or grouping of edges that correspond to a single boundary is required.

One of the most successful methods in this category for scanned image segmentation is the edge-detection operator created by taking the Laplace derivative of a Gaussian kernel [BAL82] [JAI89]. This method has an adjustable parameter (i.e., the full-width-half-maximum or the standard deviation σ^2 of Gaussian kernel), which requires user interaction. The user interaction may cause difficulty in automating the segmentation.

While the edge-detection method can guarantee the formation of regions with closed boundaries, these boundaries are often inaccurate since the edge-detection is very sensitive to noise, particularly between regions with small contrast differences.

A modification to the edge-detection method is the so called tracking method. The technique of tracking consists of those algorithms which track an edge or curves of objects. An initial pixel is identified as belonging to a curve or boundary, and successive pixels are examined until the entire boundary has been traversed. The acceptance criteria can depend on the contrast of the edge or its shape. Tracking often yields incomplete curves due to incomplete acquired borders. Techniques have been devised to enable bridging of these gaps on the tracked boundaries. A number of studies have been published regarding these techniques [BAL82].

5.3.2 Region-based Segmentation

Region Detection Methods: The simplest technique in this category is *thresholding*. The gray value or intensity of each pixel (or voxel in 3-d images) is compared to some threshold values, (as most edge-detection methods do to gradient), and the pixel is assigned to one of a few categories, depending on whether the threshold is exceeded or not. The threshold values are usually selected from a histogram of the image.

While thresholding methods focus on the difference of pixel values or intensities, the *region growing* method looks for groups of pixels with similar intensities. In its simplest form, the method starts with one pixel, called a seed, and then examines other pixels in the seed's neighborhood in order to decide whether all have similar intensities. If they do, then they are grouped together to form a region. In this way, regions are grown out of single pixels. More advanced forms do not start from pixels but with a partition of the image into a set of small regions. A uniformity test is then applied to each region, and if the test fails the region is subdivided into smaller elements [CHO91]. This process is repeated until all regions are uniform. Then regions are grown out of small regions, rather than pixels. The growth from the small regions uses a more sophisticated uniformity test on a region and its nearby regions.

One uniformity criterion compares the maximum difference between the value of a pixel and the average over a region including the pixel. A somewhat different definition of uniformity can be made by comparing the statistics over a region with the statistics evaluated over its parts. If they are close to each other, then the region may be called uniform. For example, one can evaluate the co-occurrence matrix [CON85] over each of the parts, and then compare the matrices with the region's matrix. If they are similar, the region is said to be uniform. In the growth from small regions, this statistical test is very useful. If the matrices of a region and its neighborhood are similar, the union of these regions belongs to a class.

An extension of the region growing and uniformity-testing methods is the splitting-and-merging technique [BAL82]. A simple example of this method starts with the entire image as the initial segment. Then each current segment is successfully split into quarters if the segment is not homogeneous enough as tested by a uniformity criterion. After the spit, the uniformity test is applied to a pair of adjacent quarters. If the test is satisfied, the two quarters are merged into a region. The process stops when additional splitting or merging is no longer possible. In another example, the image is represented as a quad-tree with the top of the tree corresponding to the entire image, the next level to the four quadrants of the image, and so on. The splitting-and-merging starts with the quarter at some intermediate level of the quad-tree. The a quarter is found to be non-uniform, then it is replaced by its four subsquares (split). Conversely, if four squares are found that form a uniform square, they are replaced by the uniform square (merge). This process may continue recursively until no more splits or merges are possible.

5.3.3 Segmenting Log Images by Multi-thresholding

Given the strong variation in wood density between different types of defects and between different species of hardwood logs, one or more *fixed* threshold are not appropriate for separating the log CT image into distinctive regions. In this study log images that have been filtered using the above 3-d adaptive filter are thresholded on an image-by-image basis, using a multi-thresholding scheme described in this chpater [ZHU91c] [ZHU91f].

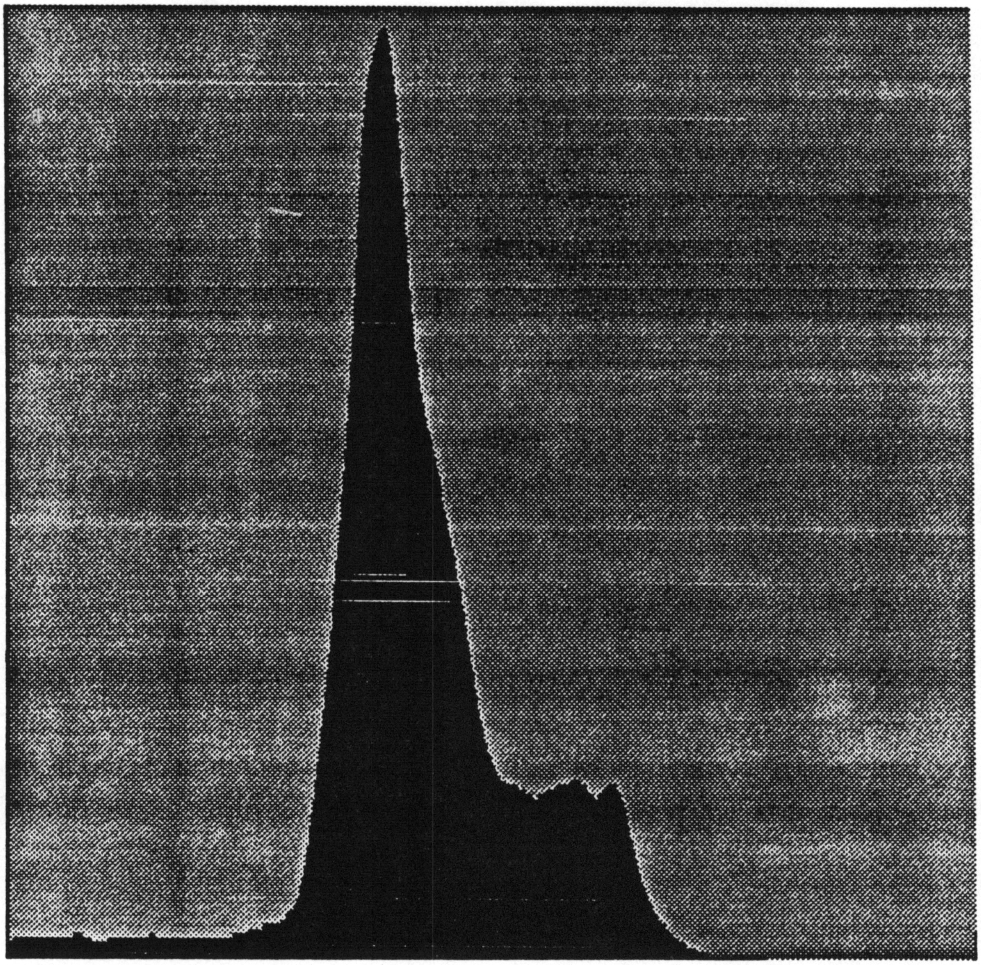

Fig. 5.2 The histogram of image YP01.21

showing only gray levels from 200 to 2,047

In this method, a histogram is first computed from the image data of each filtered image, and it is smoothed with 1-d Gaussian function to eliminate the spurious peaks in it. Fig. 5.2 illustrates an example histogram computed from a CT log image (sample no. Rk11.20). The proposed multi-thresholding operation is based on this smoothed version of the image histogram. According to the analysis on the data base in chapter 4, an ordinary mage contains pixels representing background, decay, splits, bark, knots, and clear wood. Since bark and knots both have similar CT-numbers, they are temporarily treated like a single type of defects and will be separated by the scene recognition module.

Accordingly, three thresholds $\{T_1, T_2, T_3\}$ are computed from the smoothed histogram $h(k)$ of an image. These three threshold values are determined according to the following criteria:

(1) T_1: $T_0 < T_1 < T_2 - d$, where T_0 and d are adjustable constants.

(2) T_2: the location of the maximum of $h''(k)$, the second derivative of $h(k)$.

(3) T_3: the location of the last zero-crossing of $h'(k)$, the first derivative of $h(k)$.

Using the above three thresholds, $\{T_1, T_2, T_3\}$, image segmentation produces a number of regions that have rugged boundaries, as well as a small number of spurious defect regions of different sizes. In order to facilitate the later processing steps and to improve defect recognition accuracies of the vision system, this latter category of regions needs to be eliminated before 3-d region detection (volume growing).

For this purpose, morphological operations [SER82] [HAR87] such as erosion and dilation are applied to the segmented image to remove the spurious regions and to smooth the rugged boundaries of defect regions detected by segmentation [ZHU91e].

Let variable x, y, and $b \in E^2$, where E^2 is a two dimensional space of integer numbers. Denote a digital image by X, structuring element by B, which is defined on a finite mask Ω, then $X \supseteq E^2$ and $B \supseteq E^2$. Accordingly, if we denote $B_y = \{y+b \mid x \in X, y \supseteq E^2\}$, the these two morphological masks can be expressed by the following operations:

(1) erosion operation: $X \otimes B = \{y \mid B_y \supseteq X\}$

(2) dilation operation: $X \oplus B = \{x+b \mid x \in X, b \in B\}$

In image erosion, a structuring element B scans the image X in a raster order, and it eliminates a pixel of X if none of its neighboring pixels in Ω has the same value as it has. Whereas in image dilation, the gray levels of all the neighboring pixels in Ω are changed to that of the center pixel. These morphological masks can be defined by a series of windows of size N x N, with N = 3, 5, 7, and so on.

In this study, an image erosion operation is first performed on the segmented image to get rid of those small, spurious areas. As a second morphological step, an image dilation is performed to restore those pixels of the real defect regions that have been eliminated by the erosion operation. Fig. 5.4 shows an original red oak image (sample RK12.05), image segmentation, image erosion (N = 3), and image dilation (N = 3).

5.4 Object Detection by 3-D Volume Growing

The above filtering-segmentation and erosion-dilation processes produce a number of uniform regions in each 2-d image which, when grouped together in 3-d, represent 3-d information of the different wood defects inside a log. In this study, the 2-d version of the connected component labeling (CCL) algorithm [SHI87] has been modified to create a 3-d version, called *3-d connected volume growing* algorithm, to segment or group together individual 2-d regions on consecutive slices in 3-d integral objects.

Inside a log, defects manifest themselves in varying shapes. For instance, a knot in 3-d would appear like a paraboloid [LEE91], bark like a generalized cylinder, a hole like a cylinder, and a split like a ribbon, etc. To identify the proper 3-d volumes of potential defects, the proposed 3-d volume growing algorithm uses the concepts of 6- or 18-neighborhood connectiveness [BAL82]. In this way, pixels with similar CT attributes (e.g., CT-numbers) on consecutive segmented images are grouped together, giving a number of connected volumes in 3-d.

To describe this 3-d connected volume growing algorithm, let us first define the variables and procedures used in the algorithm. For an input 3-d image, consisting of a sequence of consecutive slices (pre-segmented images), denote the gray level value at point (k,i,j) and its assigned label (symbol) by f(k,i,j) and g(k,i,j) respectively, where (k,i,j) represents the (i,j) point (location) on the *k*th slice in a sequence of S pre-segmented images slices. Furthermore, let $p_1, p_2, \ldots, p_n$ denote the image pixel values of a set of n pixels, and $l_1, l_2, \ldots, l_n$ the labels at these points.

The 3-d volume growing algorithm that has been developed for the machine vision system is comprised of the following 4 procedures:

(1) LABEL(f, g)

(2) RESOLVE(Parent, ID)

(3) MERGE(l_i, l_j)

(4) FIND(int)

5.4.1 Procedure LABEL(f, g)

Procedure LABEL(f, g) assigns a set of m labels, $\{l_1, l_2, ..., l_m\}$, to the input 3-d image f(k,i,j) according to the pixel attributes and spatial connectivity. The output symbolic image, g(k,i,j), signifies the aspect of spatial connectivity that exists amongst pixels belonging to the same 3-d regions (objects). When raster scanning a sequence of S images, an image label l_i is given to each pixel of each image in the sequence. This label is to identify the pixel as part of a 3-d entity. Because our primary goal is to differentiate defects from clear wood and air, we need not label clear wood and air. For this purpose, a binarization process is adopted in whereby all defect pixels are marked 1 and the remaining pixels are marked 0.

In segmenting a 3-d image in a sequential fashion, to process the *k*th slice, pixels on the (*k-1*)th and (*k+1*)th slices are used so that the aspect of inter-slice connectivity is taken into consideration. Let us denote the image gray level value at the current location (k,i,j) by p_0, and its associated label by l_0, respectively. In the proposed 3-d volume growing algorithm, only pixels at the following N (N = 9) neighboring points of p_0 are used:

(*k-1*)th slice: {(k-1, i, j), (k-1, i-1, j), (k-1, i+1, j), (k-1, i, j-1), (k-1, i, j+1)};
*k*th slice: {(k, i-1, j-1), (k, i-1, j), (k, i-1, j+1), (k, i, j-1)}.

Let the pixel value at the neighborhood of pixel p_0 and their associated labels be denoted by $\{p_i\}$ and $\{l_i\}$ respectively, where i = 1, 2, ..., N. Note that the gray level and label at the previous center point (k-1, i, j) is now expressed as p_1 and l_1 respectively. Then Procedure LABEL(f, g) can be described by the following algorithm:

```
Procedure LABEL(f, g)
initially, SYMBOL = 0
for $p_0 != 0$ and $\{p_n, n = 1, 2, ..., N\}$
case 1.   if ($p_0 = p_n$), then
              $l_0 = l_n$
              if ($p_i = p_j$ AND $l_i != l_j$, for i, j = 1, 2, ..., n), MERGE($l_i$, $l_j$)
case 2.   if ($f_0 != p_n$), then
              if ($f_1 = 0$), SYMBOL = SYMBOL + 1, $l_0$ = SYMBOL
              else $l_0 = l_1$
case 3    if ($p_0 = p_n$ for all n), then
              $l_0 = l_1$
              for n = 2 to N, do
              if ($f_n != f_1$) MERGE($f_n$, $f_1$)
              enddo
return
```

5.4.2 Procedure RESOLVE(Parent, ID)

After applying the procedure LABEL(f, g) as described above, a tree of labels is created as a data structure for each individual 3-d entity or volume of the 3-d image. However, procedure MREGE tends to merge two or more volumes together by connecting them into an integral region. Thus, some of the trees so created may contain multiple labels that represent multiple entities in the scene.

Procedure RESOLVE(Parent, ID) is devised to resolve the ambiguity amongst these multiple labels. Its input is a 1-d array Parent(k) that is a set of M pointers used to connect labels at individual pixel locations. The output is a different 1-d array ID(k) containing M' distinct labels, M' < M. Secondly, to generate a digital image, IMG(k,i,j), for the labeled 3-d image, Procedure FIND(int) is used to convert values of the array ID(k) into IMG(k,i,j), the 3-d digital image of the labeled scene. Procedure RESOLVE can be described as follows:

```
Procedure RESOLVE(Parent, ID)
step 1.    initialization k = 0
           for i = 1 to M, do
           if Parent(i) != ROOT, then
           k = k + 1
           ID(i) = k
           enddo
step 2.    at each defect point (k, i, j)
           int = g(k, i, j)
           l= FIND(int)
           IMG(k, i, j) = ID(l)
return
```

5.4.3 Procedure MERGE(l_i, l_j)

In the above algorithm, procedure MERGE(l_i, l_j) is a subroutine in which two individual voxels with labels l_i and l_j are merged into an integral 3-d entity. To facilitate this merge operation, a tree data structure is created for each object and the labels of these two voxels are stored in two nodes of the same tree. To signify the parenthood of a node in a tree, a pointer from a node l_i is designated as a parent Parent(l_i). To perform merge of two nodes, we must first find their respective parents, denoted by F_1 and F_2, and then merge them according to the values of F_1 and F_2. In this way, all the voxels that are connected but have different labels in a sequence of the labled CT images will be merged onto the same volume representing a 3-d object. Initially, the root of each tree is assigned a label of ROOT = -1. Procedure MERGE(l_i, l_j) accomplishes this goal and can be expressed as follows:

```
Procedure MERGE($l_i$, $l_j$)
input node: $l_i$, $l_j$
$F_1$ = FIND($l_i$)
$F_2$ = FIND($l_j$)
if ($F_1 < F_2$) then Parent($F_2$) = $F_1$
if ($F_2 < F_1$) then Parent($F_1$) = $F_2$
return
```

In the above, l_i and l_j are two labels to be merged onto the same tree. FIND(int) is another procedure that will be described below. F_1 and F_2 are two integers that represent the parents of nodes l_i and l_j in the tree structure. Procedure MERGE(l_i, l_j) establishes a connecting bond between two nodes l_i and l_j by creating a pointer from the node of smaller value to the other node.

5.4.4 Procedure FIND(int)

Each time a merge operation takes place using the above trees structure, it is necessary to first find the parents of the two nodes in the tree that are to be merged. To serve this purpose, a procedure called FIND(*int*) is defined, where variable *int* is an integer number representing a label l_i. This procedure performs two functions: (1) update the parent of the variable int until it points to the root of a tree; and (2) update the parents of all the nodes on the tree that are above the variable *int*. It is expressed as follows:

```
Procedure  FIND(int)
temp1 = int
do while (Parent(temp1) > 0)
    temp1 = Parent(temp1)
enddo
temp2 = int
do while (temp2 < temp1)
    itemp = Parent(temp2)
    Parent(temp2) = temp1
    temp1 = itemp
enddo
FIND = temp1
return
```

5.5 Results

The image segmentation method discussed in the above has been tested with the CT log images in the data base. Fig 5.2 illustrate the histogram computed from a CT image of red oak. The threshold values T_1, T_2, and T_3 can be computed from a smoothed version of this histogram using the method described previously, and they are used to segment the image into regions for knots, bark, split, and clear wood.

Fig. 5.1 shows image segmentation results (sample LOG1.65) that are obtained by using the Gaussian filter [LEE80], the 2-d [UNS90], and 3-d adaptive filter. It is clearly seen that the 3-d adaptive filter could eliminate most of the annual rings while preserving the texture structure of knots, bark, and clear wood. Fig. 5.3 illustrates another example of image segmentation (sample RK11.20) that are obtained using σ-filter [LEE80], the 2-d [UNS90] and 3-d adaptive filters.

Fig. 5.4 illustrates one example of erosion and dilation on a CT image. It shows the original image, segmentation, erosion, and dilation of a slice from a red oak log (sample RK12.05).

Fig. 5.5 shows the segmentation of a red oak slice that contains a lengthy split at the center of the log. Fig. 5.5 (a) is the original CT image of the slice, and Fig. 5.5 (b) is the segmented image after using the proposed 3-d adaptive filtering to eliminate the rings.

Finally, Fig. 5.6 and Fig. 5.7 depict the result from using the proposed 3-d labeling algorithm where 4 segmented images in a sequences (samples LOG4.06 to LOG4.09) are labeled using a 16-neighborhood connectiveness. Fig. 5.6 contains the original images of these 4 slices, and Fig. 5.7 contains the labeled objects. On all these 4 slices, the outside bark, the center knot, the center split, and the outer split are connected into 4 integral entities with labels 1, 2, 3, and 4 respectively. For purposes of illustration, the gray levels of these 4 images have been re-scaled manually. If each of these 4 slices is labeled individually (in 2-d), they contain 8, 73, 10, and 59 regions respectively, and the total number of the labeled regions is 150. Whereas using the proposed 3-d connectiveness labeling method on the 4 images (in 3-d), the total number of the labeled regions is 73. If region elimination is adopted to remove those regions that are smaller than a threshold T, the total number of regions is reduced to 87 in the former 2-d case, and 4 in the latter 3-d case. Due to the fact that this image is not morphologically filtered, clusters of small dots around the knot on some of these 4 slices are observed.

5.6 Summary

This chapter has discussed a 3-d image segmentation method which consists of four basic steps. In particular, it has discussed (1) a 3-d adaptive filter to remove the unwanted high frequency rings from log CT images; (2) image segmentation using multiple-thresholding; (3) image morphological operations (erosion and dilation) to eliminate spurious areas while smoothing defect boundaries; and (4) a 3-d connectiveness labeling algorithm. Experiment with the images in the data base has demonstrated that the described 4-step segmentationa method is efficient in separating defects from clear wood and background while preserving the properties of defects. Output from this 3-d volume growing algorithm is a number of 3-d objects that are to be recognized or interpreted by the high-level scene analysis module to be discussed in the next chapter.

In addition, this 3-d segmentation approach can also perform quantitative estimation of the structure of a 3-d object, and this volumetric information can be used in recognizing unknown structure in a scene. This estimate can be achieved by counting the number of voxels that have the same label li assigned by the proposed 3-d volume growing algorithm. Any volume smaller than a preset threshold value is eliminated by merging it with its nearest neighboring volume or with the background. This further merging process usually eliminates false defects resulted from segmentation, and retains the well-connected 3-d objects as defects, such as knots, splits, decays, and holes.

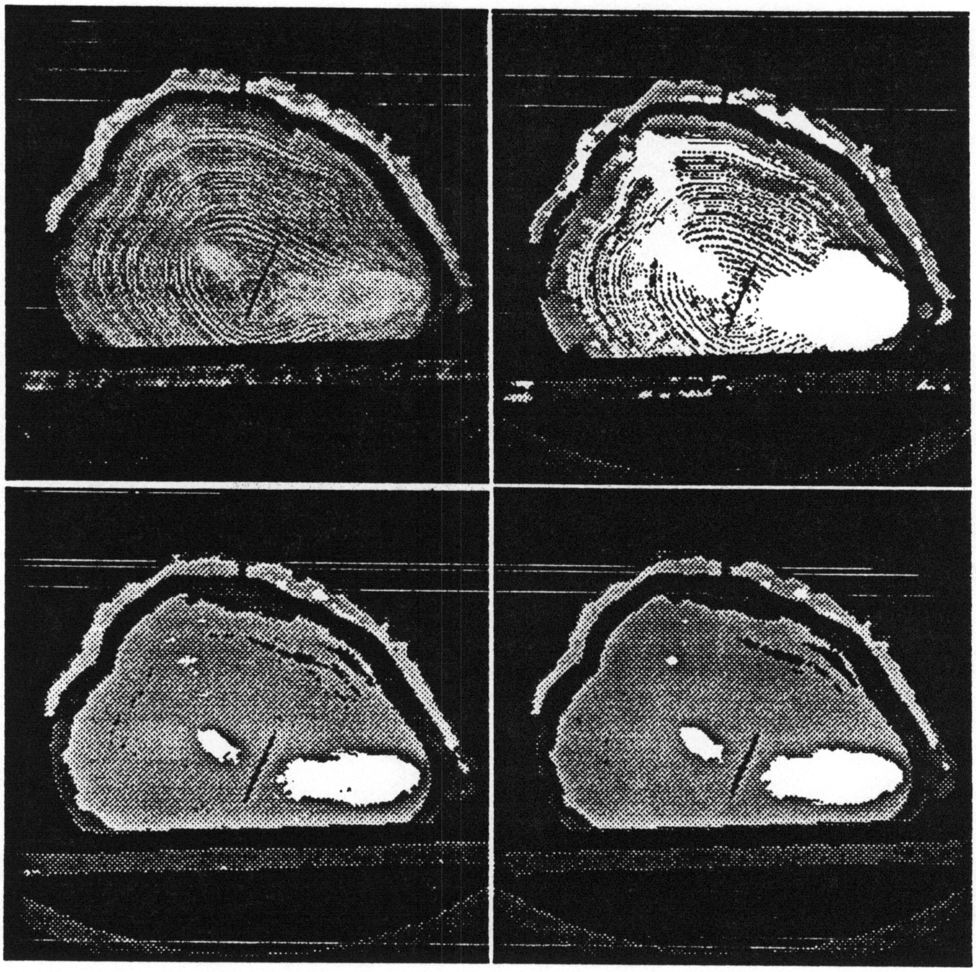

Fig. 5.3 Sample image Rk11.22: original (a), segmentation using σ-filter (b), Unser's filter (c), and the new 3-d adaptive filter (d)

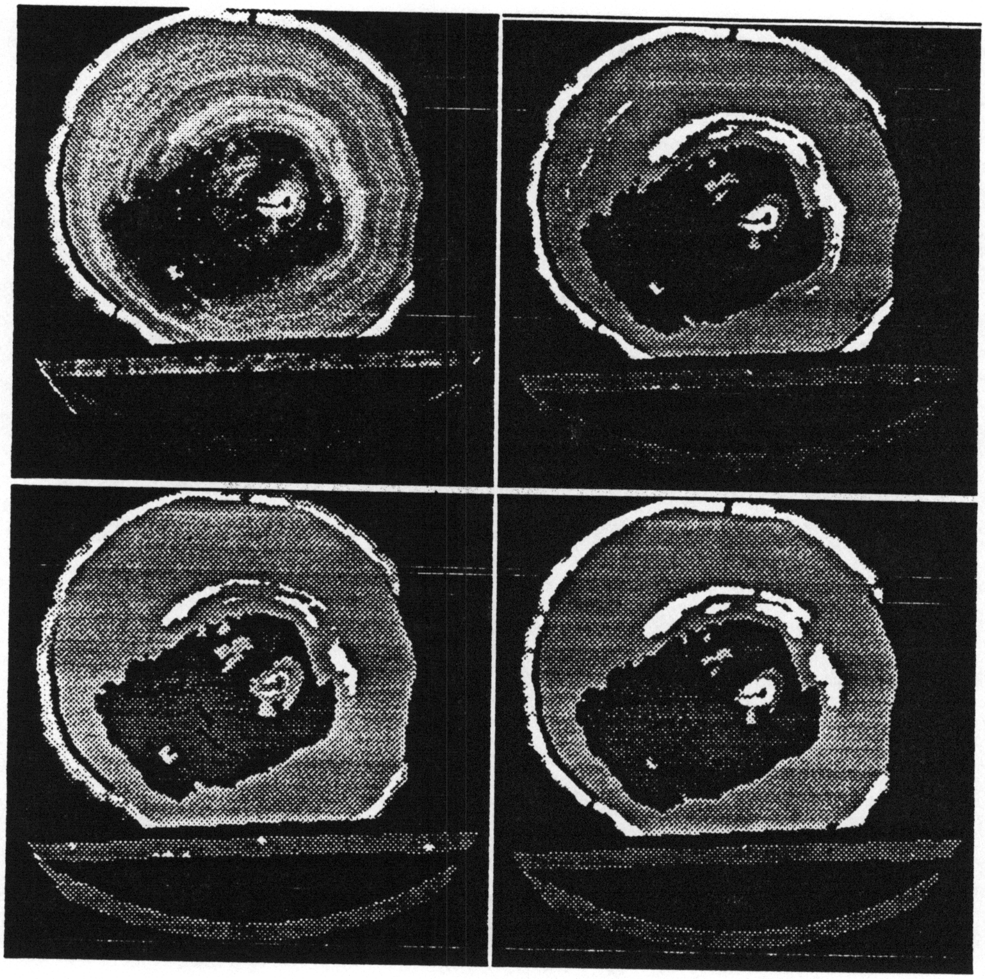

(a) (b)

(c) (d)

Fig. 5.4 Sample image RK12.05: original (a), the segmentation (b), erosion (c), and dilation (d)

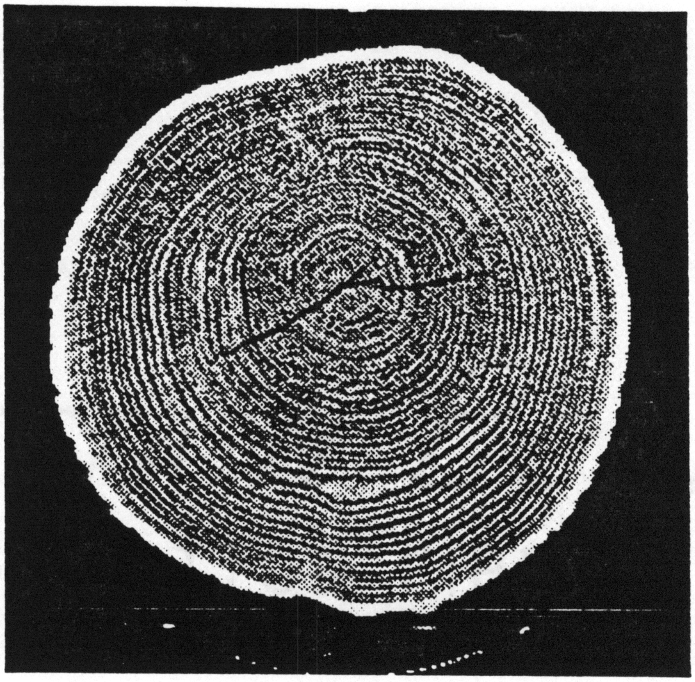

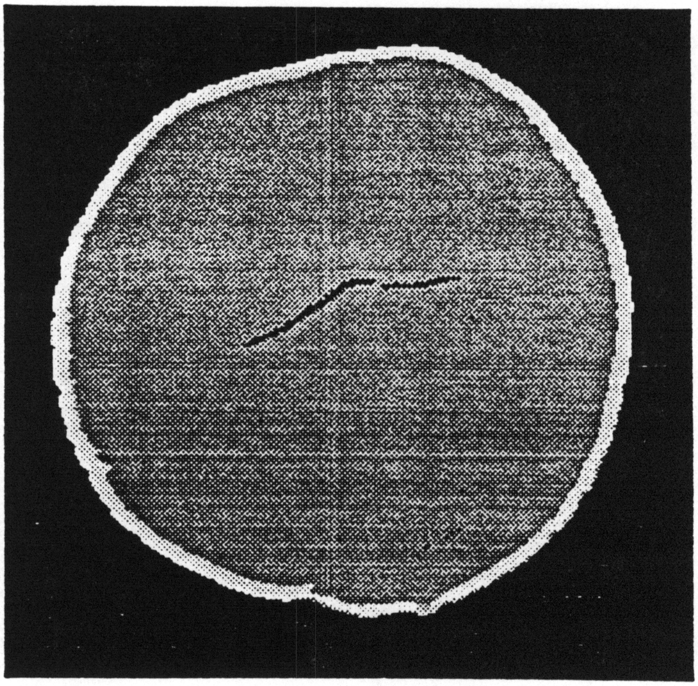

Fig. 5.5 Sample image Log3.10: original (top), and segmentation (b)

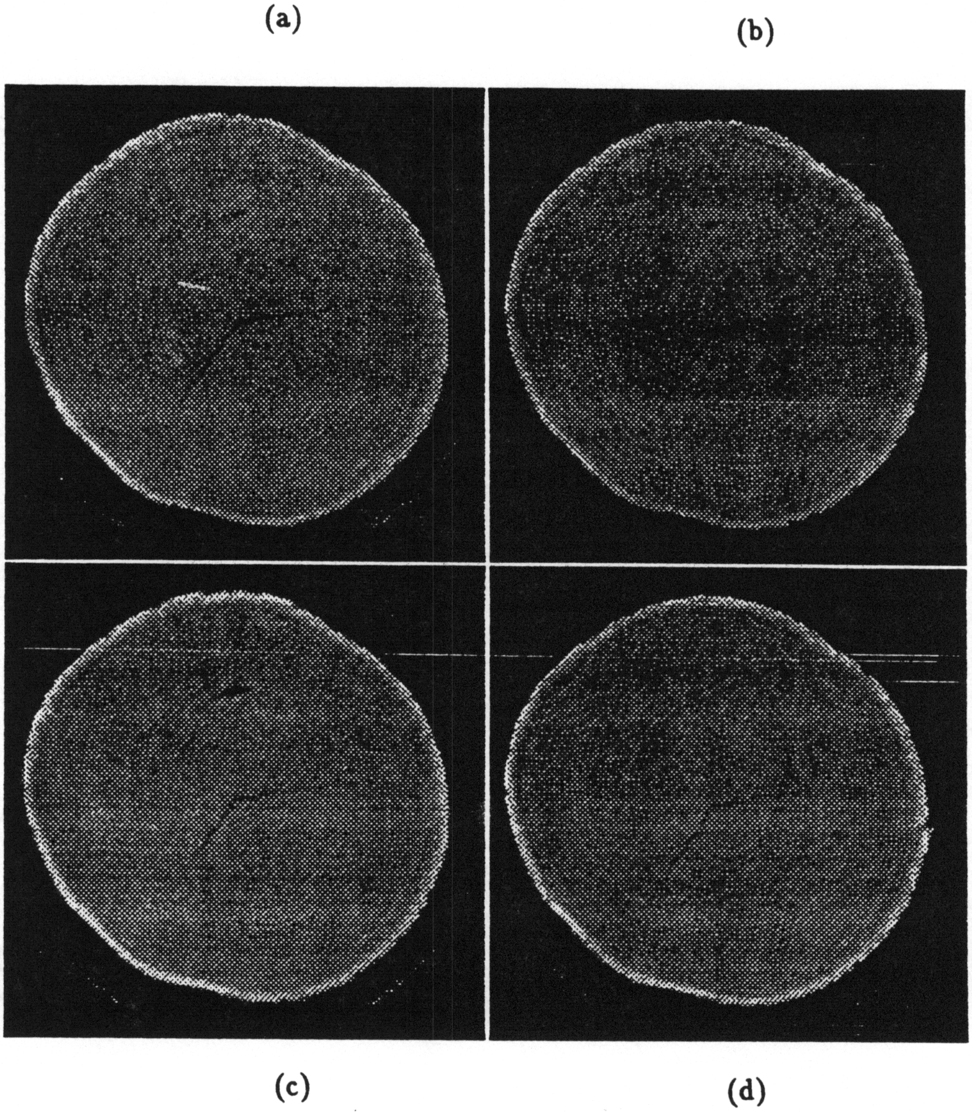

Fig. 5.6 (a-d) Sample image Log4.06-09: 4 slices in a sequence

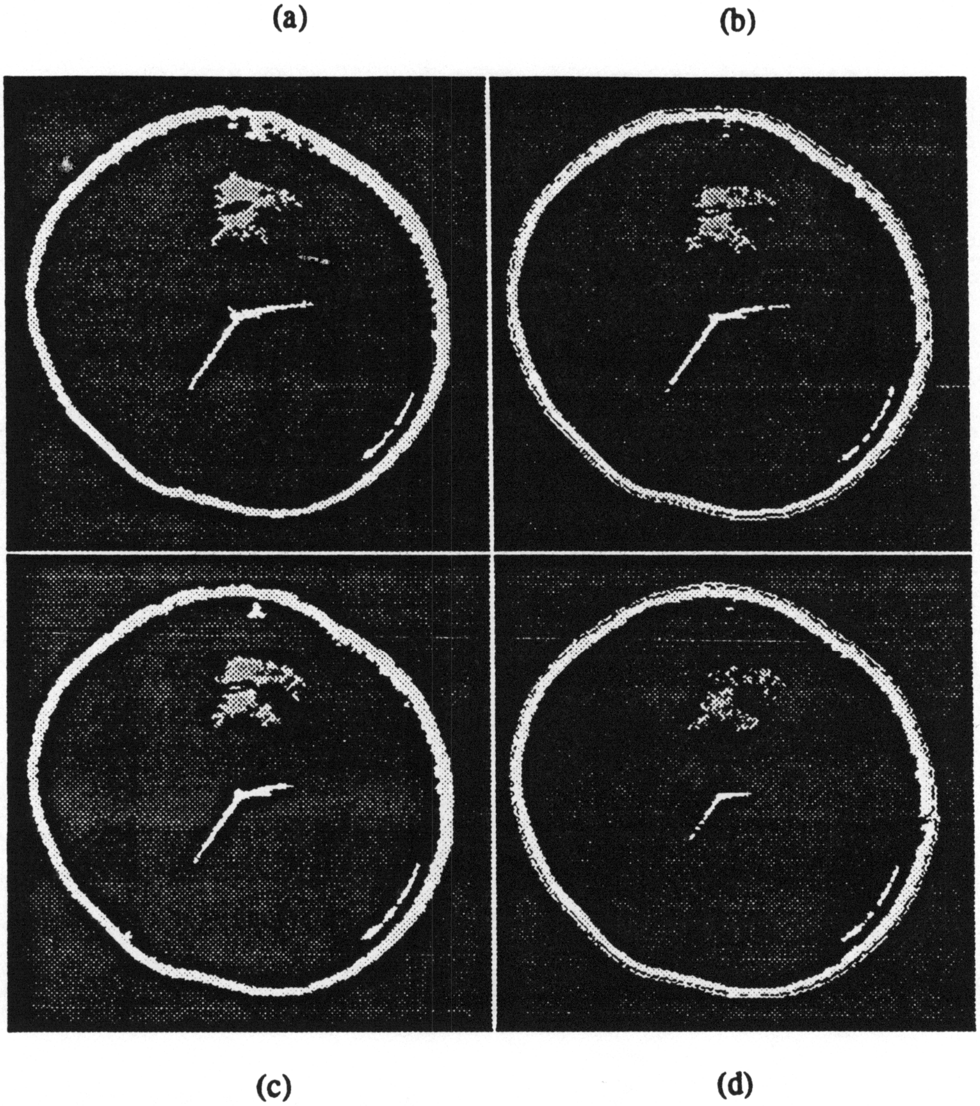

Fig. 5. 7 The 3-d volume growing result of the images in Fig. 5.6

Chapter 6
Scene Analysis Module

This chapter describes the scene analysis involved in log inspection. It reviews the general aspects of 2-d and 3-d shape analysis as a means of object recognition. Finally it presents a knowledge-based approach to log defect recognition. In particular, it describes a set of defect features that seem to be appropriate for hardwood log classification, and applies the Dempster-Shafer (D-S) theory of evidential reasoning to perform object recognition under uncertainty.

6.1 Problem Statement

Defect properties or features derived from hardwood log CT images, such as density, texture, geometric properties, and topological relationships, could all be used to interpret or infer the identity of internal log defects as they manifest themselves in CT imagery. The purpose of the scene analysis module of the machine vision system discussed in this work it to extract features or properties from the CT imagery and use them to recognize or categorize the various defects, using some type of reasoning algorithm. Because log CT images are rich in wood grain textures, texture analysis for wood detection is also an very important research topic and it is treated in the next chapter. This chapter concentrates on defect classification by 3-d object recognition.

Given the CT characteristics of wood defects, as discussed in Chapter 4, statistical or analytical classification procedures alone are difficult to successfully implement. Less exacting methods are required on this scene analysis problem [BUC84] [QIA90] [PEA86]. A heuristic, knowledge-based (rule-based) recognition system is described in [CHO90] for identifying *surface* defects in sawn lumber. Knowledge-based systems are flexible in that special rules can be written to handle exceptions [GOR85]. Combining domain independent low-level image heuristics with domain specific heuristics in a high-level module creates a very general recognition mechanism, one that can handle different wood species in automated log inspection.

In addition, the integration of information from multiple log defects requires a computer program that models complex relationships similar to the reasoning or judgment process of an experienced log grader, who evaluates the over-all log condition by analyzing information from available indicators on internal and surface defects. These relationships must be acquired from so-called domain experts. This acquisition usually requires a prototyping approach with several iterations. Furthermore, since false positive can not be excluded totally, the vision system must be able to indicate the reason for any detection generated - explanation component of a knowledge-based system - to allow the human grader to check the validity of the detection result.

A knowledge-based approach meets these requirements on two counts: (1) it provides functionality for defining complex relationships on a higher cognitive level than third generation computer languages, thereby facilitating the required iterative design of prototypes; and (2) the explicit definition of knowledge to be used in a knowledge base to enable the required explanation of the system's conclusions by a comparatively simple trace and analysis of the inference process.

In most practical cases, however, our observation of objects is *inexact*, our representation of objects is ambiguous or *fuzzy*, and our propositions about hypotheses based on a collection of evidence are *uncertain*. Uncertainty arises from a variety of sources, such as unreliable and incomplete information, imprecision in measurements, and ambiguities in object descriptions, and so forth. Moreover, when an object is represented by a number of features which may or may not be independent with each other, the decision that could be reached about the identity of the object needs to be based on the information or evidence from all the knowledge sources - belief propagation or information pooling.

To tackle the imprecision in representing ambiguous information about wood defects, the Dempster-Shafer model for imperfect knowledge [DEM67] [SHA76] is adopted to present log defect features. The evidential reasoning method based on Dempster's rules [DEM67] is used to combine evidence about an object that is collected from different knowledge sources. It is an efficient method for reasoning under uncertainty, since by this theory, evidence that only partially favors a hypothesis should not be construed as also partially supporting its negation. This means, belief about the negation of a hypothesis does not depend on belief in the hypothesis itself.

Because of the above, the machine vision system proposed in this study adopts a knowledge-based (rule-based) approach to perform 3-d object recognition. An intuitive, simple rule-based expert system for the log inspection task was first studied and tested on a number of images [ZHU91d] [ZHU91e] [ZHU92b]. More recently, a vision system of which the inference engine is based on the theory of inexact reasoning has been developed. In the current vision system, the knowledge representation is based on the Dempster-Shafer (D-S) model for imperfect knowledge, and the inference engine is based on the

Dempster-Shafer theory of evidential reasoning (uncertainty reasoning). The scene analysis module of this machine vision system is comprised of the following three steps:

(1) compute image features from the labeled volumes by the segmentation module.
(2) determine the degree of beliefs of each object by the D-S model.
(3) perform object recognition by evidential reasoning.

6.2 Object Recognition by Shape - A Review

6.2.1 Object Shape Analysis

Many stages of the scene analysis module can be facilitated by the analysis of the shape of contours (outlines) in the image. For example, object recognition may be strongly guided by the expected shapes of the external outlines of the wood defects to be recognized. Once a boundary of a specified structure has been determined, either by automated or manual methods, it is expected that there is sufficient specific information contained in the size, configuration, and orientation of the boundary. The quantification and analysis of these quantities is generally referred to as shape analysis.

Shape analysis methods may be classified into two general categories: decision-theoretical classification methods [BIN82] [DUD73] [DEV82] [ZHU92c] and syntactic classification or description methods [PAR77] [KFU82]. Decision-theoretical methods extract well-defined (in a mathematical sense) shape features and employ classic statistical decision theory to classify the original shapes. Syntactic or structural methods, on the other hand, classify shapes by reducing them to fundamental subpatterns, sometimes called primitives or morphs. These subpatterns may be defined to provide considerable flexibility.

The use of decision-theoretical methods may be made rigorous and may draw on a significant amount of research and statistical estimation and detection theory [JAI89]. This approach is often useful when geometric and variant measures are extracted and used as shape descriptors. The primary goal of such methods is classification of a shape into one of several known categories. The feature extraction portion of the decision-theoretical shape analysis methods operates on a contour and generates numeric parameters (measurements). These parameters are directly and strongly dependent on contour shape and relatively insensitive to contour position or orientation (invariant when subject to rotation and translation). A shape analysis method based on objects' boundary feature is described in [ZHU92c]. In this study, an object is represented by its *fuzzy* boundary. Object classification is achieved by image registration and object subtraction.

Syntactic methods are closer to an intuitive concept of pattern recognition [PAR77] [KFU74]. They attempt to reduce shape to a collection of subpatterns that correspond to a limited number of ideal shape constituents. The identities of the fundamental building blocks of these shapes and their relationship may then serve to classify or to describe a shape. Although the rigorous mathematical foundation of syntactic methods is less well developed than that of decision-theoretical ones, this approach is readily understandable and offers great promise for future development. Syntactic methods of shape analysis requires that the information in the contour to be decomposed into a set of primitive shapes. The primitives are the low-level of pattern elements and provide a succinct and complete description of the contour shape in terms of previously specified structural relations.

6.2.2 3-D Shape Analysis

The information content in 3-d contours is considerably higher than that of planar (2-d) contours. Since the 3-d shape of anatomic structures of log may contain correspondingly large amounts of information useful for log sawing, it is advantageous to explore methods for extraction and classification of information from the 3-d structures. Attempts to characterize 3-d shapes fall into two categories. The first category employs a 2-d projection of a 3-d figure, whereas the second category uses serial sections formed by passing parallel planes through a 3-d figure.

Attempts at using 2-d projections include the work in [TSI74], which devised a 3-d shape grammar that can determine whether two shapes are the same, or mirror images, or are dissimilar. [TSI74] also has analyzed 3-d shapes from perspective drawings. Other attempts have been made to partially use and analyze 2-d views or projections of 3-d objects [ROB65] [BAL82] [SHI87]. However, the characterization of 3-d shape using 2-d projections is a difficult task that has not yet proven to be completely successful.

If a 3-d object is specified by serial sections, then the object may be analyzed in terms of generalized cylinders [BAL82]. Cross-sectional contours of a generalized cylinder are specified as a function of the distance measured along a line perpendicular to the cross-sections. Elliptic cylinders were used in [GIP75] where each cross-sectional contour is an ellipse. These cylinders are restricted so that the slices are always parallel to a coordinate plane.

Cuzzi [CUZ77] has suggested several approaches to the characterization of 3-d shapes using serial sections. Cuzzi [CUZ77] first standardizes an object by calculating its inertia tensor, using the centroid of the object as the original of the coordinate system. Diagonalizing the inertia tensor then yields new X, Y, and Z axes for the object. Finally, the coordinates are transformed by scaling the object volume to a standard volume. When all objects are standardized, then differences in surface point coordinates are due to shape differences. If the cross-sections are convex and a cylinder coordinate system is used, then the radius measurements, for a set of Z values and a set of angle values, give a set of measurements sensitive to the shape of the object. The measurements, however, are sensitive to the manner in which the Z values and angle values are chosen. Cuzzi [CUZ77] has also derived analytical expressions, called surface equations, that specify the coordinates of all surface points for a given object.

It has been found by Cook [COO78] that once the object has been standardized and transformed by Cuzzi's transformation, the contours formed by the intersection of the planes in the 3-d object are unique. There are three such curves for each object, and they may be defined as the canonical curves or contours associated with a 3-d object. Hence, the analysis of the shape of the 3-d object may be reduced to the analysis of its canonical contours.

[DHA91] describes an anatomical knowledge-based computer vision system that interprets CT and MRI images of the human chest cavity. The approach utilizes a low-level image analysis system with the capacity of analyzing the data in both bottom-up (or data-driven) and top-down (or model driven) modes to improve the high-level recognition process. The system applies the knowledge of reference anatomy at both the 2-d slice-based analysis level and the 3-d volume-based analysis level. The process of recognizing an object is implemented as hierarchical labeling of regions. The control strategies are capable of postponing the recognition process of an object if the confidence in the matching process is not sufficient to label the object according to the model. The final labeling of such an object is delayed until more information is derived by analyzing other parts of the image in which the high-level analysis has more confidence for recognizing the objects. This additional information affects the relational description of the object when it is re-analyzed by the system. The relative emphasis among the knowledge sources can be changed according to the type of knowledge, and the belief in the knowledge used. The knowledge base consists of anatomical models stored as frames for various cross-sections of the chest-cavity. Each model uses a multi-resolution representation of the structural and relational description of the organs and their parts present in the specific cross-section. After the initial labeling process, each organ is reconstructed in 3-d and analyzed for its surface continuity.

[PAM91] and [PAM92] review the most recent research on 3-d scene interpretation, including 3-d object recognition, 3-d sensing techniques, modeling and representation of 3-d objects, and specific applications of 3-d interpretation models. It is noted that most of the 3-d-from-2-d approaches to recognition use an hypothesize-and-test paradigm in which small groups of image features are matched to small groups of model features to form initial hypotheses about an object shape. these hypotheses can then be verified by further examination of data, typically by using the transformation inherent in the hypothesis to align the object model with the image.

One key issue that plagues object recognition is dealing with the inherent uncertainty of data measurements from real devices and real scenes. [WHA92] discusses the interpretation of scene geometry in the form volumetric models. Ambiguity is described as a local probabilistic property of the misfit error surface in a parametric space. It introduced the *uncertainty image* to demonstrate the notation of uncertainty as a local property of the model's surface. It also proposed a technique that can use this information to plan a new direction of view that minimizes the ambiguity of subsequent interpretation.

Most current recognition systems, including those reviewed in [PAM91] and [PAM92], have focused on objects for which simple geometric models exist. A very version of the recognition problem deals with objects with complex shapes for which exact geometric models are difficult to obtain. [STR91] addresses this problem, arguing that contextual information is central to solving it. It provides a description of a context-based system operating on real data. Experiments on outdoor imagery has already demonstrated competence beyond what is believed attainable with other existing vision systems.

Although most of the methods discussed in the above are based on theoretical studies, they are suited, in most cases, to the object recognition tasks where the objects have regular shapes or they can be approximated by mathematical functions, such as cylinder, sphere and ellipsoid, or physical and anatomical models. For the log defect recognition task studied in this work, the various wood defects have quite irregular shapes which can not be described using one of the above methods. Instead, a set of *basic features* from these hardwood defects have been determined and used to form a feature vector for object recognition. They are described in the next section.

6.3 Log Defect Representation in 3-D

6.3.1 3-D Characterization of Log Defects

Due to different growth conditions and various biological reactions to the natural environment, log defects have varying appearances, as has been listed in Table 4-1 and

Table 4-2 of chapter 4. For instance, knots will in general appear as round or elliptic in a 2-d image and as ellipsoidal or paraboloid in a 3-d image [FUN85] [LEE91]. Topologically, certain defects are frequently located at certain locations within a log. For example, bark is always on the outmost layer of logs, most splits (except shake) occur near the heart of a log, and when compartmentization takes place in a wounded log, stain will appear as a wide ring structure to cover (protect) the wood from biological erosion. Finally, information about discoloration, associated with decaying fungi in a log, may also be obtained from the digital CT images of the log.

In summary, except for color, features derived from log CT images, such as density, texture, geometric properties, and topological relationships, can all be used to interpret or infer the internal defect structures and geometry of the log. Based on analysis of the CT images in the data base, the 3-d characteristics of hardwood defects can be categorized into the following three major types: *shape* related, *orientation* related, and *intensity* related features. They have been chosen and will be used in the knowledge-based scene analysis module of the machine vision system.

Shape: There are four features that are related to the object shape, they are 1) compactness, 2) elongation, 3) variation of cross-sections, and 4) moments of inertia.

1) *Compactness* : Compactness is defined as the ratio of an objects surface area to its volume. It is used to indicates whether an object is round or compact, with a sphere having the maximum compactness value of 1.0.

2) *Elongation* : Elongation in 2-d is defined as the ratio of the longer axis to that of the shorter axis of the object. A 3-d object has three axes (orientations of inertia) that can be

used to define more than one elongation. However, computing the elongation of a 3-d object is more complex than that of a 2-d object [BEE65], but can be approximated by averaging the 2-d elongation values of all the 2-d slices of the 3-d object. For lengthy and narrow objects, such as splits and compartmentization-related stains [BRO63] in the log images, the elongation value is relatively larger than those of other defects.

3) *Variation of cross-sections*: Depending on the defect, the cross-sectional areas of any 3-d object may have different types of variation. Some defects, such as knots, may experience more significant variation than others, such as pith, bark, and stain. Therefore, a measure of cross-sectional change in an object is an adequate feature used to differentiate the various defects in hardwood logs.

4) *Moment of inertia* : Moment of inertia of a 3-d body is obtained by computing the integral

$$I = \int r^2 dm.$$

If the body is made of a homogeneous material of density ρ, we have $dm = \rho dV$ and write

$$I = \rho \int r^2 dV.$$

It can be readily seen that this integral depends only upon the shape of the body. Therefore, moment of inertia of an object is also a useful feature for its recognition.

Orientation: In a straight log, the growth orientation of each defect is, in general, determined by the physiological conditions of the wood material. For instance, knots will always grow from the pith outward in an orientation that can be measured by an angle Φ between the Z-axis of the log and the knot center. Previous studies have shown that angle values for knots are usually larger than for holes and can be determined statistically [LEE91]. On the other hand, other defects, such as stain, bark and pith, have relatively smaller angles ranging from 0 to 15 degree. Since the exact calculation of the orientation of a 3-d object of arbitrary shape is somewhat involved and requires solving a cubic equation [BEE65], this dissertation proposes a simplified method to estimate the orientation of an object. This method is described in detail in the next section.

Intensity: Since pixel intensity in a CT image is a direct measure of the x-ray attenuation coefficient of the material, it must be used as one of the prominent properties of the object in this CT study. There are three ways of describing the intensity of the pixels in 3-d object. The first one is to calculate the average value of pixel intensities in the object, the second one is to calculate the variation (standard deviation) of the intensities, and the third is to calculate the central moments of pixel intensities within an object. According to the study described in chapter 4 on image data evaluation, we have observed that some different defects may have the same average intensity, but have different intensity variations. Therefore, the pixel intensity and its variation of an object should be included in the feature vector for object recognition. In addition, the central moments of an object reflect the distribution of the object, and should be useful for object recognition.

6.3.2 Definition of Features

After the 3-d volume growing operation, the scene analysis module extracts a vector of basic features (properties) as described in the above from each of the resulting volumes (objects). The selection of the set of basic features extracted is problem-dependent. As an example, a set of basic features extracted for the problem of hardwood log inspection are shown below.

First, let us denote a labeled object by $O(x,y,z)$ with volume V and total pixel number P. This 3-d object $O(x,y,z)$ consists of N slices of 2-d image functions $f_i(x,y)$, $i = 1, 2, ..., N$. Each of these image functions is defined over a region R_i, $i = 1, 2, ..., N$, in the X-Y coordinate system, and each has a cross-sectional area $S_{area}(i)$. Then for each volume (object), a set of 7 *basic features* f_i, $i = 1, 2, ..., 7$, are extracted by the scene analysis module. These are:

1) *Average_Angle* (Φ): The average angle is defined as the average of N angles between the Z-axis and the N lines, each connecting the centroids of two of the N consecutive slices in a 3-d object. It can be expressed as

$$\Phi = (1/N)\sum_{i=1}^{N}\theta_i, \qquad \theta_i = \arctan(dz/D_i) \tag{6-1}$$

where dz is the slice spacing (8 mm), and D_i is the distance between the centroids of the *i*th and *(i+1)*th slice, and for the two centroids at (x_i, y_i) and (x_{i+1}, y_{i+1}), D_i is computed by

$$D_i = \sqrt{(x_{i+1}-x_i)^2 + (y_{i+1}-y_i)^2}$$

2) *Compactness* (C): The compactness of 3-d object can be approximated by the ratio of the object surface, S, to its volume, V, and can be expressed by

$$C = S / V \tag{6-2}$$

3) *Average_Elongation* (E): The average elongation of a 3-d object can be estimated by the average of the 2-d elongation E_i of the corresponding N planer regions in the 3-d image, expressed by

$$E = (1/N) \sum_{i=1}^{N} E_i , \qquad E_i = (\sqrt{M_{20}(i) - M_{02}(i)} + 4M_{11}(i)) \,/\, M_{00}(i) \qquad (6\text{-}3)$$

where

$$M_{mn}(i) = \sum_{(x,y)\in R_i} (x-x_0)^m (y-y_0)^n f_i(x,y), \quad m,n = 0, 1, 2.$$

is the *mn*th order central moment about the centroid ((x_0, y_0)) of the *i*th image function $f_i(x,y)$ over the region R_i [JAI85].

4) *Area_Variation* (**A**): This shape-related feature is the normalized variance of area values of N 2-d cross-sections belonging to the same 3-d object, and it is defined as

$$A = Var\_S_{area} \,/\, Ave\_S_{area} \qquad (6\text{-}4)$$

where Var_S_{area} and S_{area} are the variance and average of area values of N slices in a 3-d object.

5) *Object_Intensity_Ave* (μ): This intensity-related feature is defined as the average of pixel intensity (CT-number) of an object, and it can be computed iteratively from the average value $\mu(i)$ of N individual slices R_i (i=1,2,...,N) of the object, with $\mu(i)$ being the average of the pixel intensity of the *i*th slice

$$\mu = (1/V) \sum_{(x,y,z)\in V} O(x,y,z) = (1/N) \sum_{i=1}^{N} \mu(i) \qquad (6\text{-}5)$$

6) *Object_Intensity_Var* (σ): This intensity-related feature is defined as the standard deviation of the pixel intensity (CT-number) of an object, and it is calculated by

$$\sigma^2 = (1/V) \sum_{(x,y,z)\in V} [O(x,y,z) - \mu]^2 \qquad (6\text{-}6)$$

7) *Moment_of_Inertia*: (**I**): The shape-related feature is calculated as follows:

$$\mathbf{I} = \sum_{(x,y,z)\in V} [(x-x_0)^2 + (y-y_0)^2]O(x,y,z) \qquad (6\text{-}7)$$

where x_0 and y_0 are the x and y coordinates of the centroid of the 3-d object.

6.4 Imperfect Knowledge Representation: D-S Model

The *basic features* f_i , i = 1, 2, ..., 7, defined in section 6.3.2, are used in the **test set** Π of the scene analysis module. There are 7 tests in this test set Π, and they are denoted by

Π_Φ, *Average_Angle* test,

Π_C, *Compactness* test,

Π_E, *Average_Elongation* test,

Π_A, *Area_Variation* test,

Π_μ, *Object_Intensity_Ave* test,

Π_σ, *Object_Intensity_Var* test,

Π_I, *Moment_of_Inertia* test.

To accomplish the defect recognition task, these tests Π_i are applied in different combinations and orders to the different 3-d objects that have been produced by the 3-d volume growing algorithm. The output from each of the tests provides the vision system *partial* **evidence** (knowledge or belief in the evidence) to support or refute a hypothesis about the identity of the object. Based on a collection of partial evidence, the vision system arrives at a *consensus* - a final decision on the identity of the defect, by using the Dempster's rule of *evidence combination* [DEM67].

As is well known, our knowledge of the real world objects could be imperfect, and our belief in the evidence can be uncertain for various reasons [BUC84] [PEA86] [SHA76]. In the machine vision system under study, our knowledge of the different wood defects is imperfect, imprecise, or fuzzy. The approach to object recognition used in this study is knowledge-based; both the evaluation and combination of each knowledge source's response are based on the application of the Dempster-Shafer (D-S) theory of evidence [SHA76]. A similar approach has been adopted in a machine vision system for inspecting the surface defects in hardwood *lumber* [CHO91], and in a drainage network evaluation system DNESYS [QIA90].

Given an object, each of the basic features is calculated to give a group of confidence values that the object should be classified to each of the types of defects. The reason for using multiple basic features rather than a single feature lies in that multiple sources of evidence are, in general, more likely to provide a reliable indicator than a single source of evidence is. No single piece of evidence by itself is sufficient for determining the identity of an object because of the nature of the uncertainty in the information. However, each piece of evidence provides a grain of support for hypotheses about the object identity, which can be pooled into more certain support for the hypothesis. Confidence values so generated are then combined to produce a final confidence or belief value using Dempster's rule of combination. The identity of an object is classified as the one for which the confidence value is maximum.

There are a number of reasons for selecting D-S theory for this scene analysis module over other reasoning schema, e.g., Bayesian probability reasoning theory [DUD79], fuzzy logic [ZAD75], and MYCIN's certainty factor model [BUC84]. The main disadvantages of the Bayesian theory include: 1) *A priori* probabilities must be assigned, an assignment that is difficult, if not impossible, to accomplish in practice. 2) It is difficult to represent the measure of ignorance [HEN88]. The MYCIN's certainty factor model is an *ad hoc* technique that is based on certain preconditions [BUC84]. In fact, the Dempster combination rule includes the Bayesian rule and certainty factor model as special cases [GOR84]. This leaves fuzzy logic method as the remaining possibility. Suppose there is one feature with very low confidence value and several other features with high confidence. Then final confidence value computed using fuzzy logic intersection operations is completely determined by the lowest confidence value, even if many other features have good credibility. This seems to be inconsistent with the human decision making process. On the other hand, Dempster's rule of combination seems to efficiently pool independent evidence (information) from multiple knowledge sources [SHA76]. In the above case, the final confidence is affected not only by the lowest confidence but other confidence values as well. Thus the final confidence computed in such a case would not be as pessimistic as the value computed using fuzzy intersection operations. In addition, D-S theory has the capacity of representing the degree of ignorance in complex domains [DEM67]. Detailed general comparisons of several uncertainty reasoning schema including the D-S theory can be found in the literature [HEN88] [LEE87].

In the D-S theory of evidence, a *frame of discernment* Θ is defined as a finite set of mutually exclusive hypotheses. For a specific question or task, a set is a frame of discernment if 1) its elements are interpreted as all possible answers to a question, and 2) exactly one of these elements is the correct answer. For the wood defect inspection problem under study, all possible answers to the question " what is the identity of the defect?" include: knot, split, pith, bark, stain, decay, and hole. Therefore, the frame of discernment in this case is

$$\Theta = \{\text{knot, split, pith, stain, decay, hole}\} \tag{6-8}$$

Any subset X of Θ, $X \subset \Theta$, is a hypothesis about the answer to a question, that is, about the identity of an object (defect). For instance, when applied to an object some of the tests Π_i generate evidence that the identity of the object could be {knot}, {decay}, or {decay or knot}. In set notation, this is denoted by the following subsets

X = {the defect is a knot} or denoted as {knot}
X = {the defect is a decay} or denoted as {decay}
X = {the defect is a decay *or* a knot} or denoted as{decay $\cup$ knot}

In case of uncertainty, the identity could be either knot or decay based on partial information extracted from a 3-d volume (defect).

In Bayesian theory of probability, the posterior probability changes as evidence is acquired [DUD79]. Likewise, in D-S theory, the belief in evidence may vary. It's customary in D-S theory to think about the ***degree of belief in evidence*** as analogous to the **mass** of a physical object. That is, the mass of evidence support a belief. The **evidence measure**, symbolized by the letter m, is analogous to the amount of mass. Associated with each piece of evidence is a basic probability assignment (*bpa*), denoted as m(X), that represents the impact of the evidence on the subsets of Θ, i.e., the probability assigned to the subset X. The quantity m(X) can be viewed as the portion of total belief assigned exactly to X. The function m(X) maps the power set of Θ (2^Θ) numbers between 0 and 1. This mapping is formally expressed as

$$m: \quad P(\Theta) \Rightarrow [0,1]. \qquad (6\text{-}9)$$

According to the D-S theory, the *bpa* must satisfy the following two properties:

1) the basic probability number of a null event $\varnothing$ is 0, $m(\varnothing) = 0$; and

2) the sum of *bpa* for all subsets of Θ must be 1, $\sum_{X \subset \Theta} m(X) = 1$.

A fundamental difference between the D-S theory and probability theory is the treatment of **ignorance**. Probability must distribute an equal amount of probability even in ignorance, i.e., when there is no information available about a hypothesis. For example, probability theory assigns probability *uniformly* to N possibilities X_i, i = 1, 2, ..., N, when there is ignorance, i.e., each of these possibilities X_i is assigned the same amount of probability $P(X_i)$, according to the so called uniform probability density function (*pdf*)

$$P(X_i) = \frac{1}{N}, \quad i = 1, 2, ..., N.$$

This assignment is made (in desperation) by using the **principle of indifference** . The extreme case of applying the principle of indifference occurs when there are only two possibilities, such as A and its negation A'. Probability theory will assign a probability of 50% to A and A' even when there is no knowledge at all, since probability theory says that

$$P(A) + P(A') = 1. \qquad (6\text{-}10)$$

This means, anything which does not support *must* refute, since ignorance is not allowed in the Bayesian probability.

The D-S theory does not force belief to be assigned to ignorance or refutation of a hypothesis. Instead, the belief or mass determined by the *bpa* mapping function $m(X)$ is assigned only to those subsets of the frame of discernment Θ, called *focal elements* of Θ, to which one wishes to assign non-zero belief, i.e., $m(X) > 0$, $X \subset \Theta$. Any belief that is not assigned to a specific subset is considered **no belief** or **nonbelief** and just associated with Θ. Belief that refutes a hypothesis is **disbelief**, which is *not* nonbelief.

For example, suppose that after applying to an object one of the tests Π_i, this test assigns to the subset $X = \{knot\}$ a *bpa* of

$$m_i(knot) = 0.7$$

where $m_i(.)$ refers to the evidence or belief supported by the *i*th test. The rest of the total belief is left with the frame of discernment Θ as nonbelief, since there is no evidence to support otherwise, i.e.,

$$m_i(\Theta) = 1 - 0.7 = 0.3$$

The above illustrates the major difference between D-S possibility theory and Bayesian probability theory. In probability theory the above requires

$$P(\text{knot}) = 0.7, \qquad P(\text{non-knot}) = 0.3$$

In Bayesian probability theory, if the belief in knot by the *i*th test is 0.7, then the disbelief in knot must be 0.3. Instead, the 0.3 in D-S theory is held as nonbelief in the frame of discernment by $m_i(\Theta)$. This means *neither belief nor disbelief* in the evidence to a degree of 0.3. We belief that the object is a knot to a degree of 0.7 and are reserving judgment of 0.3 in disbelief and the additional belief in knot. It is very important to realize that the assignment of 0.3 to the frame of discernment Θ does not assign *any* value to the proper subsets of Θ even though these subsets may include knot, such as

$\{\text{knot} \cup \text{decay}\}, \{\text{knot} \cup \text{split}\}, \{\text{stain} \cup \text{knot}\}$.

In the scene analysis module of the vision system under discussion, each test from the test set $\Pi = \{\Pi_\Phi, \Pi_C, \Pi_E, \Pi_A, \Pi_\mu, \Pi_\sigma, \Pi_I\}$ maps the evidence that is extracted from the detected objects into a *bpa* $m_i(.)$, a set of discrete mass values between 0 and 1, i.e.,

$$m_i(X) = [0, 1] \text{ for any } X \subset \Theta, i = 1, 2, ..., 7. \tag{6-11}$$

where $m_i(.)$ could be replaced by one of a set of the *bpa* mapping functions $\{m_\Phi(.), m_C(.), m_E(.), m_A(.), m_\mu(.), m_\sigma(.), m_I(.)\}$, depending on the particular test used. In general, each test Π_i is a function of a measurement made on the object (basic feature f_i) and a parameter vector T_i, i.e.,

$$\Pi_i = g_i(f_i,T_i) \tag{6-12}$$

The parameters T_i's are the thresholding values that are determined either from training experiments with image data base, or by experts in the field of hardwood log grading.

In the scene analysis module, the *bpa*'s are implemented as a set of discrete table look-up functions embedded in the knowledge base of the vision system. Evidence strengths are extracted from the knowledge base by consulting with these look-up tables, tables that are created by experimenting with the images available in the data base. For instance, the two tests that are designed for inspecting knots are Average_Angle test Π_Φ and Area_Variation test Π_A. Associated with these two tests are two evidence mapping functions, $m_\Phi(.)$ and $m_A(.)$, together with parameters t_Φ and t_A. These two *bpa* mapping functions are respectively defined by

bpa Mapping Function $m_\Phi(.)$ by Test Π_Φ:

if $(T_\Phi > t_\Phi)$

$$m_\Phi(X) = \begin{cases} 0.9 & X = \{\text{knot}\} \\ 0.05 & X = \{\text{decay}\} \\ 0.05 & X = \{\Theta\} \end{cases}$$

else

$$m_\Phi(X) = \begin{cases} 0.1 & X = \{\text{knot}\} \\ 0.6 & X = \{\text{bark} \cup \text{decay}\} \\ 0.3 & X = \{\Theta\} \end{cases}$$

bpa Mapping Function $m_A(.)$ by Test Π_A:

if $(T_A > t_A)$

$$m_A(X) = \begin{cases} 0.9 & X = \{\text{knot}\} \\ 0.1 & X = \{\Theta\} \end{cases}$$

else

$$m_A(X) = \begin{cases} 0.6 & X = \{\text{bark} \cup \text{decay}\} \\ 0.4 & X = \{\Theta\} \end{cases}$$

The *bpa*'s for the other tests all have the similar format as the above examples.

6.5 Recognition by Combination of Evidence

Interpretation of real world images is a difficult task because of uncertainties arising when formulating hypotheses based on noisy image data and imprecise models about how different objects might appear in the scene. In addition, different hypotheses about the identity of one object may even conflict. Therefore, some mechanism of recognition that is based on the theory of *reasoning* is needed in a vision system to resolve this type of decision conflicts. Dempster-Shafer theory of evidential reasoning is especially suited to integrating evidence from different knowledge sources. Because by D-S model, evidence that only partially favors a hypothesis should not be construed as also partially supporting its negation, which means, belief about the negation of a hypothesis does not depend on belief in the hypothesis itself.

Mechanism for Focus of Attention: As stated above, there are 7 tests that are targeted to different types of hardwood log defects. For example, the *Average_Angle* test Π_Φ is designed to inspect knots, and the *Compactness* test Π_C is to inspect pith, and so forth. However, to recognize a candidate object with minimal computational complexity of the analysis possible, our vision system employees a *focus of attention* mechanism.

To each object that has been segmented by the segmentation module, the Object_Intensity_Ave test Π_μ is first applied. The purpose of this test is to roughly divide the clear wood and defects into 3 groups of *candidate objects* according to their CT-numbers: 1) group 1 - knots and bark with the highest CT-numbers, 2) group 2 - clear wood, decay and stain with medium CT-numbers, and 3) group 3 - splits, holes and pith with the lowest CT-numbers. The division is not perfect because some defects' CT-numbers tend to overlap with each other in some sample images. For example, a knot may have the same average CT-number as bark, and a stain (white rot) may have the same CT-number as clear wood. Nevertheless, this division does provide the vision system a *focus of attention* mechanism that seems able to guide the other tests of the scene analysis module.

Next, a subset of the test set Π are determined and applied to objects belonging to the 3 groups of the *candidate objects*. Responses of these objects to each of these tests give a set of partial evidence (also called *evidence strength*) to the different hypotheses about the identities of the objects. Note that results of test from test set Π may logically conflict, but others may still verify a hypothesis. The D-S theory selects a belief function that is able to synthesize all partial knowledge and to achieve a multi-criteria optimization. The evidence provided by each test Π_i is represented as a *bpa* over a hypothesis space spanned by Θ. An individual hypothesis, such as X = {the defect is a *knot*}is supported or refuted depending on the response of an object to its corresponding tests. Each such test Π_i merely contributes to the overall support, and the effect of Π_i on a hypothesis is determined by its *evidential strength* or degree of confirmation. An inference network that propagates evidence strength can then be constructed using the Dempster's rule of combination [DEM67] [GIA89].

Let m_1 and m_2 be the *bpa* of two independent pieces of evidence obtained by applying two tests Π_1, and Π_2 to one object. Denote X and Y as any two subsets of the frame of discernment Θ, $X \subset \Theta$, and $Y \subset \Theta$. Since Dempster's rule of combination is commutative and associative, m_i's from the two tests can be combined regardless of order. Then the new *bpa* m(A), for any A $\subset \Theta$, can be calculated using Dempster's rule of combination given by

$$m(A) = \begin{cases} k \sum\limits_{x \cap y = A} m_1(X) m_2(Y) & \text{if } A \neq \varnothing \\ 0 & \text{if } A = \varnothing \end{cases}$$

$$K = \frac{1}{1 - \sum\limits_{x \cap y = \varnothing} m_1(X) m_2(Y)}$$

where k is a normalization factor [GOR85]. When there are more than two tests, the above rule of evidence combination still can be used. Each time a pair of m_i's is combined and the resulting *bpa* is combined with the *bpa* generated by the next test. The same procedure can be applied N-1 times until all the N *bpa*'s have been combined.

At the final stage of reasoning, a single hypothesis among others is determined, if and only if the belief function has a maximum value that is greater than T_Θ, a threshold specified in the knowledge base. The object is recognized as defect type i if the discrete value of the combined *bpa* $m(X_i)$ is maximum and is above the preset threshold T_Θ.

6.6 Preliminary Results

In the experiment with the log images that are available in the data base, the frame of discernment Θ is smaller than that given in Eq. (6-8) and consists of a finite number of exhaustive and mutually exclusive subsets, each of which is one of the following hypotheses:

1. An object is a knot, denoted as K.
2. An object is a rot (decay), denoted as R.

3. An object is bark, denoted as B.

In the experiments, the thresholds T_i's associated with each test are at present determined by observation. In addition the threshold value T_Θ, which is used to select a single hypothesis from final evidence strengths, is specified in the knowledge base, and is set to $T_\Theta = 0.5$. This means, when the possibility of a hypothesis is maximum among all hypotheses and is equal or greater than half of the total chances (50%), we select that hypothesis.

Due to the limited CT log images in the data base, only two segments of defective hardwood logs have been selected. They contain knot, bark, and rot (decay) that spreads cross 10 to 20 slices of CT imagery. As a consequence, only these 3 types of hardwood defects are presently inspected by the scene analysis module described in this chapter. Accordingly, only 4 of the designed 7 tests Π_i are chosen and implemented in the inference engine of the knowledge-based vision system. They are Π_μ, Π_Φ, Π_I, and Π_A. When additional image data are available, the remaining 3 tests (or other new tests) could be easily added to the set of these 4 tests to make the task of object recognition more reliable. The steps involved in the object recognition are described by the following experiment.

To illustrate one experiment example of evidence combination in the procedure of object recognition, let us consider pooling the three *bpa*'s $m_I(.)$, $m_A(.)$ and $m_\Phi(.)$ after applying three tests Π_I, Π_A and Π_Φ to a 3-d object (defect). This defect of unknown type is located near the center of the log segment in Fig. 6.1, where 4 consecutive slices from sample log YP01 are shown. Fig. 6.2 and Fig. 6.3 illustrate the segmentation and 3-d volume growing results of these 4 slices. This detected object near the log center has already been categorized as a group 1 candidate object (knot or bark) by the *focus of attention* mechanism, i.e., the *Object_Intensity_Ave* test Π_μ. The three *bpa*'s $m_I(.)$, $m_A(.)$, and $m_\Phi(.)$ are implemented as a set of discrete table look-up functions expressed by

$$m_I(X) = \begin{cases} 0.8 & \{KB\} \\ 0.2 & \{\Theta\} \end{cases}, \quad \text{for } T_I < t_I.$$

$$m_A(X) = \begin{cases} 0.6 & \{RB\} \\ 0.4 & \{\Theta\} \end{cases} \quad \text{for } T_A < t_A.$$

$$m_\Phi(X) = \begin{cases} 0.9 & \{K\} \\ 0.05 & \{R\} \\ 0.05 & \{\Theta\} \end{cases} \quad \text{for } T_\Phi > t_\Phi.$$

where K, B, and R represent knot, bark, and rot (decay), and t_I, t_A and t_Φ (in degree) are the thresholding values of the corresponding test. In the experiment with the log CT images available from the data base, these thresholds have been determined to be $t_I = 100$, $t_A = 50$, and $t_\Phi = 15$ (degree), respectively. First, the inference engine of the knowledge-based system propagates the evidence by combining together the two *bpa*'s, $m_I(.)$ and $m_A(.)$, into a new *bpa* denoted by $m_{IA}(.)$

$$m_{IA}(X) = \begin{cases} 0.48 & \{B\} \\ 0.32 & \{KB\} \\ 0.12 & \{RB\} \\ 0.08 & \{\Theta\} \end{cases}$$

Then, $m_{IA}(.)$ is combined with $m_\Phi(.)$, and the resulting *bpa*, $m_{IA\Phi}(.)$, is

$$m_{IA\Phi}(X) = \begin{cases} 0.057 & \{B\} \\ 0.838 & \{K\} \\ 0.024 & \{R\} \\ 0.014 & \{RB\} \\ 0.038 & \{KB\} \\ 0.009 & \{\Theta\} \end{cases}$$

From this final *bpa*, one can see that knot (K) has the maximum evidence strength of 0.838 and it is greater than the preset threshold value T_Θ, $T_\Theta = 0.5$. The vision system has therefore correctly identified the object near the log center as a knot. Note that, if only partial information (evidence) from two tests Π_I and Π_A is used in the decision-making process, the system would have wrongly identified the object as bark (B), according to the $m_{IA}(.)$ given above.

The same procedure of evidence pooling has been applied to the thin and circular object on the boundary of the log segment (Fig. 6.3), and this defect has been classified as bark correctly. The complete recognition results are shown in Fig. 6.4, which illustrates part of a 15-slice long log segment.

6.7 Summary and Discussions

In this chapter, we have discussed the problem of scene analysis, reviewed the general issue of object recognition by shape analysis, and applied the D-S theory to the problem of hardwood defect recognition in a knowledge-based machine vision system. In particular, we have discussed research on the application of both D-S theory and the concept of evidential reasoning in order to address the issues involved in the scene analysis module. A set of 7 ***basic features*** have been defined that seem to be appropriate for the 3-d defect recognition task. Experimental examples with 2 segments of logs that contain knot, rot (decay) and bark show the efficacy of the knowledge-based approach, although additional experiments with significantly more images are needed to assess the performance of the method.

It has been argued that knowledge-based systems must reason from evidential information, i.e., from information that is to some degree uncertain, imprecise, and occasionally inaccurate. This is no less true of knowledge-based vision systems that operates in the domain of compute-based scene analysis. Recent work has suggested that the work of Dempster and Shafer (D-S) provides a viable alternative to Bayesian-based probability techniques for reasoning from evidential information.

Our domain of application is knowledge-based machine vision. The D-S theory and the concept of evidential reasoning are the foundations of a developing framework for knowledge-based systems, such as general-purpose machine vision system, that must reason in complex domains about their perception. Some experimental results from this study highlight the benefits of employing these technologies in an industrial vision system. That is, by using previously unavailable information such as the amount of ignorance and ambiguity a hypothesis exhibits, the system is able to correctly recognize a significantly greater number of objects in a 3-d image.

Despite the progress of research in D-S theory, there remain a significant number of problems with respect to the technology we have explored in this chapter and its use in knowledge-based systems. For instance, although the D-S theory has relieved us from the burden of specifying complete probability models, a formal theory for generating mass function (*bpa*) m(.) remains unavailable. It is believed that this latter problem is more tractable than the former. Furthermore, at present there is no computational theory for the integration of "fuzzy-based" approaches to uncertain reasoning with the D-S theory of belief functions.

The features used to represent 3-d objects in the scene analysis module are based on the object's shape, orientation, and X-ray attenuation variation. However, there are other features of defects that can be extracted from their images. Closely examining the CT images of hardwood logs reveals that there is a distinct textural pattern in each of the types of defects. It is, therefore, possible to develop a method to extract the texture information from the detected objects and use the texture feature to design an additional hypothesis test, called texture test Π_t. This texture test will help improve the performance of the scene analysis module since it adds the knowledge about wood texture to its knowledge base. Chapter 7 describes in detail a stochastic method for extracting this texture information from log CT image. It also presents two efficient procedures for texture discrimination with experimental results. Finally, it discusses the possibility of incorporating the texture test in the scene analysis module of the machine vision system.

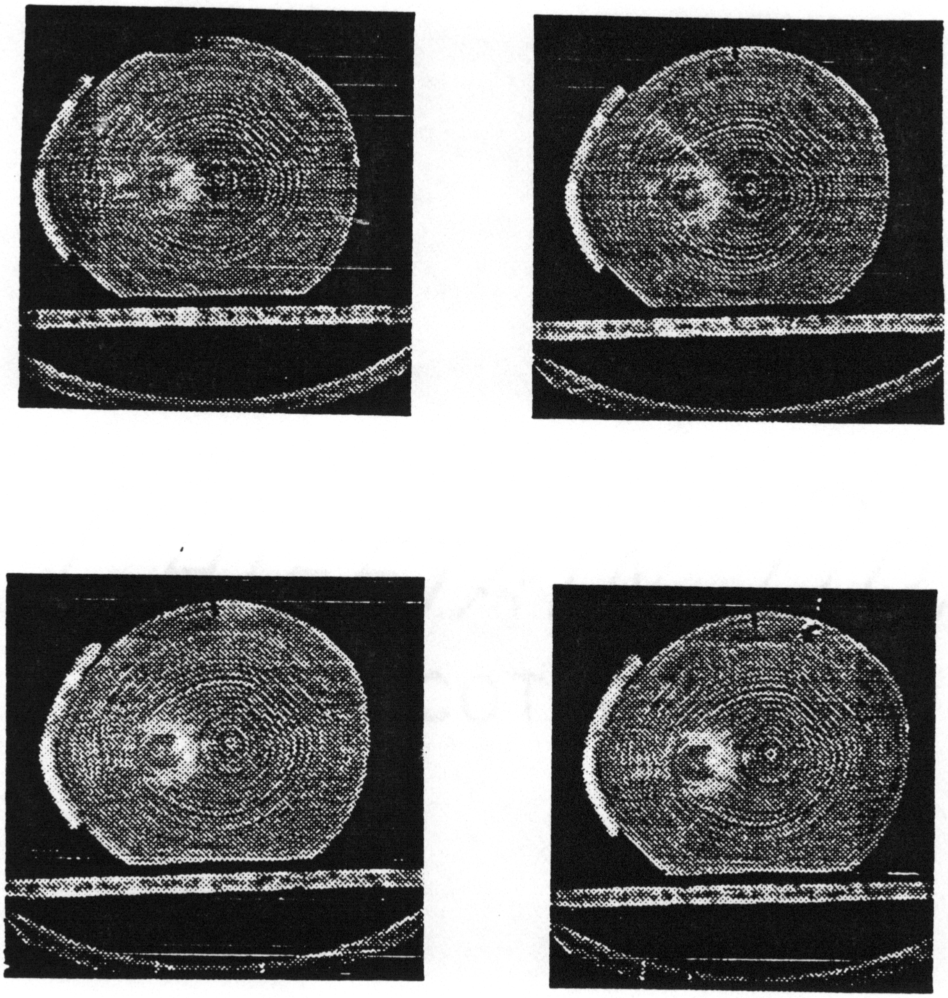

Fig. 6.1 4 consecutive slices YP01.02-05 (clockwise from upper left)

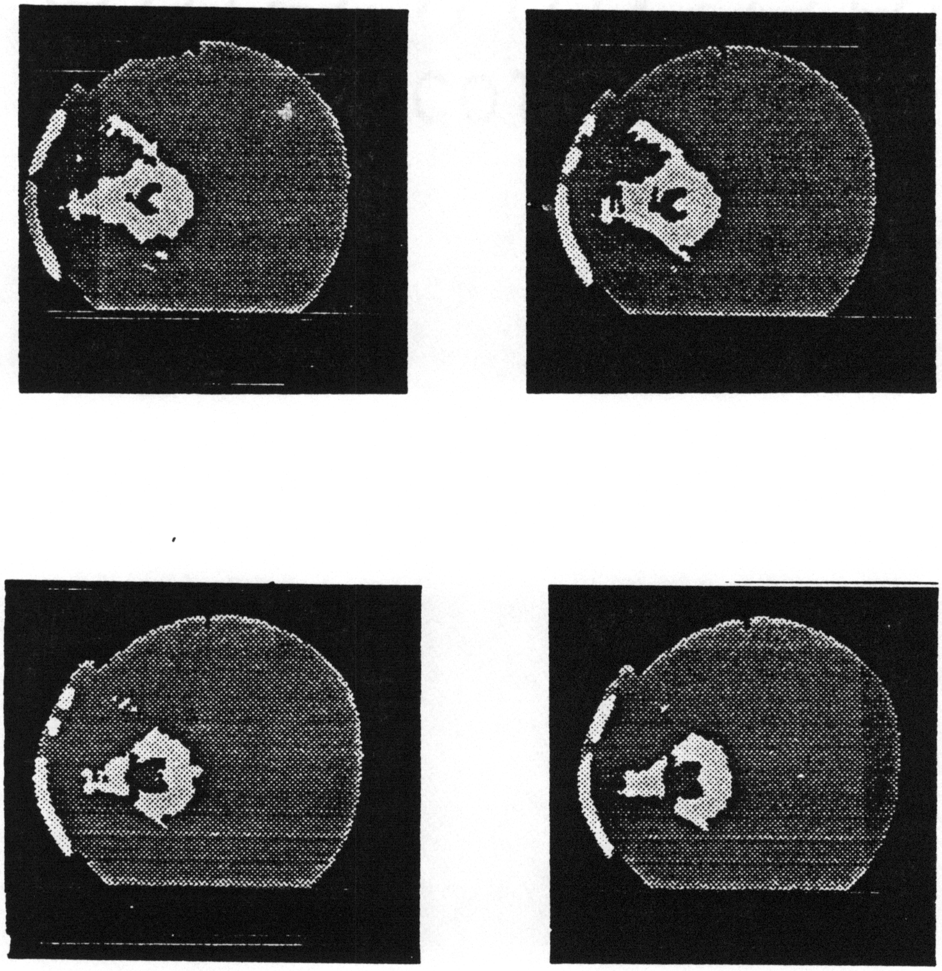

Fig. 6.2 The segmentation result of the images in Fig. 6.1

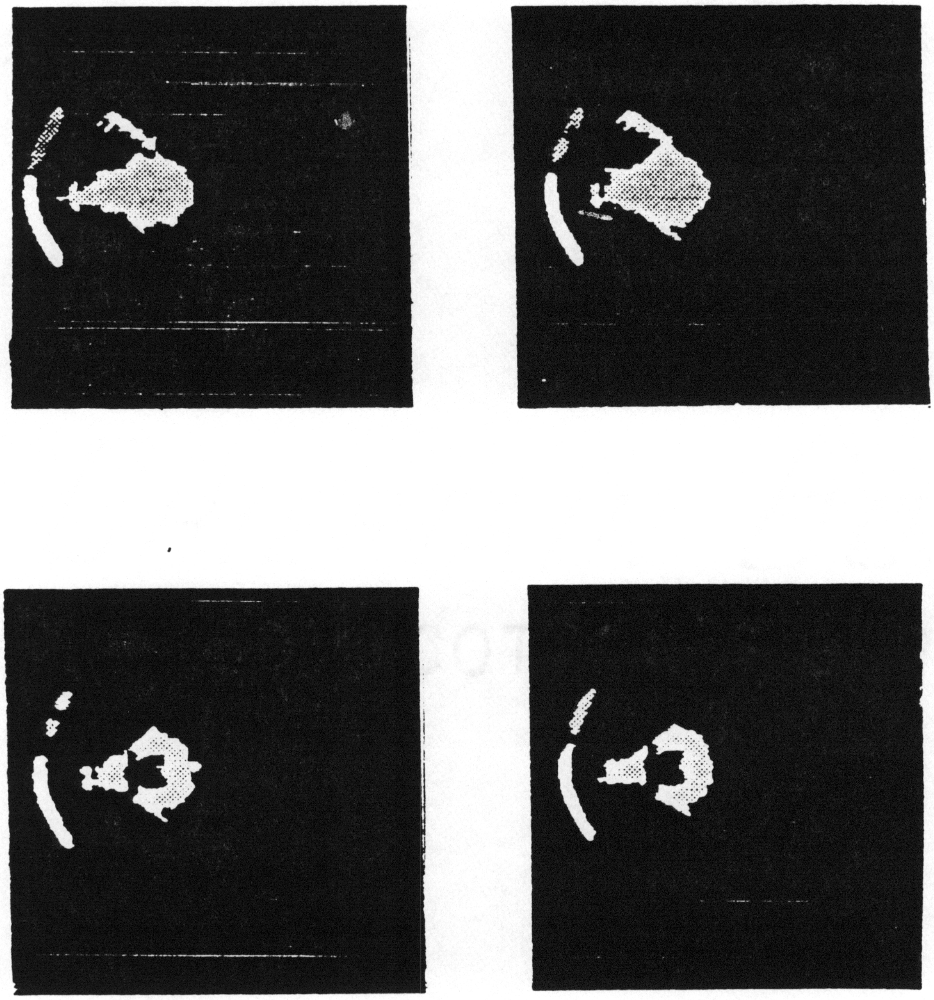

Fig. 6.3 3-d growing of the images in Fig. 6.2, each object assigned a label

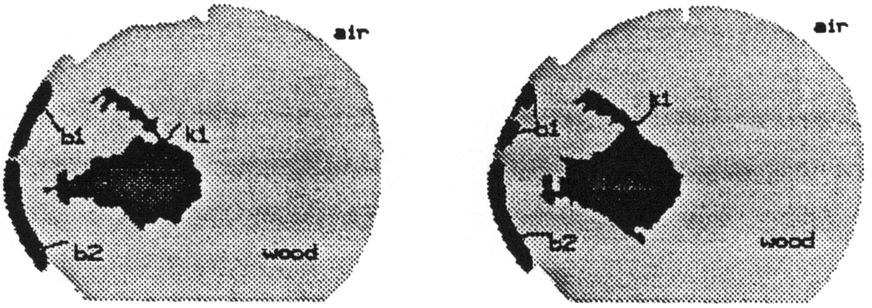

slice 1 slice 2

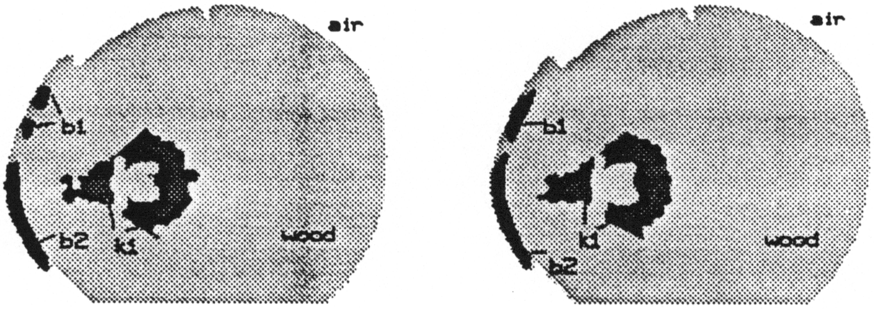

slice 3 slice 4

Fig. 6.4 Object recognition of Fig. 6.3 by evidential reasoning

Chapter 7
Wood Texture Modeling

In Chapter 6, the scene analysis module of the log inspection vision system is described. In this scene analysis module, a set of basic features are computed from each of the objects detected by the segmentation module of the vision system. In essence, this set of basic features represents the information about the objects' 3-d shape, spatial orientation, and X-ray attenuation coefficient variations. To develop a reliable machine vision system for log inspection, information about other properties of the objects should be acquired and integrated in the object recognition process. According to Chapter 4, wood grains in log CT images exhibit textural patterns, patterns that can be utilized to recognize different objets in log CT images.

The textural patterns exhibited by different wood grains are, in fact, indicative of the different structures of each of the types of grading defect and clear wood in the log. For example, knots have quite a different texture structure than decay and clear wood in log CT images. This difference, however, can not be described by the shape- or orientation-based features defined in Chapter 6. Instead, new features based on the defects' textural patterns must be defined and used to differentiate the grading defects by their different textures.

This chapter represents the first application of Spatial Auto-Regressive (SAR) modeling to wood texture analysis by CT. It describes an iterative robust algorithm for wood texture modeling that is based on the stochastic field theory [ZHU91h] [ZHU93]. In particular, we provide the background and definition of the texture analysis problem, describe a robust model estimation algorithm, and present a discrimination scheme based on a circular correlation distance, along with the texture classification results with log CT images. Due to the limited scope of this dissertation, the problem of how to integrate the texture feature in the scene analysis module of the vision system will not be addressed.

7.1 Background and Problem Definition

Texture is observed in the structural patterns of surfaces of objects, since many natural scenes, such as wood (Fig. 7.1 and Fig. 7.2), sand, grass, and cloth, are made of various textural structures [BRO66]. Image texture is a very important and useful feature for representing and identifying the various defects in our log inspection vision system.

The term texture generally refers to repetition of basic texture elements called *texels*. A texel contains several picture elements called *pixels*, whose placement could be periodic [CON89], quasi-periodic or random [JAI89]. Natural textures are generally random, whereas man-made textures are often deterministic or periodic. Texture may appear coarse, fine, smooth, granulated, rippled, regular, irregular, or linear. In image analysis, textures are broadly categorized into two basic groups, statistical and structural (syntactic). Statistical textures are characterized by their statistical properties, such as the random field model parameters [ZHA90] and concurrence matrix [CON81], whereas structural textures are determined both by the texels and by their displacement rules, deterministic or random [HAR79]. We will concentrate on statistical texture analysis since this seems the most appropriate for application to the log inspection.

Image texture is an important feature used in analyzing objects of interest in image analysis and computer vision applications. Texture characteristics play a major role in image classification and interpretation. In classification, texture features can be used to discriminate and label regions of an image, such as crop identification in an aerial photograph, and medical diagnosis of an X-ray photograph. Texture features can also be used in scene segmentation and identification in an image understanding or computer vision system, for example, in robot vision and industrial inspection. Therefore, the determination of proper texture features is the key to these applications. There are many approaches to choosing image texture features. Some of those based on statistical techniques are: the Fourier power spectrum [HAR79], gray level co-occurrence matrices [CON81], the decorrelation method, and visually perceived properties [LIN90]. Some of those based on parametric models are the mosaic model, the autoregressive model, and Markov random field models [KAS86]. A stochastic method of image texture analysis has been reported in [KOI89] where it is successfully used to classify the surface defects on wood boards.

This chapter explores the application of a stochastic texture modeling method in the machine vision system. In particular, we describe a parametric model-based method for representing the spatial stochastic processes -- wood grain textures; with the grain texture of each defect and the clear wood being modeled by a parametric random field model. A spatial autoregressive (SAR) model [KAS86] is adopted to characterize the stochastic property of wood grain textures, and the model parameters are used to discriminate different wood defects. A robust parameter estimation algorithm is applied to obtain the model parameters associated with different defects that can occur inside a log. By defining a distance measure based on a circular correlation [ZHU91h], a simple minimum distance classifier is constructed for texture discrimination. Using the estimated model parameters, the classifier assigns an unknown defect into one of the prototypical defects. Experimental results with CT images from different red oak wood show the efficacy of the proposed approach.

7.2 Stochastic Field-Based Texture Modeling

As described in chapter 5, a segmented image contains a number of regions, each representing a potential defect such as split, knot, bark, stain, or decay. For each defect region of unknown class that has been detected on a log CT slice, a Gaussian spatial autoregressive (SAR) model is defined on a neighborhood system to model the spatial directional dependence of wood grains, i.e., each pixel value is modeled as a weighted sum of the values of its neighboring pixels plus a Gaussian white noise process. For each homogeneous region, the SAR model parameters are estimated using a least squares (LS) estimation approach. This set of SAR parameters as well as the gray level mean and variance are then employed as a feature vector in a supervised texture discrimination scheme.

Julezs [JUL62] pointed out that human beings can only distinguish between textures which are different in the first and second order statistics. Following this basic line, a number of statistical texture algorithms have been developed during the last two decades to analyze a wide variety of textural images. They can be further classified into two major categories: statistical technique-based methods [CON81] [HAR79] and parametric model-based methods [GEM84] [DER86] [JEN89].

In the first category, pixel gray levels are directly used to extract texture features, such as run-length statistics, gray value moments, power spectrum, and those derived for the gray level co-occurrence matrix (GLCM) [CON81] [HAR79]. In the second category, it is assumed that homogeneity of a textural region depends only on the configuration of neighboring pixels in the texture. By extending to integer domain, the Gibbs random field model, a model of magnetic domains studied in quantum mechanics, is used to model textures in texture analysis and synthesis with impressive results [GEM84] [DER86]. On the other hand, to take into account the spatial correlation property of textures, 2-D autoregressive models are introduced to texture analysis technique. More recently, several more sophisticated texture models called compound Gaussian Markov random fields (CGMRF) [SRI89] and doubly stochastic Gaussian random fields (DSGRF) [JEN89] are used for surface interpolation as well as texture segmentation.

To represent the texture of a homogeneous region, the image intensity surface needs be well characterized with a small number of features such as model parameters. Statistical image models have already been used to characterize the spatial interdependence of individual pixel values in different textures [BRO66] [KAS86]. Many images that are similar to natural textures, such as cork, grass, wood grain, etc., have been successfully synthesized by random field models. In the random field model approach, a pixel gray level is described as a linear weighted sum of the gray levels of the neighboring pixels and a noise sequence. The sample image can then be characterized by the parameters of the model equation. A spatial autoregressive model [KAS86] is a 2-D autoregressive model that behaves very much like 1-D autoregressive model in time domain.

Let the subset of gray values of an M x M image region be represented by $\{y(s)\}$ where the coordinate index $s = (i, j) \in \Omega$ with $\Omega = \{(i, j) \mid 1 \leq i \leq M, 1 \leq j \leq M\}$. Currently a square window is chosen for simplicity, but the method can be easily extended to other windows. Then an independent Gaussian random field [ZHA90] can be represented by

$$y(s) = f + w(s) \tag{7-1}$$

where f is a constant signifying the image field mean value, w(s) is a 2-d zero-mean Gaussian white noise process with unknown variance σ_w^2. Under this model assumption, f and σ_w^2 are the feature values that represent the textural image field. Although this model has been used to model certain simple textures, it could not fully characterize the wood grain textures under study.

In the following, a second type of random field is studied and used as the model for defect recognition in the vision system. It is assumed that the subset $\{y(s)\}$ satisfies the so called Gaussian causal or spatial autoregressive (CAR or SAR) model in a toroidal lattice system [KOI89]:

$$y(s) = \Theta^T z(s) + \sigma w(s) \tag{7-2a}$$

where Θ is the parameter vector consisting of p unknown coefficients θ_i, i = 1, 2, ..., p, z(s) is the neighborhood vector containing the lexicographically ordered image data from a particular neighborhood system, and where w(s) is a white noise process of zero mean and unit variance. The model parameter vector Θ, the gray level mean μ, and the standard deviation σ are to be estimated from the CT image, and together they comprise the feature vector for each individual wood texture.

By assuming the Markov property of g(i,j), and by the independence of the w(i,j) process, the joint probability density function (*pdf*) of all pixels y(s), $s = (i, j) \in \Omega$, is given by

$$p\{y(s),\, s \in \Omega \mid \Theta,\sigma\} = \frac{1}{(2\pi\sigma^{MM/2})} \exp\{-\frac{1}{2\sigma^2} \sum_{s\in\Omega} [y(s)-\Theta^T z(s)]^2\} \qquad (7\text{-}2b)$$

where z(s) is the neighborhood vector defined in the above.

Our object is to find the parameter $\{\Theta, \sigma\}$ so as to maximize $p\{y(s), s \in \Omega \mid \Theta,\sigma\}$. Since $p\{y(s), s \in \Omega \mid \Theta,\sigma\}$ is an exponential function, we can first take a logarithm operation on it, then set its partial derivatives with respect to Θ and σ to zero, respectively. This leads to the following maximum likelihood estimates of the parameters Θ and σ:

$$\Theta_{LS} = [\sum_{s\in\Omega} z(s)z(s)^T]^{-1}[\sum_{s\in\Omega} z(s)y(s)] \qquad (7\text{-}2c)$$

$$\sigma_{LS}^2 = \frac{\sum_{s\in\Omega} [y(s) - \Theta_{LS}^T z(s)]^2}{M^2} \qquad (7\text{-}2d)$$

7.3 An Iterative Robust Estimation Algorithm

To account for the unrealistic Gaussian assumption for the image data in a potential region, a contamination model [HUB81][KOI89] is introduced to take into consideration the effects of outliers, the data points that are far away from their cluster centers. In this approach, the observed image $\{y_a(s)\}$ is expressed as

$$y_a(s) = y(s) + u(s) \qquad (7\text{-}3)$$

where the noise process u(s) is independent of y(s) and identically distributed with a Gaussian mixture density H given by [HUB81]

$$H = (1-\alpha)F + \alpha G \tag{7-4}$$

consisting of two components: a degenerate central component F and a contamination component G. For instance, F can be a Gaussian distribution with zero-mean and variance σ_F^2, and G an arbitrary distribution characterizing the *outliers* in the image data, such as the zero-mean Laplacian distribution. The iterative algorithm described below, however, does not depend on the explicit forms of F and G. In the above, α is a small fraction of contamination (typically $\alpha < 0.2$), defined as the ratio of the number of *outliers* in the data to the total number of data. The model expressed in (7-1) states that the majority of the image data (a fraction $1-\alpha$) is distributed according to F, and a minority of the image data (a fraction α) is distributed according to G.

In the robust estimation method, called the generalized M-estimation, proposed in [HUB81], the texture model parameters $\{\Theta, \sigma\}$ in (7-2a) are determined from an observed image $y_a(s)$ by minimizing the following index $J(\Theta,\sigma)$:

$$J(\Theta,\sigma) = \sum_{s\in\Omega} W_1(s) \Big[\rho\Big[\frac{r(s)}{\sigma}\Big] + a\Big] \sigma \tag{7–5}$$

where a is an optimization constant, r(s) is the residual $r(s) = y_a(s) - \Theta^T z(s)$, ρ is the Hampel robustifying function, and $W_1(s)$ is a weighting function. The objective here is to minimize (7-5) with respect to the parameter vector Θ and the variance σ. By using a stochastic approximation in the steepest gradient method [KOI89] [LJU83], the following iterative algorithm is derived to simultaneously estimate Θ and σ, at each time instant $k = 1, 2, 3,\ldots k$. The iterative estimation algorithm is expressed as follows:

$$\Theta(k+1) = \Theta(k) + \gamma\Big[\sum_{s\in\Omega} z(s)W_1(s)\,\varphi'\Big(\frac{r_k(s)}{\sigma(k)}\Big)\Big]^{-1}\Big[\sum_{s\in\Omega} z(s)W_1(s)W_2\Big(\frac{r_k(s)}{\sigma(k)}\Big)r_k(s)\Big] \tag{7-6}$$

$$\sigma^2(k+1) = \frac{\sum\limits_{s\in\Omega} W_1(s)\chi\left(\frac{r_k(s)}{\sigma(k)}\right)\sigma(k)^2}{\sum\limits_{s\in\Omega} \beta W_1(s)} \qquad (7\text{-}7)$$

with γ being a convergence step size that satisfies $0 < \gamma < 2$, $W_1(s)$ and $W_2(x)$ are two weighting functions defined as [KOI89]

$$W_1(s) = \frac{\varphi[[z(s)^T z(s)/\sigma_y{}^2 p]^{0.5}]}{[z(s)^T z(s)/\sigma_y{}^2 p]^{0.5}} \qquad (7\text{-}8)$$

$$W_2(x) = \frac{\varphi(x)}{x} \qquad (7\text{-}9)$$

In the above equations, function $\chi(x)$ is defined by the following expression

$$\chi(x) = x\varphi(x) - \rho(x) \qquad (7\text{-}10)$$

and the constant β is equal to E_Φ, the mean value of the squared Hample robustifying function $\varphi^2(r(s))$ over Φ,

$$\beta = E_\Phi[\varphi^2(r(s))] \qquad (7\text{-}11)$$

where E_Φ denotes the expectation over the standard normal distribution N(0,1).In the above equations, $\sigma_y{}^2$ is the gray level value variance calculated over the given image region, and the odd function $\varphi(x)$ is the first derivative of the Hampel robustifying function [KOI89] $\rho(x)$ defined by

$$\varphi(x) = \begin{cases} x & |x| \leq a \\ a\ \mathrm{sign}(x) & a < |x| \leq b \\ a\ \mathrm{sign}(x)\frac{c-|x|}{c-b} & b < |x| \leq c \\ 0 & |x| > c \end{cases} \tag{7-11a}$$

which is the first derivative of the even, Hampel robustifying function $\rho(x)$

$$\rho(x) = \begin{cases} \frac{x^2}{2} & |x| \leq a \\ a\ |x| - \frac{a^2}{2} & a < |x| \leq b \\ a\ \frac{c\ |x| - 0.5x^2}{c-b} - \frac{a^2}{2} - \frac{ab^2}{2(c-b)} & b < |x| \leq c \\ \frac{a}{2}\ (c+b-a) & |x| > c \end{cases} \tag{7-11b}$$

The parameters in functions $\varphi(x)$ and $\rho(x)$ should satisfy the relationship $a = 0.5(c-b)$ [HUB81], and they are chosen here as $a = 2.0$, $b = 2.5$, and $c = 4.5$. The above algorithm starts with the initial values, $\Theta(0)$ and $\sigma(0)^2$, set equal to their least squares (LS) solutions, i.e.

$$\Theta(0) = \Theta_{LS} = [\sum_{s \in \Omega} z(s)z(s)^T]^{-1}[\sum_{s \in \Omega} z(s)y(s)] \tag{7-12a}$$

$$\sigma(0)^2 = \sigma_{LS}^2 = \frac{\sum_{s \in \Omega} [y(s) - \Theta(0)^T z(s)]^2}{M^2} \tag{7-12b}$$

It has been shown [HUB81] that the above robust algorithm, as expressed by equations (7-6) and (7-7), will converge if it starts with proper initial values. A possible candidate is the LS estimate. The iteration is stopped when the maximum of the absolute differences in the parameter estimates found by two consecutive iterations of the algorithm is equal to or less than 0.0001 .

7.4 Texture Discrimination Scheme

In applying the proposed texture analysis method to wood defect recognition, a 8-pixel symmetrical neighborhood system or prediction mask for the center point (0,0) is chosen as {(+1,0), (0,+1), (-1,0), (0,-1), (-1,-1), (-1,+1), (+1,-1), (+1,+1)} [KAS86]. Eleven feature values, including the eight coefficients $\{\theta 1, \theta 2, ..., \theta 8\}$, an estimate of the error variance σ^2 at convergence, the image sample mean μ_y and sample variance σ_y^2 are chosen to construct a feature vector for each candidate defect region. Having chosen features, we can adopt a Bayesian or other standard rule for classification. A minimum distance classifier [DUD73] is employed because of its simplicity and low computational requirements, which is especially important in the later stages of the vision system. In the proposed scheme, the distance between a candidate feature vector and *a standard vector* is defined as the difference of 1.0 and the maximum of the circularly shifted correlation coefficient vector [ZHU93]. The higher a *candidate vector* is correlated with a *standard vector*, the shorter is the distance.

For texture pattern training, representative rectangular windows in a standard orientation are selected from each class of defect images, and their feature values are estimated and averaged to create a standard feature vector against which a candidate feature vector associated with a region is to be compared. Since there exists a strong directionality in the wood grain process and the selected rectangular windows may have varying orientations with respect to a standard orientation, each candidate feature vector is circularly shifted until the maximum correlation is achieved between it and the standard vectors. Texture discrimination is then performed by examining the maximum correlation coefficient, and the candidate texture is classified as the texture type for which it has the highest correlation.

The defect recognition scheme can be described by the following two steps, *partial correlation* and *full correlation*. Since the only components of a feature vector that are direction-dependent are the eight SAR model parameters, a partial correlation with circular shifting is performed first between the first eight feature values of a candidate vector and the standard vectors. Second a full correlation is calculated to include the three remaining features, i.e., the estimated error variance, and the image sample mean and sample variance. For the 11 bit image data used in this study, the first quantity of these three remaining features has a fairly small value, whereas the other two quantities have relatively large values. Therefore, these three feature values need to be properly scaled by two different weighting constants α_1 and α_2 so that they are given approximately the same weight as the eight model parameters. In particular, the value of the estimated error variance is scaled by constant α_1, while those of the image sample mean and sample variance are scaled by constant α_2.

Let us denote the properly weighted *standard feature vector* and *candidate feature vector* by U and V respectively, with $U = [u_1, u_2, ..., u_p, ... ,u_N]^T$, $V = [v_1, v_2, ..., v_p, ...,v_N]^T$, $p = N_1$ the number of estimated SAR model parameter features ($p = 8$), and $N = N_1 + N_2$ ($N = 11$) the total number of features selected for recognition. The element of U are derived from the standard features as follows

$u_i = \theta_i$; $i = 1, 2, ..., p,$
$u_{p+1} = \alpha_1 \sigma^2$,

$u_{p+2} = \alpha_2 \mu_y$,

$u_{p+3} = \alpha_2 \sigma_y^2$.

The elements of V are defined similarly, based on candidate feature.

The *partial correlation*, denoted by PC(k) , is defined as

$$PC(k) = \frac{\sum_{i=1}^{N1} U_i V_{i+k}}{\sqrt{\sum_{i=1}^{N1} U_i^2}\sqrt{\sum_{i=1}^{N1} V_i^2}}, \quad k = 0, 1, 2, ...N_1 - 1. \tag{7-13}$$

and the *full correlation*, denoted by FC(k) , is defined as

$$FC(k) = \frac{\sum_{i=1}^{N1} U_i V_{i+k} + \sum_{i=1}^{N2} U_i V_i}{\sqrt{\sum_{i=1}^{N} U_i^2}\sqrt{\sum_{i=1}^{N} V_i^2}}, \quad k = 0, 1, 2, ..., N1 - 1 \tag{7-14}$$

where $N = N_1 + N_2$, with $N_1 = 8$ the number of the estimated SAR model parameters and $N_2 = 3$ the number of the weighted features. Having defined FC(k) as in equation (7-14), the *distance* between two vectors U and V , denoted by d , can be expressed as

$$d = 1 - \max\{FC(k), k = 0, 1, 2, ..., N-1\} \quad (7\text{-}15)$$

This value is then forwarded to the minimum distance classifier that assigns a candidate defect to the type of defect for which the *distance* d retains the minimum value.

7.5 Experiment Results

The experimental results for the proposed method were obtained with CT images of two different red oak logs [ZHU93]. Fig. 7.1 and Fig. 7.2 each show one slice of these two logs. Fig. 7.1 (a) is the 22nd slice from a sequence of images for the first red oak log. Fig. 7.1 (b) exhibits its segmentation which contains barks, knots, a split, and clear wood; the latter occupying most of the image area. Fig. 7.2 (a) and (b) are the corresponding images for the 5th slice from the second red oak log, containing a brown decay and bark.

Using the model and algorithm described previously, the features of each defect were estimated from several image slices and their values averaged, to produce a standard feature vector for each defect type. A CT image was 256 x 256 x 11 bits with gray levels ranging from 0 to 2047 by a gray level transformation. After image segmentation, windows of appropriate sizes and orientations were selected for each potential defect region. The original image data within such windows were standardized by removing the mean value and then scaling by the standard deviation. First, 3- and 4-pixel neighborhood systems were tried as the SAR model masks. Since each wood grain is highly correlated with all its eight neighbors, these *partial model* masks did not produce consistent parameter estimates for the textures under study. Next the 8-pixel neighborhood system was selected as the SAR model mask. Eleven feature parameters were estimated, using the proposed iterative estimation algorithm. These parameters were then cross-correlated with each of the standard vectors, and the calculated correlation values were input to the minimum distance classifier to determine the defect type of a candidate region.

In the first experiment, 7 bark regions from 2 image slices (slices 20 and 24 of red oak section 11), 7 decay regions from 1 slice (slice 1 of red oak section 12), and 7 knot regions from 2 slices (slices 21 and 22 of red oak section 11) were selected as a training set and used to create the standard feature vector. Classification was then conducted with the training set, and the resulting classification accuracies were 71.4, 100, and 100 percent for decay, bark, and knot regions respectively. A testing set of 15 bark, 21 decay and 13 knot candidate regions was selected from 14 different image slices (including those used in the training)and classification conducted by the above described method. To achieve stable solutions, the step size of the iterative algorithm was selected as $\gamma = 0.01$. Since the typical value of the estimated variance is on the order of 10^{-1}, whereas those of the image sample mean and variance are from 10^{-3} to 10^{-5}, the weighting constants were chosen as $\alpha_1 = 100$, and $\alpha_2 = 0.0001$ so that all features are approximately equally treated by the classifier. Two sets of experiments on defect recognition were conducted with log image samples available from the Wood Image Library at the Spatial Data Analysis Laboratory. The following defect recognition accuracies were obtained with the testing set: 80 percent for bark regions with 3 out of 15 barks misclassified as decays; 81 percent for decay regions with 4 out of 14 decays misclassified as knots; and 100 percent for knot regions with no misclassification.

In the second experiment, a two-level tree structure was employed to construct a new classifier similar to that used in [KOI89]. The first level classifies candidates into two gross groups by examining the estimated value of the error variance, whereas the second level performs a correlation operation using the other ten features similar to the minimum distance classifier in the first experiment. In this case we report a 100 percent classification accuracy for each of the three groups of defects, and for both the training and the testing data sets described above. Correlation coefficients calculated in both experiments and detailed texture match results are available in [ZHU93].

Given the CT image data of the wood species available, the current method for wood texture analysis can identify clear wood as well as several prototypical defects, such as bark, decay, and knot. As CT image data for more species become available, this texture analysis method could be enhanced to classify other defects as well, such as stains, mineral streaks, holes, etc.

7.6 Summary and Discussions

In this chapter, a stochastic field-based approach for wood texture analysis has been presented. In particular, an iterative robust image modeling algorithm is applied to the problem of defect recognition in the machine vision system for log inspection. Experiments show that the described texture modeling method seems capable of discriminating several defects, including knots, decay, and bark, from the clear wood. It is expected that other major grading defects, such as stain, compression wood, mineral streaks and etc., might be recognized as well, when additional image data are collected from these log samples.

Experiments also indicate that the causal 3-neighborhood [KOI89] and the symmetrical 4-neighborhood configurations are not appropriate for modeling wood grain textures; that textures of the same grain, due to the wood growth process, demonstrate scale- and orientation-variation at different locations on each CT log image; and that many image preprocessing methods (histogram equalization, adaptive noise smoothing, or pixel interpolation in the circular model [KAS86]) tend to adversely affect the discrimination power of the described texture modeling method.

One of the major difficulties in texture modeling is the texture variance problem; i.e., the same texture may behave quite differently when its scale or orientation changes. Although there have been several research papers on the theoretical aspects of the texture invariance problem [FAN91], more practical methods are needed for a robust approach to modeling real-world wood textures. In future research, the initial value problem of the iterative algorithm also needs to be studied further, and solutions like the L_1 and the high breakdown estimates could be selected as the initial values [ROU87]. Moreover, more robust methods need to be developed to compute the covariance matrix, which is closely related to the weighting coefficient W1(s) in equation (7).

Yet another avenue of research is to incorporate the texture property of an object with its geometric and topological properties in the scene analysis module of the vision system. As such this scene analysis module can identify the object more accurately, since it uses all the information that can be obtained from the object. This can be accomplished by designing an additional test, called texture test Π_t, that assigns partial evidence to the various elements in the hypotheses space. Then the same method of evidence combination as discussed in Chapter 6 can be applied to accurately recognize the object.

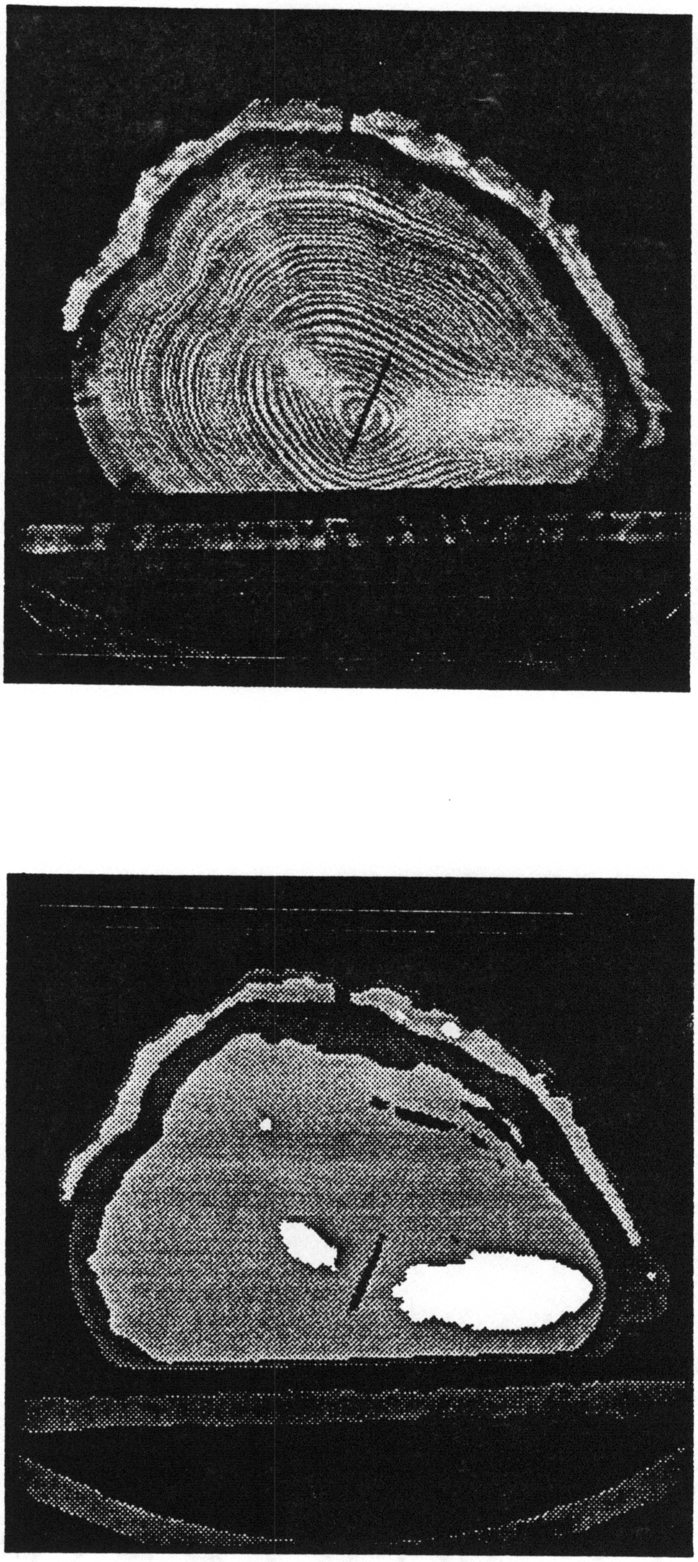

Fig. 7.1 Sampel image RK11.22 with bark and knot textures (top), and the objects whose texture models are iteratively estimated (bottom)

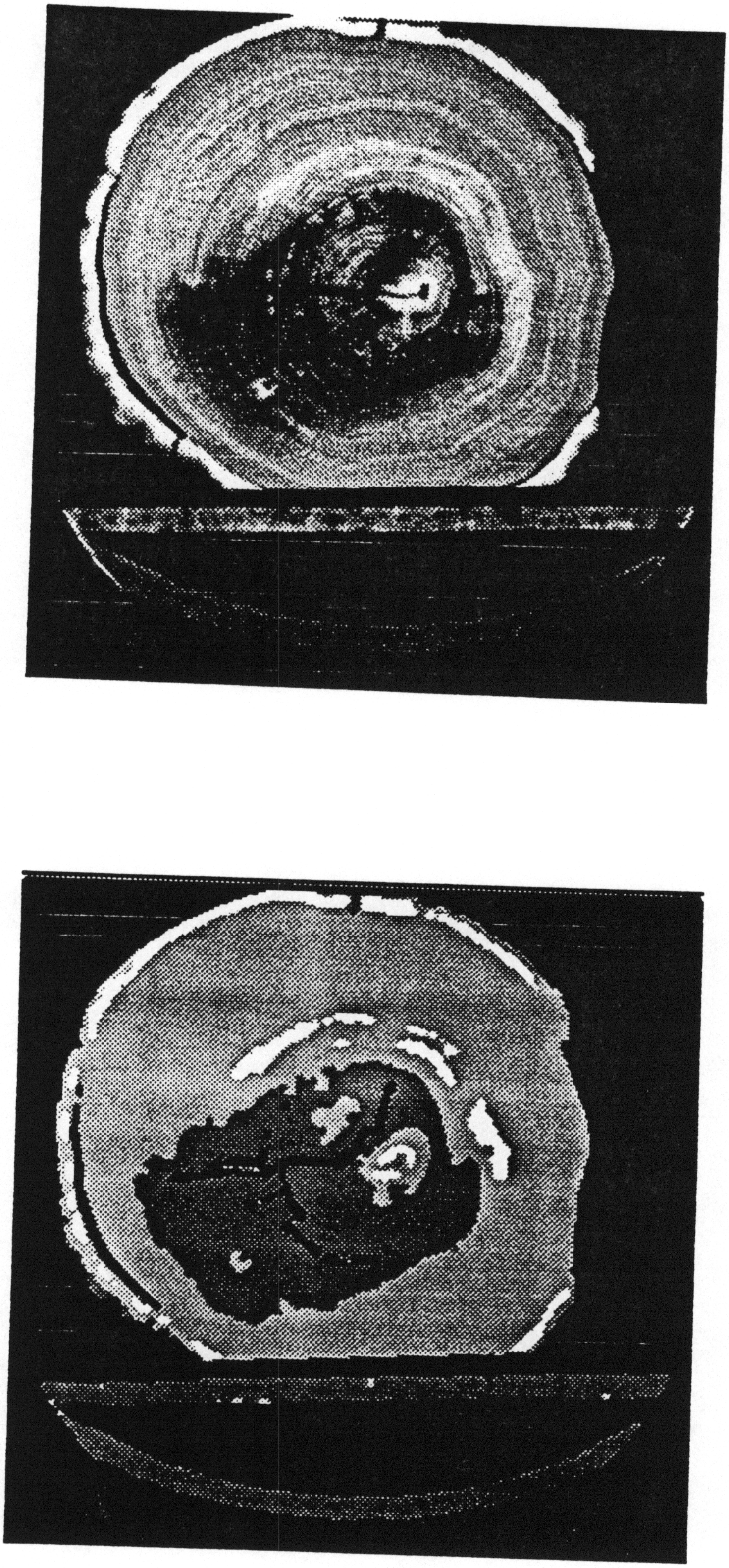

Fig. 7.2 Sample image RK12.05 with decay and stain textures (top), and the objects whose texture models are iteratively estimated (bottom)

Chapter 8
Conclusions

Due to the increasing demand on and the decreased availability of trees, there has been increased research into ways to better utilize this valuable natural resource in general, and to improve the value yield of a log in particular. To optimize the value of the material, either veneer or lumber, produced from a log requires information on the internal structure and geometry of grading defects prior to primary cutup. This information is used for two purposes: 1) to determine whether to process a log as veneer log or sawlog as the former is worth ten times more than the latter, and 2) to determine how to maximize the value of the resulting wood products by optimizing the cutting pattern of the initial breakdown. Several parallel research projects have been carried out elsewhere to simulate log grading and log sawing on computers, in search for an optimal method to saw logs so that the log value recovery can be maximized. While results from these efforts look promising, they do not fully utilize the indispensable information about real-world defects in logs, since previously there was no way of seeing into the inside of the log. Several scientific studies have shown that a 7 to 21 percent improvement in log value recovery can be achieved by log inspection using such technologies as microwave, ultrasound and laser. Although these conventional detecting technologies have been studied to some extend, there has been no serious effort at applying the internal scanning methods to the automated log inspection.

The recent developments in overcoming the crucial limitation of invisibility of internal defects are made possible by the advanced nondestructive testing (NDT) methods.

Technological advances in CT and MRI imaging have reached the point that these techniques can be applied to log inspection to automate the logging industry. However, methods for analyzing the scanned image data are not available yet. For these advanced sensing modalities to be of utility requires not only that defects manifest themselves in the sensor imagery in a manner in which they can be detected easily, but it also requires the existence of computerized methods for automatically interpreting this sensor imagery. While a good deal of work has gone into demonstrating that certain defects do manifest themselves in images produced by the various sensors, no systematic approach has been undertaken to study the important issues associated with designing an automated system for log inspection.

This dissertation attempts to establish the feasibility of using CT imaging for hardwood log inspection. In particular, it aims to achieve three basic objectives. These are: 1) to establish a log image data base that is representative of most hardwood species, so that the designed analysis methodology can be tested on a set of real-world log data; 2) to evaluate the images in the data base and determine which hardwood grading defects can be detected by the CT imaging modality, i.e., to assess the technical feasibility of this technology; and 3) to devise a systematic methodology for automatically segmenting and interpreting CT imagery of logs.

A knowledge-based machine vision system is described in this dissertation. It is comprised of three major components - a data collection unit, a low-level module for image segmentation, and a high-level module for scene analysis. This system has the following desirable properties: 1) the data collecting component should be able to capture most common hardwood grading defects defined in the standard log grading rules; 2) the image segmentation is robust and species-independent, so that important features could be accurately extracted from images of different species; 3) the scene analysis is able to handle the imprecision of knowledge representation and the uncertainty in hypothesis tests, so that it can recognize real-world log images with sufficient certainty.

As an important first step, a red oak and yellow poplar log image data base has been established. It consists of two different data presentations, a set of CT imagery and set of color photographs of cross-sections of the logs. Comparison of the CT imagery with the corresponding color photographs shows good correlations between the two sets. An analysis of the data base indicates that (1) for red oak logs, the CT imaging modality can capture most defects including knots, splits, holes, and decay, while mixing some pixels of bark with those of stain and not being able to differentiate between bark and clear wood in some log image samples; and that (2) for yellow poplar logs, the imaging method could capture knots, bark, and clear wood, as well as being able to differentiate sapwood and heartwood in green logs.

To design a robust, and species-independent image segmentation methodology, several methods were used: (1) A 3-d adaptive filter was developed for image smoothing. This smoothing operation is necessary to assure the robustness of the segmentation module by eliminating the unwanted parts from the original image data, while preserving the needed image details such as the narrow, lengthy splits. (2) An adaptive segmentation algorithm was used that is based on the concept of dynamic multiple thresholding. Operating on a slice-by-slice fashion, this adaptive segmentation is necessary to assure the species-independence of the methodology. It has been shown to be efficient at separating defects from clear wood and the image background (air). (3) A 3-d volume growing algorithm was developed that can group individual regions on 2-d slices into a finite number of 3-d objects. These 3-d objects in turn represent potential defects in the log that need to be recognized by the scene analysis module.

To devise an intelligent 3-d scene analysis method for object recognition, a knowledge-based approach was adopted. Since this method combines domain-independent image heuristics in the low-level module with domain-specific heuristics in the high-level module, it is a very general recognition mechanism suitable to discern different defects in an automated fashion. It also has the advantage of being flexible so that additional knowledge sources or tests could be included easily to deal with exceptions. Although still at its infancy, the development of machine vision systems has been studied extensively in the recent years. Most current recognition systems have focused on objects for which simple geometric models exist. This dissertation studied a very different version of the 3-d recognition problem, i.e., it involved objects with complex and arbitrary shapes for which exact geometric models are difficult, if not impossible, to obtain. Based on the analysis of the data base, a set of *basic features* have been defined and used to design a set of hypothesis tests for recognizing the identities of the various objects. To cope with the imprecision and uncertainty in representing object information, the Dempster-Shaffer model for knowledge representation was adopted for use. As a viable alternative to the Bayesian-based probability theory, the Dempster's method of evidential reasoning was employed to resolve conflicts that may exist among different hypotheses. It has been demonstrated to be an efficient method for reasoning under uncertainty, since by this theory, evidence that only partially favors a hypothesis should not be construed as also partially supporting its negation. As such, the proposed vision system seems to be able to recognize log defects of irregular 3-d shapes.

As a last topic, this dissertation also studied a stochastic field-based approach to wood textures analysis. In particular, it contributes the first application of Spatial Auto-Regressive (SAR) modeling to wood-grain texture analysis of CT images of hardwood logs, and an iterative robust method for image modeling was developed. Experiments show that the described texture modeling method appear capable of discriminating between clear wood and several defects, including knots, decays, and bark. Our study also indicates that the causal 3-pixel and the symmetric 4-pixel masks are not appropriate for modeling wood textures; that textures of the same grain, due to different growth processes, exhibit scale- and orientation-variation; and that some image pre-processing methods tend to adversely affect the discrimination power of the described modeling method. However this texture analysis method must be integrated with the machine vision system as an additional *texture test*, so that information about the important texture feature of grading defects can be used to improve object recognition.

The above methods in the image segmentation and scene analysis modules have been tested with CT images from the data base described in Chapter 4. Experiment results indicate that the image segmentation module can separate clear wood from knots, splits, holes, decay, and bark; the scene analysis module can recognize knots, decay (rot), and bark. These methods have been found to be robust and species-independent. These results also demonstrate that a CT-based machine vision system can be developed to locate and identify internal defects in hardwood logs. Furthermore, this general and robust methodology could also be used with other imaging modalities, such as MRI and ultrasound, in other industrial inspection applications.

Nevertheless, this research is limited, and further research is needed to fully address all the issues associated with automatically locating and identifying internal defects of logs.

Our research indicates that there is significant variation in wood properties amongst different sample images, thus making log image analysis a complicated problem in practice. It is suggested that future research efforts should be directed toward the following issues.

1) *Collecting additional data*: additional CT images of different logs are needed to verify the validity of CT imaging modality, to study the characteristics of the various defects, and to test the performance of the vision system using the SDT methods of Chapter 4.

2) *Augment image segmentation*: CT images contain more information content than human beings can percept. The current image segmentation module can only derive regional and volumetric information from the intensity images. By defining other possible image features derivable from CT images, such as the *dual energy* features of the x-rays, the image segmentation performance could be augmented significantly.

3) *Refine scene analysis*: despite the progress of research in D-S theory, there remain a significant number of problems with respect to the technology we have explored in this dissertation and its use in knowledge-based systems. For instance, although the D-S theory has relieved us from the burden of specifying complete probability models, a formal theory for generating mass function (*bpa*) remains unavailable. It is believed that this latter problem is more tractable than the former. Furthermore, at present there is no computational theory for the integration of "fuzzy-based" approach to uncertainty reasoning with the D-S theory of belief functions. Developing such a theory or method would fill in the gap between the two important branches of the approximate reasoning study.

4) *Improve texture modeling algorithm*: a more practical method is needed to address texture variation problems, so that the estimators could be more invariant. For the initial estimate of texture models, solutions like the L_1 and the high-breakdown estimates could be selected as the initial values.

5) *Integrating texture method in scene analysis module*: yet another avenue of research is to design a texture test, Π_t, in the scene analysis module using defects' texture. This new test will provide additional evidence about the identity of each of the types of the grading defects, so as to improve the identification accuracy of the scene analysis module in machine vision system for log inspection.

References

[ARA90] P. Araman, T.H. Cho, D. Zhu and R. W. Conners, "Computer vision systems for hardwood logs and lumber", *Artificial Intelligence Applications in Wood Manufacturing, XIXIUFRO Congress*, Montreal, Canada, Aug. 5-20, 1990

[BAL82] D. H. Ballard and C. M. Brown, Computer Vision, Englewood Cliffs, New Jersey: Prentice-Hall, Inc. 1982.

[BAR88] S. Bartlett, C. Cole, and R. Jain, "Automatic solder joint inspection," *IEEE Transactions on Pattern Analysis and Machine Intelligence*, vol. PAMI-10, no. 1, pp. 31-44, Jan. 1988.

[BEE65] F. Beer and E. R. Jonston, Jr. Vector Mechanics for Engineers, 3rd edition, New York: McGraw-Hill Book Company, 1965.

[BIN82] T, O, Binford, "Survey of model-based image analysis systems," *Internal Journal of Robotics Research*, Vol. 1, no. 3, pp. 18-64, 1982.

[BIR91] R. Birkeland and W. Han, "Ultrasonic scanning for internal log defects," *Proc. of 4th International Conference on Scanning Technology in The Wood Industry*, October, 1991.

[BRO63] B. L. Browning, The Chemistry of Wood, New York: John Wiley Sons, 1963.

[BRO66] P. Brodatz, Textures - A Photographic Album for Artists and Designers, Toronto: Dover Publishing Co., 1966.

[BRU89] C. C. Brunner, M. S. White, F. M. Lamb, and J. G. Schroeder, "CORY: a computer program for determining dimension stock yields," *Forest Products Journal*, vol. 39(2), pp. 23-24, 1989.

[BUC84] B. Buchanan and E. Shortliffe, Rule-Based Expert Systems: The MYCIN Experiments of the Stanford Heuristic Programming Project, Addison-Wesley Co., Reading, MA, 1984.

[BUS90] R. Bush, S. Sinclair and P. Araman, "Match your hardwood lumber to market needs," *Southern Lumberman*, vol. 251, No. 8, pp.24-27, August, 1990.

[CHA89] S. J. Chang "Economic feasibility analysis of the NMR fast imaging scanner," *Proc. of 3rd International Conference on Scanning Technology in Sawmilling*, pp. 1-5, October, 1989.

[CHA91] S. J. Chang, M. Cohen and P. C. Wang, "Ultrafast scanning of hardwood logs with an NMR scanner," *Proc. of 4th International Conference on Scanning Technology* in The Wood Industry, October, 1991.

[CHO90] T-H. Cho, R. W. Conners and P. Araman, "A computer vision system for automatic lumber detection using blackboard expert system method," *Proc. 10th International Conference on Pattern Recognition*, Atlantic City, NJ, June, 1990.

[CHO91] T-H. Cho "A knowledge-based machine vision system for automated industrial web inspection," Doctoral Degree Dissertation, Dept. of Electrical Engineering, Virginia Polytechnic Institute & State University, Blacksburg, VA, May 1991.

[CON81] R. W. Conners and C. Harlow, "A Theoretical comparison of texture algorithms," *IEEE Trans. on Pattern Analysis and Machine Intelligence*, vol. 2 no. 3, pp. 204-222, May 1981.

[CON83] R. W. Conners, C. McMillin and et al, "Identifying and locating surface defects in wood: Part of an automated lumber processing system," *IEEE Transactions on Pattern Analysis and Machine Intelligence*, vol. PAMI-5, no. 6, pp.573-583, Nov. 1983.

[CON89] R. W. Conners and C. T. NG, "Developing a quantitative model of human preattentive vision," *IEEE Transactions on System, Man and Cybernetics*, vol. SMC-19, no. 6, pp.1384-1407, Nov/Dec. 1989.

[COO78] Larry Cook, "Fourier-walsh shape descriptors and applications to radiographic image processing," Doctor of Philosophy Degree Dissertation, Electrical Engineering Department, University of Missouri-Columbia, December, 1978.

[COP93] G. Coppini, M. Demi, R. Poli and G. Valli, "An artificial vision system for x-ray image of human coronary trees," *IEEE Transactions on Pattern Analysis and Machine Intelligence*, vol. PAMI-15, no. 2, pp. 156-162, Feb, 1993.

[CUZ77] J. R. Cuzzi, "A general analytical method for evaluating differences in shape,: Preliminary Report, Biostereometrics Laboratory, Baylor College of Medicine, Houston, TX, 1977.

[DAV92] J. Davis and P. Wells, "Computed tomography measurement on wood," *Industrial Metrology*, vol. 2, no. 3/4, pp. 195-218, 1992.

[DEA91] CHERRY JUBILEE: A Guide to Today's Most Popular Cherry Veneers, 2nd Edition, The Dean Company, Princeton, WV, 1991.

[DEM67] A. P. Dempster, *Annals of Mathematical Statistics*, vol. 38, pp. 325-423, 1967.

[DER86] H. Derin and W. Cole, "Segmentation of texture images using Gibbs distribution," *Computer Vision, Graphics and Image Processing*, vol. 35, pp.72-98, 1986.

[DEV82] P. A. Devijver and J. Kittler, Pattern Recognition: A Statitstical Approach, Englewood Cliffs, New Jersey: Princtice Hall, 1982.

[DHA91] A. Dhawan and L. Arata, "Knowledge-based 3D analysis from 2D medical images," *IEEE Engineering in Medicine and Biology Magzine*, vol. 10 no. 4, pp. 30-37, December, 1991.

[DOI69] K. Doi, "Investigation of rdiological images," *Proc. Rad, Image Information*, vol. 2, pp. 264-270, 1969.

[DUD73] R. Duda and P. Hart, Pattern Classification and Scene Analysis, New York: John Wiley, 1973.

[DUD79] R. Duda, P. Hart, and R. Reboh, "A computer-based consultant for mineral exploration, " Technical Report, SRI International, Menlo Park, CA, 1979.

[ENG66] H. A. Enge, Introduction to Nuclear Physics, Reading, MA: Addison-Wesley Publishing Company, 1966.

[EGA75] J. Egan, Signal Detection & ROC Analysis, New York: Academic Press, 1975.

[FAN91] Z. Fan, F. Cohen adn S. Attali, "Automated inspection of textile fabriscs using textural models," *IEEE Transactions on Pattern Analysis and Machine Intelligence*, vol. PAMI-13, no. 8, pp.803-808, August. 1991.

[FUN85] B. V. Funt and E. C. Bryant, "A computer vision system that analyzes CT-scans of sawlogs, " *Proc. of IEEE Conference on Computer Vision and Pattern Recognition*, pp. 175-177, 1985.

[GEM84] S. Geman and D. Geman, "Stochatic relaxation, Gibbs distribution, and the Bayesian restoration of images," *IEEE Transactions on Pattern Analysis and Machine Intelligence*, vol. PAMI-6, pp. 721-741, 1984.

[GIP75] J. Gips, Shape Grammars and Their Uses, Basel, Birkhauser Verlag, 1975.

[GOO72] D. J. Goodenough, "Radiographic applications of signal detection, Doctoral Degree Dissertation, University of Chicago, 1972.

[GOR85] J. Gordon and E. Shortliffe, "The MYCIN experiments of the Stanford heuristic programming project," in Rule-Based Expert Systems, Ed. B. Buchanan and E. Shortliffe, Addison-Wesley, Reading, MA, 1985.

[GRU91] S. Grundberg and A. Gronlund, "Methods for reducing data when scanning for internal log defects of hardwood logs with an NMR scanner," *Proc. of 4th International Conference on Scanning Technology in The Wood Industry*, San Francisco, CA, October, 1991.

[HAR79] R. M. Haralick, "Statistical and structural approaches to textures," *Proceedings of IEEE*, vol. 67, no. 5, pp.786-804, 1979.

[HAR87] R. M. Haralick, S. Sternberg and X. Zhuang, "Image analysis using mathematical morphology," *IEEE Transactions on Pattern Analysis and Machine Intelligence*, vol. PAMI-9, no. 7, pp. 523-550, July, 1987.

[HAR88] Y. Hara, H. Doi, K. Karasaki and T. Iida, "A system for PCB automated inspection using fluorescent light," *IEEE Transactions on Pattern Analysis and Machine Intelligence*, vol. PAMI-10, no. 1, pp. 69-78, 1988.

[HAR91] T. Harless, F. Wagner, F. Taylor, V. Yadama and C. McMillin, "Methodology for locating defects within hardwoodlogs and determining their impact on lumber-value yield," *Forest Products Journal*, vol. 41(4), pp. 25-30, 1991.

[HAT85] Y. Hattori and Y.Kanagawa, "Non-destructive measurement of moisture distribution in wood with a medical CT-scanner," *Mokuzai Gakkaishi*, vol. 31, pp. 974-982, 1985.

[HEN88] S. J. Henkind and M. Harrison, "An analysis of four uncertainty calculi," *IEEE Trans. on Systems, Man, and Cybernetics*, vol. 18, no. 5, pp. 700-714, 1988.

[HER78] G. T. Herman, "An introduction to some basic mathematical concepts of computed tomography," Roentgen-Video-Techniques for Dynamic Studies, Ed. P heintzen and J. Bursch, Georg Thieme Publishers, Stuttgart, Germany, pp.253-260, 1978.

[HOD90] D. Hodges, W. Anderson and C. McMillin, "The economic potential fo CT scanners for hardwood sawmills," *Forest Products Journal*, vol. 40, no. 3, March 1990.

[HUB81] P. J. Huber, Robust Statistics, New York: John Wiley & Sons 1981.

[JAI89] A. K. Jain, Fundamentals of Digital Image Processing, Englewood Cliffs, New Jersy: Prentice Hall, 1989.

[JEN89] F. Jeng and J. W. Woods, "Texture discrimination using double stochastic gaussian random fiels," *Proceedings of IEEE International Conference on Accoustics, Speech, and Signal Processing*, pp. 1675-1678, May 1989.

[JUL62] B. Julesz, et at., "Invisibility of humans to discriminate between visual textures that agree in second order statistics-revisited," *IRE Transactions on Information Theory*, vol. IT-8, no. 1, pp.84-92, Feb. 1962.

[KAK88] A. Kak and M. Slaney, Principles of Computerized Tomographic Imaging, New York: IEEE Press, 1988.

[KAS86] R. L. Kashyap, "Image models ," in Handbook of Pattern Recognition and Image Processing, New York: Academic Press, 1986.

[KFU74] King-Sun Fu, "Syntactic methods in pattern recognition," in *Mathematics in Science and Engineering*, vol. 112, New York: Academic Press, Inc., 1974.

[KFU82] F. S. Fu, Syntatic Pattern Recognition and Applications, Englewood Cliffs, NJ: Prentic-Hall, 1982.

[KIN79] E. A. King, "An operating defect detector," presented at *The North American Sawmill and Plywood Clinic*, Portland, OR, March,1979.

[KLI88] P. Klinkhachorn, J. P. Franklin, C. W. McMillin, C. W. Conners and H. A. Huber, "Automated computer grading of hardwood lumber," *Forest Products Journal*, vol. 38, no. 4, pp. 67-69, April, 1988.

[KLI90] D. E. Kline, *personal communication*, Wood Science and Forest Products Department, Virginia Polytechnic Institute and State Univerisity, 1990.

[KLI92] D. E. Kline, and C. Regalado, "Optimum edging and trimming of hardwood lumber," *Forest Products Journal*, vol.42, no.2, pp.8-14, Feb., 1992.

[KOI89] A. Koivo and C. Kim, "Rubost image modeling for classification of surface boards," *IEEE Transactions on Systems, Man, and Cybernetics*, vol. SMC-19, no. 6, pp. 1659-1666, Nov/Dec., 1989.

[KOL68] Franz F. Kollmann and Wilfred A. Cote, Jr. Principles of Wood Science and Technology (I), Solid Wood Berlin: Spring-Verlag, 1968.

[KOM80] Dry Kiln Operator's Manual, National Hardwood Lumber Association, 1980.

[KUH63] D. E. Kuhl and R. W. Edwards, "Image separation radioisotope sanning of the liver and brain," *Radiology*, vol. 83, no. 5, pp. 926-936, 1964.

[LEE80] J. S. Lee," Digital image enhancement and noise filtering by the use of local statistics," *IEEE Trans. on Pattern Recognition and Machine Intelligence*, vol. 2, no. 2, pp. 165-168, 1980.

[LEE91] S. C. Lee, G. Qian, J. Chen and Y. Sun, "Determine a maximum value yield of a log using an optical log scanner," *Proc. of IEEE Conference on Computer Vision and Pattern Recongnition*, Meno, HI, Jan., 1991.

[LEV82] C. Levi, J. Cray, E. McCullough and R. Hattery, "The unreliability of CT-numbers as absolute values," *America Journal of Radiology*, vol. 139, pp. 443-447, 1982.

[LID90] D. Lide (Ed.), Handbook of Chemistry and Physics, 10th Edition, Englewood Cliffs, New Jersey: CRC Press, 1990.

[LIN88] L. O. Lindgren, "Non-destructive measurements of density and moisture content in wood using computerized tomography," Technical License Thesis, Royal Institute of Technology, Stockholm, Sweden, 1988. (in Swedish).

[LIN91] L. O. Lindgren, "Medical CAT-scanning: x-ray absorption coefficients, CT-numbers and their relation to wood density," *Wood Science and Technology*, vol. 25, pp. 341-349, Berlin: Spring-Verlag, 1991.

[LIN90] Z. Lin and Y. Attikiouzel, "2-d linear predication model-based decorrelation method," *IEEE Trans. on Pattern Analysis and Machine Intelligence*, vol. 11, no. 6, pp. 661-665, June, 1990.

[LJU83] L. Ljung and T. Soederstroem, Theory and Practice of Recursive Identification, Cambridge, MA: The MIT Press, 1983.

[MAL56] F. B. Malcolm, "Effect of defect placement and taper setout on lumber grade yields when sawing hardwood logs," Technical Report, No. 2221, *USDA Forest Service Forest Products Laboratory*, Madison, WI, p.7, 1956.

[MAR87] P. Martin, R. Collet, P. Barthelemy and G. Roussy, "Evaluation of wood characteristics: internal scanning of materials by microwave," *Wood Science and Technology*, vol. 21, no. 4, pp. 361-371, April, 1987.

[MCM84] C. W. McMillin, R. W. Conners and H. A. Huber, "ALPS - a potential new automated lumber processing system," *Forest Products Journal*, vol. 34, no. 1, pp. 13-20, 1984.

[MET69] C. E. Metz, "A mathematical investigation of radiosotope scan image processing," Doctoral Degree Dissertation, University of Pennsylvania, 1969.

[MUL84] R. Mull, "Mass estimates by computed tomography: physical densities from CT-numbers," *America Journal of Radiology*, vol. 143, pp. 1101-1104, 1984.

[NAG80] M. Nagao and T. matruyama, A Structural Analysis of Complex Aerial Photographs, New York: Plenum, 1980.

[NEW81] T. H. Newton and D. G. Potts, Ed. Radiology of The Skull and Brain: Technical Aspects of CT, St. Louis, MO: The C. V. Mosby Company, 1981.

[NHL86] National Hardwood Lumber Association, Rules for the measurement and inspection of hardwood and cypress lumber, Menphis, TN, 1986.

[OCC88] L. G. Occena and J. M. Tanchoco, "Computer graphic simulation of hardwood log sawing ," *Forest Products Journal*, vol.38, no.10, pp.72-88, Oct., 1988.

[OCC89] L. G. Occena and J. M. A. Tanchoco, "Pattern directed extraction and characterization of defect configurations in solid log models," *Artificial Intelligence in Engineering*, Vol. 4, no. 3, pp. 144-154, March, 1989.

[PAM91] W. L. Grimson and D. P. Huttenlocher (Eds.), Special Issue on Interpretation of 3-D Scenes, Part I, *IEEE Trans. on Pattern Analysis and Machine Intelligence*, vol. 13, no. 10, October, 1991.

[PAM92] W. L. Grimson and D. P. Huttenlocher (Eds.), Special Issue on Interpretation of 3-D Scenes, Part II, *IEEE Trans. on Pattern Analysis and Machine Intelligence*, vol. 14, no. 2, Febuary, 1992.

[PAN70] A. J. Panshin and C. deZeeuw, Textbook of Wood Technology, vol. I, 3rd Ed., New York: McGraw-Hill Book Co., 1970.

[PAR77] T. Parvlidis, Structural Pattern Recognition, New York: Sping-Verlag, 1977.

[PEA86] J. Pearl, "On Evidential Reasoning in a hierarchy of hypotheses," *Artificial Intelligence*, vol, 28, pp. 9-15, 1986.

[QIA90] J. Z. Qian, "DNESYS - A Knowledge-based Drainage Evaluation System," Doctoral Degree Dissertation, Department of Electrical Engineering, Virginia Polytechnic Instiute and State University, Blacksburg, Virginia, April, 1990.

[RAS73] E. D. Rast, D. L. Sonderman and G. L. Gammon, A Guide to Hardwood Log Grading, U.S.D.A. Forest Service General Technical Report NE-1, Northeastern Forest Experiment station, Broomall, PA, 1973.

[REG91] C. Regalado, "Optimization of edging and trimming operations for red oak lumber," Master of Science Degree Thesis, Wood Science and Forest Products Department, Virginia Tech, 1991.

[ROB65] L. Roberts, "Machine perception of 3-d solids," in Optical and Electro-Optical Information Processing, J. Tippet (Ed.), MIT Press, Cambridge, MA, 1965.

[ROS73] A. Rose, Vision: Human and Electronics, New York: Plenum Press Corp, 1973.

[ROU87] P. J. Rousseeuw and J. Leray, Robust Regression and Outlier Detection, New York: John Wiley & Sons, 1987.

[ROW84] R. Rowell, Ed., The Chemistry of Solid Wood, America Chemistry Society Advances in Chemistry Series, No. 207, ACS, Washington, D.C., 1984.

[SER82] J. Serra, Image Analysis and Mathematical Morphology, New York: Academic Press, 1982.

[SHA76] G. D. Shafer, A Mathematical Theory of Evidence, Princeton University Press, Princeton, NJ, 1976.

[SHA88] P. A. Shadbolt, "Some aspects of non-destructive testing using computerised tomography," Master of Science Degree Thesis, Department of Applied Physics, Chrisholm Institute of Technology, Australia, Sept., 1988.

[SHI87] Y. Shirai, 3-Dimensional Computer Vision, New York: Springer-Verlag, 1987.

[SRI89] C. Srinivas and M. D. Srinath, "CGRF model image segmentation and restoration," *Proceedings of IEEE International Conference on Accoustics, Speech, and Signal Processing*, pp. 1586-1589, May, 1989.

[STA75] S. J. Starr, C. Metz, L. Lausted and D. Goodenough, "Visual detection and localization of radiographic images," *Radiology*, vol. 116. pp. 533-538, 1975.

[STE89] P. H. Steele and F. W. Taylor, "Hardwood sawing methods to maximize value and volume: preliminary results," *Proceedings of the 7th Annual Hardwood Symposym*, U.S. Hardwood Research Council, pp. 149-157, May, 1989.

[STR91] T. M. Strat and M. A. Fischler, "Context-based vision: recognizing objects using information from both 2-d and 3-d imagery," *IEEE Trans. on Pattern Analysis and Machine Intelligence*, vol. 13, no. 10, pp. 1050-1065, October, 1991.

[SZY81] R. Szymani and K. A. McDonald, " Defect detection in lumber: state of the art," *Forest Products Journal*, vol. 31, no, 11, pp. 34-44, 1981.

[TSA76] C. M. Tsai and Z. H. Cho, "Physics of contrast mechanism and averaging effect of linear attenuation coefficients in a computerized transversal axis tomography scanner," *Phy. Med. Biol.* vol. 21, pp. 544-559, 1976.

[TAY84] F. Taylor, F. Wagner, C. McMillin, I. Morgan and F. Hopkins, "Locating knots by industrial tomography - a feasibility stuty ," *Forest Products Journal*, vol. 34, no, 5, pp. 42-46, 1984.

[TSI74] P. P Tsiang, "Computer analysis of chest radiographs using size and shape descriptors, " Doctor of Philosophy Degree Dissertation, University of Missouri-Columbia, 1974.

[WAG89] F. Wagner, F. Taylor, D. Ladd, C. McMillin and F. Roder, "Ultrafast CT scanning of an oak log for internal defects," *Forest Products Journal*, vol. 39, November/December, 1989.

[WAN89] P. C. Wang, S. J. Chang and J. Olson, "Scanning logs with an NMR scanner," *Proc. of 7th International Nondestructive Testing of Wood Symposium*, pp. 209-219, Sept., 1989.

[WEG84] F. D. Wegnener, Wood: Chemistry, Ultrastructure, Reactions, Berlin: W. de Gruyter, 1984.

[WHA92] P. Whaite and F. P. Ferrie, "From Uncertainty to visual exploration," *IEEE Trans. on Pattern Analysis and Machine Intelligence*, vol. 13, no. 10, pp. 1038-1049, October, 1992.

[WIL80] C. R. Wilson, "Quantitative computed tomography,' in Medical Physics of CT and Ultrasound-tissue Imaging and Characterization, Ed. G. D. Fullerton adn J. A. Zagzebski, New York: American Institute of Physics, 1980.

[WIL91] W. W. Wilcox, Wood as A Building Material: A Guild for Designers and Builders, New York City, New York: John Willey & Sons, Inc. 1991.

[WON81] D. C. Wong, A. Vagnucci and C. C. Li, "Gradient inverse weighted smoothing scheme and evaluation of its performance," *Computer Graghics and Image Processing*, vol.15, pp.167-181, 1981.

[UNS90] M. Unser, "Improved restoration of noisy images by adaptive least-squares post-filtering," *Signal Processing*, vol. 20, no.1, pp.3-14, Elsevier-Science Publishers B.V., May, 1990.

[ZAD65] L. Zadeh, "Theory of fuzzy sets," *Inform. Contr.*, vol. 8, pp. 338-358, 1965.

[ZHA90] J. Zhang and J. W. Modestino, "A model-fitting approach to cluster validation with application to stochastic model-based image segmentation," *IEEE Transactions on Pattern Analysis and Machine Intelligence*, vol. 12, no. 10, pp. 1009-1017, Oct., 1990.

[ZHU91a] D. Zhu, R, Conners and P. Araman, "CT image sequence processing for wood defect recognition," *Proceedings of the 23rd Southeastern Symposium on System Theory*, The IEEE Computter Society Press, pp.75-79, March, 1991.

[ZHU91b] D. Zhu A. A. Beex, R. W. Conners and P. Araman, "Stochastic field-based object recognition in computer vision," *Proceedings of SPIE International Confernce on Stochastic Methods in Neural Networks, Signal and Image Processing, and Computer Vision*, San Deigo, CA, July 23-26, 1991.

[ZHU91c] D. Zhu, R. W. Conners and P. Araman, "3-d signal processing in a computer vision system," *Proceedings of IEEE International Confernce on Systems Engineering*, Dayton, OH, August 1-3, 1991.

[ZHU91d] D. Zhu, R. W. Conners, D. Schmoldt and P. Araman, "CT image sequence analysis for object recognition -- a rule-based 3-d computer vision system," *IEEE International Conference on Systems, Man, and Cybernetics*, Charlottesville, VA, October 13-16, 1991.

[ZHU91e] D. Zhu, R. W. Conners, F. Lamb, D. Schmoldt and P. Araman, "A computer vision system for locating and identifying internal log defects using CT imagery," *Processings of The Fourth International Conference on Scanning Techlonogy in Wood Industry,* San Francisco, CA, pp.1-13, October, 1991.

[ZHU91f] D. Zhu, R. W. Conners and A. Araman, "CT image segmentation for defect region identification," *SPIE International Conference on Applications of Digital Image Processing XIV*, San Diego, CA, July, 1991.

[ZHU91g] D. Zhu, R. W. Conners and P. Araman, "3-dimensional image segmentation by volume growing," *IEEE and SPIE Int'l Conference on Visual Communications and Image Processing'91*, Boston, MA, Nov., 1991.

[ZHU91h] D. Zhu, A. A. (Louis) Beex, R. W. Conners and P. Araman,"Parametric modeling of CT image textures for object recognition," *Proc. 25th Annual Conference on Information Sciences and Systems*, Baltimore, MD, May, 1991.

[ZHU92a] P. Araman, D. Schmoldt, T-H. Cho, D. Zhu, R. Conners, and D. Earl Kline, "Machine vision systems for processing hardwood lumber and logs," *AI Applications*, vol. 6, no. 2, pp.13-26, April, 1992.

[ZHU92b] D. Schmoldt, D. Zhu and R. Conners, "Nondestructive testing of hardwood using CT imaging," *Proc. of 2nd Sympoiusm on Nondestructive Testing Applications*, San Diogo, CA, June 20-26, 1992.

[ZHU92c] D. Zhu, C. B. Carrig and R. W. Conners, "Canine bone e shape analysis by use of a radioagraphic image-classification system," *American Journal of Veterinary Research*, vol. 53, no. 7, pp. 1090-1095, American Veterinary Medical Association, July, 1992.

[ZHU93] D. Zhu and A. A. (Louis) Beex, "Robust spatial autoregressive modeling for hardwood texture analysis," (to appear in) *Journal of Visual Communication and Image Representation*, vol. 36. no. 9, Academic Press, Sept. 1993.

VITA

Dongping Zhu was born on December 24, 1958 in Anxiang County, Changde District of Hunan Province, the People's Republic of China. He earned a B.S. degree in Radio Electronics in 1982 and a M.S. degree in Electronics and Communication Systems in 1985, from Dalian Institute of Technology (DIT), now named Dalian University of Technology (DUT), Dalian, P. R. China. From 1982-1987, he was on the faculty in the Department of Electrical Engineering at DIT. He received a M.S. degree in May 1990, and a Ph.D. degree in April 1993, both in Electrical Engineering from Virginia Polytechnic Institute and State University, Blacksburg, Virginia. During the study at VPI&SU, he was a graduate project assistant at the Spatial Data Analysis Laboratory. Since January 1992, he has been with InVision Technologies, Inc., Foster City, California, where he is now a research project manager and staff scientist.

Dongping Zhu